EVALUATION OF REQUIRED SPLICE LENGTHS FOR REINFORCING BARS IN MASONRY WALL CONSTRUCTION

A Thesis Submitted to the College of
Graduate Studies and Research
in Partial Fulfillment of the Requirements
for the Degree of Master of Science
in the Department of Civil and Geological Engineering
University of Saskatchewan
Saskatoon

By

Roanne D. Kelln

PERMISSION TO USE

In presenting this thesis in partial fulfillment of the requirements for a Postgraduate degree from the University of Saskatchewan, the author has agreed that the Libraries of this University may make it freely available for inspection. The author has further agreed that permission for copying of this thesis in any manner, in whole or in part, for scholarly purposes may be granted by the professor or professors who supervised the thesis work or, in their absence, by the Head of the Department or the Dean of the College in which the thesis work was done. It is understood that any copying, publication, or use of this thesis or parts thereof for financial gain shall not be allowed without the author's written permission. It is also understood that due recognition shall be given to the author and to the University of Saskatchewan in any scholarly use which may be made of any material in this thesis.

Requests for permission to copy or to make other use of material in this thesis in whole or part should be addressed to:

Head of the Department of Civil and Geological Engineering

University of Saskatchewan

Engineering Building

57 Campus Drive

Saskatoon, Saskatchewan S7N 5A9

Canada

ABSTRACT

Relatively few research efforts have focused on splice length requirements for reinforced masonry, despite the significant impact of these requirements on the safety, economy, and constructability of masonry walls. The Canadian masonry provisions for splice lengths in CSA S304.1-04 are taken directly from the Canadian concrete design standard, CSA A23.3-04, and thus do not necessarily reflect factors unique to masonry construction. Provisions in American masonry standard TMS 402-13/ACI 530-13/ASCE 5-13 are based on test results of double pullout specimens, but may be overly conservative due to shortcomings of the specimen type chosen.

The purpose of this study is to examine the splice lengths needed for flexural masonry elements reinforced with bar sizes typically used in Canadian masonry construction. In this study, 27 wall splice specimens and 12 double pullout specimens were constructed. The wall splice specimens were tested horizontally in four point loading, while the double pullout specimens were tested in direct tension.

Results from the double pullout specimen testing suggest that the techniques used at the University of Saskatchewan (U of S) are reasonably similar to those of the National Concrete Masonry Association (NCMA), and are thus adequate to assess current provisions in the American and Canadian standards.

A predictive equation for the tensile resistance of spliced reinforcement was developed from the results of the wall splice specimen testing. This predictive equation was then adjusted to incorporate an adequate margin of safety for calculating splice length requirements for design purposes, using a five percent quantile approach. The adjusted predictive equation was then extrapolated to determine the splice lengths corresponding to the nominal yield strength of the reinforcement. These splice lengths were compared to current code provisions. It was found that the current CSA S304.1-04 Class B provisions, used almost exclusively in construction, are conservative for No. 15, 20, and 25 bars. In contrast, the TMS 402-13 provisions were overly conservative for all three bar sizes. Changes to the bar size factors of the current provisions for both codes were recommended to bring better consistency to the requirements of the two codes, and thus ensure the safety, economy, and constructability of masonry walls.

CO-AUTHORSHIP

All experimental and analytical work presented herein was performed by Roanne Kelln and reviewed by Dr. Lisa R. Feldman. The literature review presented in Chapter 2 of this thesis was presented at the 12th Canadian Masonry Symposium in Vancouver, Canada, in 2013 and was included in the electronic compendium of papers for this conference. Test results and analysis from the first phase of construction were presented at the 9th International Masonry Conference in Portugal in 2014 and were included in the proceedings of this conference. A journal paper discussing the results of this study will be written and submitted.

ACKNOWLEDGEMENTS

The author would like to thank the numerous individuals without whom the undertaking and completion of this program would not have been possible.

The author would like to thank her supervisor, Dr. Lisa Feldman, and advisory committee, Dr. Bruce Sparling and Dr. Leon Wegner, for their feedback and guidance throughout the program. Special thanks are also extended to Dr. Gordon Putz and Dr. Jim Kells, for their help in the course of this M.Sc. program. The help of Dr. Bickis regarding the regression analysis and quantile approach used in this study is gratefully acknowledged.

The author would also like to thank Brennan Pokoyoway and Dale Pavier, Structures laboratory technicians, for their immense help in the execution of the experimental program undertaken for this research. Their help, guidance, and feedback in the construction and testing of the test specimens in this program are greatly appreciated. Thanks are also extended to Roy Nicolas, journeyman mason of Gracom Construction, for constructing the test specimens in this program. Additionally, the author would like to thank Albert Pilon of Gracom Construction for accommodating the construction scheduling and equipment needs of this program, as well as Bob Afseth and the Saskatchewan Masonry Institute (SMI) for their financial support in terms of the labour and materials required for the construction of the test specimens in this program. Help from fellow graduate students in the construction of the test specimens, particularly in the mixing and placement of many batches of grout, is also gratefully acknowledged.

Contributions from the Natural Sciences and Engineering Research Council of Canada (NSERC), the Department of Civil and Geological Engineering at the U of S, the College of Graduate Studies and Research in the form of a Dean's scholarship, and The Masonry Society in the form of the C.T. Grimm PE Scholarship are all gratefully acknowledged. As noted above, the financial contributions of SMI are gratefully acknowledged as well.

Finally, the author would like to thank her family and friends, for supporting her throughout the journey of her M.Sc. program. Many thanks are extended to her parents, her sister, and her grandparents, for the assistance and unconditional love they have provided.

TABLE OF CONTENTS

LIST OF TABLES

LIST OF FIGURES

LIST OF ABBREVIATIONS

ACI	American Concrete Institute
ASCE	American Society of Civil Engineers
ASTM	American Society for Testing and Materials
CCMPA	Canadian Concrete Masonry Producers' Association
COV	Coefficient of Variation
CSA	Canadian Standards Association
LVDT	Linear Variable Differential Transducer
MSJC	Masonry Standards Joint Committee (TMS, ACI, and ASCE)
NCMA	National Concrete Masonry Association
PVC	Polyvinyl chloride
RMSE	Root-mean-square error
SMI	Saskatchewan Masonry Institute
TMS	The Masonry Society
U of S	University of Saskatchewan
UTM	Universal Testing Machine

LIST OF SYMBOLS

a	Loading point locations (mm)
A'_1, A'_2, A'_3, A'_4	Constants for strain-hardening region of reinforcement stress-strain curve, determined from boundary conditions
A_s	Nominal cross-sectional area of reinforcement (mm^2)
b	Width of wall splice specimen (mm)
c_{cl}	Clear cover to reinforcement (mm)
C	Resultant compressive force in masonry (kN)
d_b	Reinforcing bar diameter (mm)
d_{cs}	Lesser of: (1) the distance between the reinforcing bar and the closest masonry surface, or (2) two-thirds the distance between bars being developed (mm)
d_{eff}	Effective depth of reinforcement (mm)
d_i	Distance from centroid of i^{th} segment to neutral axis
E_m	Elastic modulus of masonry assembly (MPa)
E_s	Elastic modulus of the reinforcement (MPa)
E_{sh}	Instantaneous slope at the initiation of strain hardening of reinforcement
$F_{2\alpha,k,n-k}$	Value of the F distribution at the confidence level α with k and $n-k$ degrees of freedom
f_{av}	Average compressive strength of tested masonry prisms (MPa)
f'_{gr}	In-situ compressive strength of the grout (MPa)
f'_m	Specified compressive strength of the masonry assembly (MPa)
f'_{mt}	Compressive strength of the masonry assembly determined from masonry prism testing (MPa)
$f_m(\varepsilon_m)$	Stress in masonry at given strain, ε_m (MPa)
$f_s(\varepsilon_s)$	Stress in the reinforcement at given strain, ε_s (MPa)
f_{s1}, f_{s2}	Bar stresses at sections 1 and 2 of reinforcement, respectively, used in development of theoretical average bond stress definition
f_y	Yield strength of the reinforcement (MPa)
f_{ult}	Ultimate strength of the reinforcement (MPa)
F_s	Allowable stress in reinforcement, TMS 402-95 (psi)
I_{cr}	Fully cracked section moment of inertia (mm^4)
I_{eff}	Effective moment of inertia (mm^4)
I_g	Gross moment of inertia (mm^4)
k	Number of bar sizes considered in study
k_1	Bar location factor, CSA S304.1-04
k_2	Epoxy coating factor, CSA S304.1-04
k_3	Bar size factor, CSA S304.1-04
K	Least of minimum cover, clear spacing between adjacent reinforcement, and $9d_b$, TMS 402-13 (mm)
K_o	Strength enhancement factor, modified Kent-Park curve
K_{tr}	Transverse reinforcement index, CSA S304.1-04 (mm)
kd	Neutral axis depth (mm)
l_d	Development length (mm)

l_s	Lap splice length (mm)
$\overline{l_{s_i}}$	Mean splice length for all specimens of the i^{th} bar size (mm)
$l_{s_{ij}}$	Splice length for the i^{th} bar size and j^{th} splice length (mm)
l_m	Clear span length of wall splice specimen (mm)
M	Moment calculated using numerical moment-curvature model (kN·m)
M_a	Applied moment (kN·m)
M_{ai}	Moment at middle of i^{th} segment (kN·m)
M_{cr}	Cracking moment (kN·m)
n	Number of specimens in test database
n_i	Number of specimens of the i^{th} bar size
n_{seg}	Number of segments
P	Applied load (kN)
P_{cr}	Cracking load (kN)
s	Standard deviation of the compressive strength of the masonry assembly as determined by masonry prism testing
s_s	Standard deviation of sample set, ASTM E178
s^2	Estimated residual variance of the predictive equation
t	Thickness of wall splice specimen (mm)
t'	75th percent quantile of the non-central t-distribution
T	Tensile force in reinforcement (kN)
$T_r(\varphi)$	Tensile resistance of reinforcement at a given curvature, φ (kN)
T_r	Tensile resistance of the lap splice, reported for a single splice in reference to any wall splice specimen (kN)
T_n	Test criterion for identifying statistical outliers, ASTM E178
T_r^*	Lower 95 percent tolerance value of tensile resistance of spliced reinforcement, calculated from adjusted predictive equation
u_{avg}	Average bond stress (MPa)
x_n	Observation or data point of interest, ASTM E178
$\bar{x}$	Average value of all specimens in the sample set, ASTM E178
δ_{mid}	Midspan deflection (mm)
ε_{cm}	Strain in extreme compressive fibre of masonry
ε_i	Strain at centroid of i^{th} segment
ε_m	Strain in masonry
ε_o	Strain corresponding to maximum stress in masonry assembly
ε_s	Strain in reinforcement
ε_{sh}	Strain at the initiation of strain hardening of reinforcement
ε_{ult}	Strain in reinforcement at its ultimate strength
ε_y	Yield strain of reinforcement
γ	Bar size factor, TMS 402-13
φ	Curvature (1/m)
φ_{cr}	Curvature at initiation of cracking (1/m)
φ_i	Curvature in i^{th} segment (1/m)
φ_e	Effective curvature (1/m)
$\varphi_m(M)$	Curvature at given moment, M (1/m)
φ_{max}	Curvature at maximum load (1/m)

φ_{uc}	Curvature of uncracked section (1/m)
σ_i	Compressive stress in i^{th} segment (kN)
Δl	Segment of reinforcement in the region where the bar is being developed, used in development of theoretical average bond stress definition

CHAPTER 1 INTRODUCTION

The use of masonry as a building material has long connoted a sense of permanence, excellence, and distinction for the structures built from it. Masonry structures have a unique place-making ability that few other building materials can replicate. Modern masonry construction largely consists of reinforced masonry, as the addition of reinforcing bars to masonry elements makes masonry a cost-competitive option as a structural material. Much like reinforced concrete, reinforced masonry takes advantage of the high compressive strength of the masonry blocks and grout while using the reinforcement to provide tensile resistance appropriate for withstanding flexural loads. As such, sufficient bond between the reinforcement – grouted in-place in the cells of masonry blocks – and the grout is needed, such that stresses are transferred within the assemblage and the full capacity of the reinforcement can be developed.

In reinforced masonry construction, common features such as connections, openings, or construction details, as well as the overall lengths or heights of certain members, frequently prevent the use of continuous reinforcement. In such situations, two reinforcing bars are overlapped or spliced; however, the length of these splices must be sufficiently long for tensile stresses to be transferred between lapped bars to prevent a bond failure (Hatzinikolas & Korany 2005, Drysdale & Hamid 2005, NCMA 1999). Consequently, splice and development length requirements significantly impact the safety, constructability, and economy of masonry walls.

Despite the significant impact of splice length requirements on masonry construction, relatively few research efforts have focused on these requirements. The limited research regarding bond in reinforced masonry has historically focused on testing pullout-type specimens, due to the relative ease of construction and testing of these smaller-scale specimens. In testing these types of specimens, tension is applied directly to the lapped bars until the reinforcement ‘pulls out’ of the specimen. Pullout-type tests typically place the cementitious materials surrounding the reinforcing bars in a compressive or neutral stress state, whereas the stress state of the cementitious materials surrounding the reinforcing bars would be tensile in a flexural element (ACI Committee 408 2012). As

such, these specimens do not accurately capture the behaviour of flexural elements. Researchers studying the behaviour of reinforced concrete have identified similar shortcomings with pullout specimen testing (ACI Committee 408 2012).

Consequently, Ahmed & Feldman (2012) conducted a study comparing double pullout specimens and wall splice specimens in terms of the load-deflection behaviour and tensile resistances of spliced reinforcement. The double pullout specimens were tested by applying tension directly to the reinforcing bars. The wall splice specimens, which were 13 courses high and had the same cross-sectional geometry as the double pullout specimens, were tested in flexure using four-point loading. They reported a statistically significant increase in the capacity of wall splice specimens as compared to the corresponding double pullout specimens, with an average increase in the tensile resistance of the reinforcement of 8 percent for contact lap splices. The wall splice specimens reinforced with lap spliced bars in contact exhibited strain hardening of the bars while the reinforcement in the corresponding double pullout specimens did not show signs of strain hardening. The results of Ahmed & Feldman's (2012) work thus established the validity of using wall splice specimens for evaluations of splice length requirements for reinforced masonry.

The Canadian masonry provisions for development and lap splice lengths provided in CSA S304.1-04: *Design of Masonry Structures* (CSA 2004a) are taken directly from the Canadian concrete design code, CSA A23.3-04: *Design of Concrete Structures* (CSA 2004b), since bond has been studied extensively by reinforced concrete researchers, with tests for development and lap splice lengths dating as far back as 1876 (Abrams 1913). However, the provisions for reinforced concrete design do not account for inherent properties unique to masonry construction, including the reduced lever arms, weak bed joints, and limiting of flexural cracking to the bed joints (Ahmed 2011, Hammons et al. 1994). These properties may have a negative effect on bond strength and thus may necessitate longer lap splices than those calculated for reinforced concrete (Kisin 2014). Further investigation specific to masonry is thus needed.

Provisions for splice lengths in the American masonry code TMS 402-13/ACI 530-13/ASCE 5-13: *Building Code Requirements for Masonry Structures* (MSJC 2013a), hereafter referred to as TMS 402-13, were developed from the results of an experimental program consisting exclusively of masonry pullout specimens. Based on their experimental results, the National Concrete Masonry Association (NCMA) developed provisions for splice lengths that were first included in the 2008 edition of the American masonry code (NCMA 2009). In developing these provisions, a tensile resistance of spliced reinforcement equal to 125 percent of the reinforcing steel yield strength was targeted. As a result of the specimen type selected and tensile resistance targeted, overly conservative provisions may have resulted, since the stress state in the cementitious materials surrounding the reinforcing bars is not adequately captured in pullout specimens. The provisions of TMS 402-13 (MSJC 2013a) are significantly more conservative than those prescribed by CSA S304.1-04 (CSA 2004a) for bar sizes No. 20 and greater.

Significant differences in splice length provisions presented in CSA S304.1-04 (CSA 2004a) and TMS 402-13 (MSJC 2013a) motivate a further examination of bond in masonry construction. As such, the purpose of this research is to investigate the splice lengths required for the reinforcing bar sizes typically used in Canadian reinforced masonry construction.

1.1 Objectives of Study

The objective of this research is to establish rationalized splice lengths needed for flexural masonry elements reinforced with bar sizes within the range typically used in Canadian reinforced masonry construction (No. 15, No. 20, and No. 25 reinforcing bars). The specific objectives of this study are:

- To confirm that the construction and testing techniques used at the University of Saskatchewan (U of S) are reasonably similar to those used by the NCMA (1999, 2009)

- To develop an empirical equation to predict the tensile resistance of spliced reinforcement for No. 15, No. 20, and No. 25 reinforcing bars,

- To quantify splice lengths needed to develop a tensile resistance corresponding to the yield strength of the reinforcement for No. 15, No. 20, and No. 25 reinforcing bars,

- To compare code-to-test calculated ratios of splice lengths by dividing the splice length requirements of CSA S304.1-04 (CSA 2004a) and TMS 402-13 (MSJC 2013a) for each bar size by the test-required splice lengths corresponding to the yield strength of the reinforcement, and

- To provide recommendations for changes to the current provisions of CSA S304.1-04 (CSA 2004a) and TMS 402-13 (MSJC 2013a) to ensure adequate safety for both codes, while bringing better consistency to the requirements of the two codes.

1.2 Scope

A large scale experimental program was required to address the above-noted objectives, and involved the construction of 27 wall splice specimens and 12 double pullout specimens. The specimens were constructed over two phases of construction, due to spacing limitations in the Structures laboratory. All specimens were constructed with 200 mm lightweight hollow blocks placed in running bond. Companion specimens of block, mortar, grout, and reinforcement were produced and tested to ascertain the properties of these materials.

Wall splice specimens reinforced with No. 20 and No. 25 bars were constructed and tested in this study. All wall splice specimens were constructed with the lapped bars in contact but not tied together. Seven wall splice specimen configurations were evaluated. The configurations included walls that were 13 courses tall and 2.5 blocks wide, 13 courses tall and 3.5 blocks wide, and 15 courses tall and 3.5 blocks wide. Six replicates were constructed for the 2.5 block wide and 3.5 block wide configurations that were reinforced with No. 20 bars and 200 mm splices. The number of replicates for these two specific configurations was selected such that the differences in the tensile resistances of

the spliced reinforcement of these two configurations could be evaluated statistically. Three replicates were constructed for the remaining five configurations, which provided an estimate of variability for each of these configurations.

The database of experimental results of wall splice specimen testing from this program was bolstered by the inclusion of experimental results from previous research at the U of S by Sanchez & Feldman (2013) examining splice lengths for specimens reinforced with No. 15 bars. Further testing of wall splice specimens reinforced with No. 15 bars was outside of the scope of this experiment.

The wall splice specimens were tested under four-point loading, with load and displacement data collected during testing. Three splice lengths were tested for specimens reinforced with No. 20 bars, and three splice lengths were tested for specimens reinforced with No. 25 bars. Qualitative observations of flexural cracking during testing and internal damage upon the conclusion of testing were noted. The tensile resistance of the spliced reinforcement was determined using a numerical moment-curvature analysis, since the tension in the reinforcement could not be measured directly for these specimens without compromising the bond between the reinforcement and the surrounding cementitious materials.

In addition, 12 double pullout splice specimens were constructed, each with two splices that were 600 mm in length. These specimens were reinforced with No. 25 bars. The double pullout specimens were constructed with the lapped bars in contact, with six specimens having the lapped bars tied together and six specimens having the lapped bars not tied together. These specimens were tested in direct tension, with load and displacement data recorded during testing.

The effects of grout and mortar properties, block strength and density, block size, and effective depth to cover were excluded from the scope of this experiment. As such, these parameters were held as constant as practically possible for all specimens constructed during this study.

1.3 Layout of Thesis

This thesis contains five chapters, each described herein:

- **Chapter 1** presents an introduction to this thesis, including the background regarding bond research and splice length requirements for reinforced masonry, the objectives of this study, and the scope of this study.
- **Chapter 2** provides a review of relevant literature on splice length research and current requirements of the Canadian and American masonry standards. This chapter includes a description of the basic mechanics of bond in reinforced masonry, past works regarding bond in masonry, and selected findings from reinforced concrete research. The differences between the Canadian and American masonry standard splice length requirements are discussed. Finally, the rationale for the work in this study is presented.
- **Chapter 3** describes the experimental program of this study in detail, including the construction process employed and the test methods used to test all wall splice, double pullout, and companion specimens.
- **Chapter 4** discusses the results and analysis for the specimens constructed and tested in this study. The results of companion specimen testing of blocks, mortar, grout, masonry prisms, and reinforcing bar samples are discussed. The load histories and failure loads of the double pullout specimens are presented and then compared to the results of NCMA (1999, 2009) studies. The load deflection behaviour, qualitative damage observations during testing, and internal damage observations for the wall splice specimens are detailed. The numerical model used to determine the tensile resistance of the spliced reinforcement for the wall splice specimens is discussed. The regression analysis of the tensile resistances and the subsequent comparison to current code provisions are presented. Changes to current code provisions are then recommended.
- **Chapter 5** presents the conclusions in relation to the stated objectives and recommendations for further research derived from this study.

CHAPTER 2 LITERATURE REVIEW

The safety, constructability, and economy of masonry walls depend on splice and development length requirements, as aforementioned in Chapter 1. The assumption of perfect bond between the reinforcing steel and surrounding cementitious material requires a transfer of tensile stresses between the materials. Development and lap splice lengths must be sufficiently long to ensure the transfer of stresses. Researchers studying the behaviour of reinforced concrete structures have extensively examined bond and development and splice length requirements. However, relatively few research efforts have focused on development and splice length requirements for masonry, despite their importance.

Presented herein is a discussion of relevant literature related to splice length research and code requirements. A description of the basic mechanics of bond in reinforced masonry is first provided. Past works regarding bond in masonry are discussed, and selected findings related to reinforced concrete research are also presented based on their relevance in guiding future work on bond in reinforced masonry. The current provisions in the Canadian and American masonry standards are compared. Differences in research philosophies used in masonry and reinforced concrete are also discussed. The rationale for further work to refine and calibrate lap splice length provisions for reinforced masonry is presented.

2.1 Mechanics of Bond

In reinforced masonry construction, adequate bond between the reinforcement and the surrounding cementitious material is required for the tensile stresses to be transferred between them (Hatzinikolas & Korany 2005). Bond stresses acting along the length of the reinforcement provide the mechanism for force transfer. However, these bond stresses tend to cause movement of the reinforcing bar and the surrounding cementitious material relative to one another (ACI Committee 408 2012). Adequate bond between the reinforcement and the surrounding cementitious material is thus needed to prevent slip between them (Hatzinikolas & Korany 2005).

Figure 2.1(a) shows the end of a masonry wall where development of forces is required between the reinforcement of diameter d_b (a plain bar is shown for the purpose of illustration) and the surrounding cementitious material (MacGregor & Bartlett 2000). Tensile and compressive stresses result in the reinforcement and cementitious material, respectively (MacGregor & Bartlett 2000). The stresses developed must increase over the length of the reinforcement between the support and the midspan of the wall such that the yield strength of the reinforcement can be achieved and the wall can develop its full flexural capacity at the location of the maximum internal moment. Figure 2.1(b) shows a segment of the reinforcement in the development region of length Δl, where the stresses at sections 1 and 2 are f_{s1} and f_{s2}, respectively, where f_{s1} is less than f_{s2}. Bond stresses are present to maintain equilibrium, and these stresses act on the surface area of the reinforcement as shown. The average bond stress, u_{avg}, can be computed based on a summation of horizontal forces as follows:

$$(f_{s2} - f_{s1}) \cdot A_s = u_{avg}(\pi d_b)\Delta l \qquad \{2.1\}$$

where A_s is the cross-sectional area of the reinforcement. Rearranging Equation 2.1 and substituting $A_s = \frac{\pi}{4} d_b^2$, it then follows that the average bond stress, u_{avg}, is:

$$u_{avg} = \frac{(f_{s2} - f_{s1})d_b}{4\Delta l} \qquad \{2.2\}$$

Equation 2.2 provides an oversimplification of the bond stress for two reasons (MacGregor & Bartlett 2000, Pillai et al. 2008, ACI Committee 408 2012). First, the actual distribution of bond stresses is highly non-uniform, varying between flexural cracks where the cementitious material surrounding the reinforcement carries a portion of the tensile stress. The calculation of actual bond stresses is not possible since the flexural crack locations and exact tensile strength contributions of the cementitious material between these cracks are unknown. Second, deformed reinforcement provides a further mechanism for force transfer between the reinforcement and surrounding cementitious material through the mobilization of bearing forces of the lugs of the reinforcement on the surrounding cementitious material.

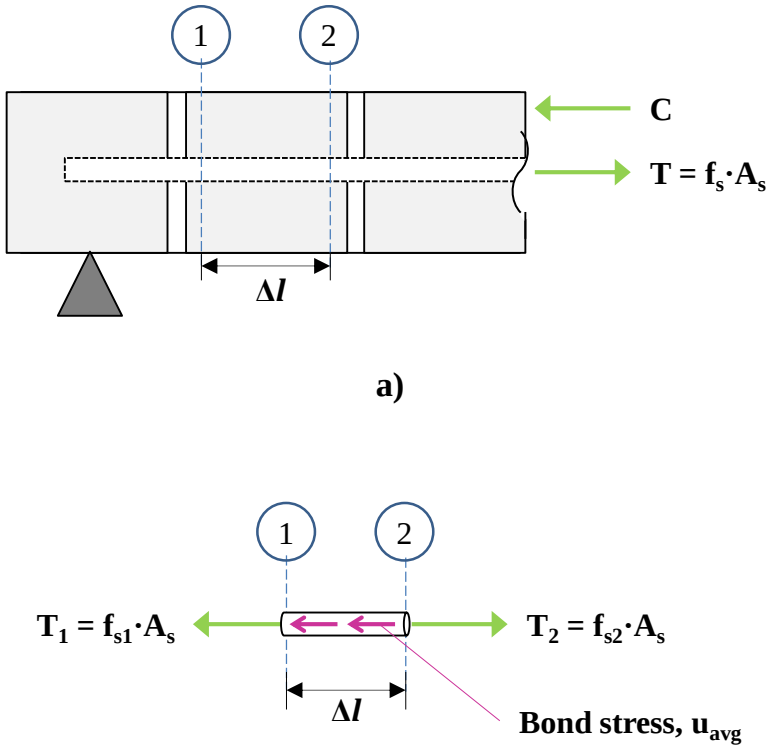

Figure 2.1. Distribution of forces and stresses along reinforcing bar segment: a) development region of a masonry element, b) bar forces (after MacGregor & Bartlett 2000)

Figure 2.2(a) shows the bearing forces exerted on a deformed reinforcing bar, which are at an angle with respect to the longitudinal axis of the bar due to the bar deformations (MacGregor & Bartlett 2000). Figure 2.2(b) shows the equal and opposite forces that are then exerted on the surrounding cementitious material. Figure 2.2(c) then shows the resolution of the forces on the concrete into longitudinal and radial components. Tensile stresses acting circumferentially on the cementitious material are caused by the radial component. These stresses will, when sufficiently large, cause the cementitious material to split and crack.

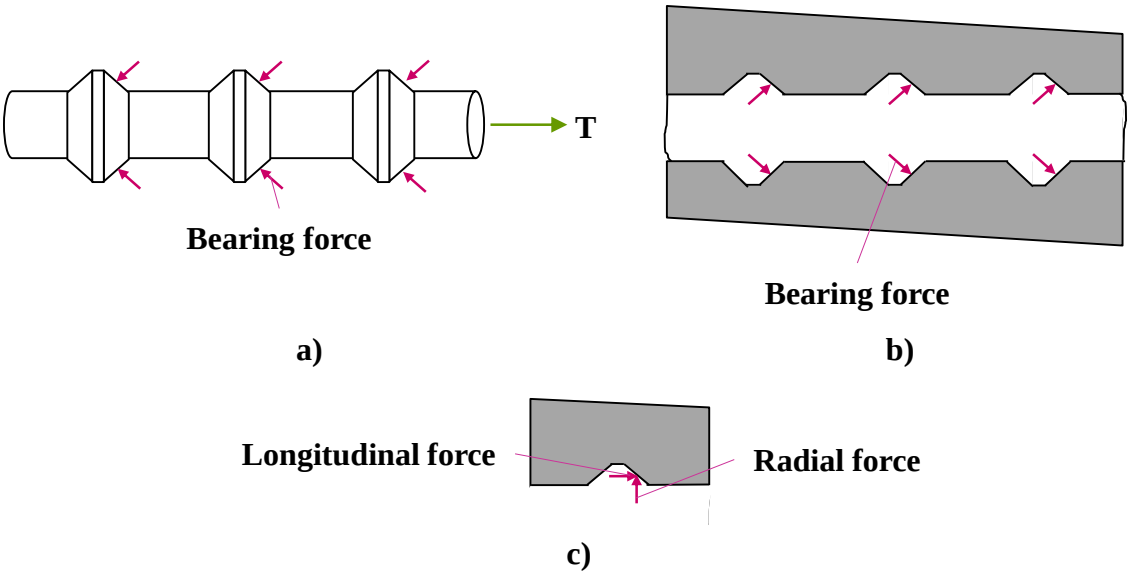

Figure 2.2. Bearing forces on deformed reinforcement: a) bar forces, b) concrete forces, and c) longitudinal and radial components of concrete forces (from MacGregor & Bartlett 2000, p. 306)

Additionally, force transfer from one reinforcing bar through the adjacent cementitious materials to a second reinforcing bar is necessary when two bars are spliced together (MacGregor & Bartlett 2000). Figure 2.3 shows the splitting cracks along the bars that occur as a result of the force transfer mechanism (MacGregor & Bartlett 2000). Splitting cracking is typically initiated at the splice ends, resulting from the change in stiffness at these locations (MacGregor & Bartlett 2000). Consequently, large transverse cracks can develop at each end of the splice.

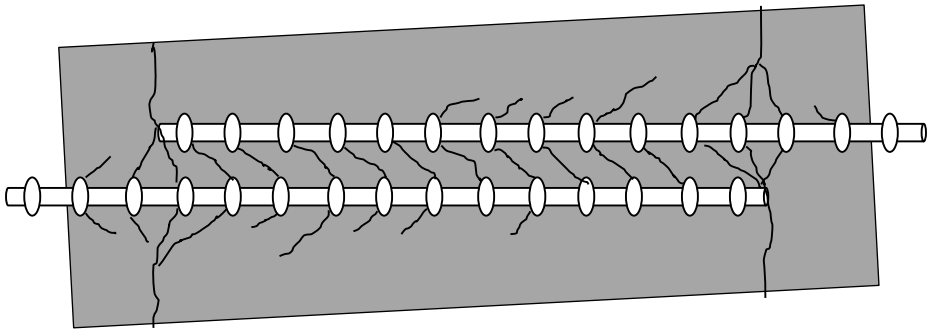

Figure 2.3. Cracking initiation in lap splices (from ACI Committee 408 2012, p.14)

2.2 Factors Affecting Bond in Cementitious Materials

There are a variety of factors that influence bond (ACI Committee 408 2012). The diameter of the reinforcing bars significantly influences bond, as larger bar sizes require longer development or splice lengths to achieve sufficient resistance to bond failure. The tensile strength of the cementitious material is also significant, and is typically reflected by the square root of the compressive strength of the cementitious material. Finally, the transverse spacing between spliced bars, if any, cementitious cover and bar spacing, bar casting position, and the presence of transverse reinforcement affect the required splice length.

Design expressions for required development and splice lengths, as included in the current Canadian and American masonry standards, have typically been empirically derived from experimental studies with an incorporation of a safety margin (discussed further in Section 2.7.2), due to the complex nature of bond in cementitious materials such as reinforced concrete and masonry (MacGregor & Bartlett 2000). Researchers conducting the experimental work from which design expressions are derived typically evaluate the tensile resistance of spliced reinforcement with variations in the structural, cementitious material, and reinforcement properties that influence bond, as described above. The resulting design expressions specify minimum required development or splice lengths as opposed to maximum bond stresses because of the highly non-uniform distribution of bond stresses, as described in Section 2.1.

2.3 Past Research Related to the Bond of Reinforcement in Masonry Construction

Most past work examining bond in reinforced masonry is based on pullout-type specimens where direct tension is applied to reinforcing bars. These specimens have historically been favoured because they are relatively easy and inexpensive to construct and relatively simple to analyze since the force applied to the spliced reinforcement is measured directly. A thorough review of all past experimental work and specimen types for bond research in masonry is provided by Ahmed (2011).

Figure 2.4 shows a double pullout specimen, which was used by the NCMA (1999, 2009) and Ahmed & Feldman (2012). Results for those specimens tested by the NCMA (1999, 2009) formed the basis of the development and lap splice length provisions in the American masonry standard, TMS 402-13 (MSJC 2013a), as discussed further in Section 2.5. These specimens minimize the effects of eccentric loads, and hence in-plane moments, by including two reinforcement splices in the panel. Double pullout specimens have shown good repeatability for contact splice specimens. Ahmed & Feldman (2012) tested eight replicates of double pullout specimens to establish the statistical significance of the results. A coefficient of variation of 2.37 percent was observed, and failure resulted due to bar pullout. Despite the aforementioned advantages, double pullout specimens still do not offer an accurate replication of the stress state experienced in the cementitious materials surrounding the reinforcement and so do not accurately capture the behaviour of walls subjected to out-of-plane flexure.

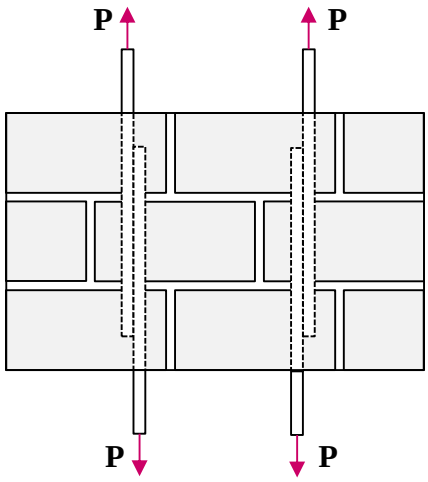

Figure 2.4. Double pullout specimen, developed by NCMA (1999, 2009) (after NCMA 1999, Ahmed 2011)

In their study, Ahmed and Feldman (2012) directly compared the capacities of wall splice and double pullout specimens. Eight replicates of each specimen type were constructed, and the wall splice and double pullout specimens were tested in four-point flexural loading and direct tension, respectively. The tensile resistance of the spliced reinforcement was determined for each specimen. They reported a statistically

significant increase in the tensile resistance of the lap-spliced bars as tested in wall splice specimens as compared to the tensile resistances of the lap-spliced bars in corresponding double pullout specimens, with increased capacities of 8.47 percent and 41.2 percent for contact and non-contact splices, respectively. The wall splice specimens reinforced with lap spliced bars in contact exhibited strain hardening of the bars while the corresponding reinforcement in the double pullout specimens failed by bar pullout at loads greater than the theoretical yield load. The higher tensile resistance of the spliced reinforcement and higher strains in the reinforcement result from the improved ductility of the wall splice specimens that cannot be evaluated using double pullout specimens.

2.4 CSA S304.1-04 Splice Provisions

The development and splice length provisions in CSA S304.1-04 (CSA 2004a) are taken directly from CSA A23.3 (CSA 2004b) with slight modifications, as discussed later in this section. Despite these modifications, many parameters unique to masonry construction, including weak bed joints, the limiting of flexural cracks to these bed joints, and reduced lever arms in members subject to flexure, are not accounted for in the masonry provisions. The aforementioned parameters likely have an effect on bond strength, thus requiring further investigation specific to masonry (Kisin 2014, Ahmed 2011, Hammons et al. 1994).

The minimum development length requirement in Clause 12.4.2.3 of CSA S304.1-04 (CSA 2004a) is:

$$l_d = 1.15 \frac{k_1 k_2 k_3}{(d_{cs} + K_{tr})} \frac{f_y}{\sqrt{f'_{gr}}} A_b \qquad \{2.3a\}$$

where k_1, k_2, and k_3 are factors for bar location, epoxy coating, and bar size, respectively (dimensionless); d_{cs} is the lesser of the distance between the reinforcing bar and the closest masonry surface and two-thirds of the distance between bars being developed in mm; K_{tr} is the transverse reinforcement index in mm; f_y is the nominal yield strength of the reinforcement in MPa; f'_{gr} is the in-situ compressive strength of the grout in MPa; and A_b is the cross-sectional area of the reinforcement in mm^2. The term $(d_{cs} + K_{tr})$ in

Equation 2.3a is limited to a maximum value of $2.5d_b$. Equation 2.3b shows the resulting equation if this maximum value is substituted into Equation 2.3a and the cross-sectional area of the reinforcement is expressed in terms of bar diameter.

$$l_d = 0.36k_1k_2k_3\frac{f_y}{\sqrt{f'_{gr}}}d_b \quad \{2.3b\}$$

Clause 12.4.2.4 of CSA S304.1-04 (CSA 2004a), presents a simplified equation applicable when the clear spacing between the lap spliced reinforcing bars exceeds two times the bar diameter:

$$l_d = 0.45k_1k_2k_3\frac{f_y}{\sqrt{f'_{gr}}}d_b \quad \{2.4\}$$

It should be noted that Equation 2.4 provides more conservative development length requirements than Equation 2.3b.

The only modifications made to these equations relative to those presented in CSA A23.3 (CSA 2004b) are the substitution of the compressive strength of the grout, f'_{gr}, for that of the concrete, f'_c, and the exclusion of an additional k factor used in CSA A23.3 (CSA 2004b) that accounts for the concrete density.

Splice length requirements in CSA S304.1-04 (CSA 2004a) depend on the calculated development length and the class of the lap splice. The required length of a Class A lap splice in CSA S304.1-04 (CSA 2004a) is equal to l_d, where a Class A lap splice is defined as one in which at least twice the required area of reinforcement is provided and no more than 50 percent of the reinforcement is spliced at a given location. A lap splice is otherwise considered a Class B splice, where the splice length must be at least 1.3 times l_d as calculated from Equation 2.3 or 2.4. In masonry wall construction, Class B splices are used almost exclusively as staggering the location of lap splices in a wall or other element is not feasible given the construction staging.

2.5 Development of TMS 402 Masonry Splice Provisions from NCMA (1999) Study

TMS 402-13 provisions (MSJC 2013a) for development and lap splice lengths were developed from the research studies conducted by the NCMA (1999, 2009). In these studies, NCMA (1999) conducted an experimental program consisting of double pullout specimens exclusively to examine splice length capacities in reinforced masonry as a function of several parameters. These parameters included bar size, splice length, cover depth, and grout compressive strength. A total of 81 double pullout splice specimens were constructed with standard 8 inch (approximately 200 mm) concrete masonry blocks. An additional 27 specimens were constructed with standard 12 inch (approximately 300 mm) concrete masonry blocks. The double pullout splice specimens were 2.5 blocks wide, with specimen heights chosen as a function of selected lap splice length such that the specimen was sufficiently long to accommodate the lap splice length. Lap splice lengths were chosen as multiples of the bar diameter, d_b, and ranged from $36d_b$ to $113d_b$. This selection of splice lengths paralleled American code provisions at that time, TMS 402-95 (MSJC 1995), which specified a development length requirement in inches as:

$$l_d = 0.002 d_b F_s \qquad \{2.5\}$$

where F_s is the allowable stress in the reinforcement in psi, specified as 24,000 psi (165 MPa) for Grade 60 (413 MPa) reinforcement (MSJC 1995).

NCMA (1999) established a database of 177 individual double pullout specimens by including the results of specimens as reported by other researchers available at that time in addition to the specimens constructed and tested in their program. A regression analysis was then performed to predict the capacity of the lap splice, T_r (lb), based on the lap splice length l_s (inches), bar diameter d_b (inches), masonry compressive strength f'_m (psi), and clear cover c_{cl} (inches):

$$T_r = -17624 + 305 l_s + 25204 d_b^2 + 322\sqrt{f'_m} + 3332 c_{cl} \qquad \{2.6\}$$

The predicted capacity of the splice, T_r, was taken as 1.25 times the force in the reinforcing bar at yield based on the nominal yield strength of the reinforcement ($A_s f_y$) and the equation was solved for the required splice length. The equation was then

simplified such that it took on the same form as that used in the Uniform Building Code (NCMA 1999). Requirements for splice lengths were set equal to the requirements for development length, l_d. The expression recommended by NCMA for development and splice length requirements, therefore became:

$$l_d = \frac{1.57 d_b^2 f_y \gamma}{K\sqrt{f'_m}} \quad (Metric) \qquad \{2.7\}$$

where γ is a bar size factor (unitless); K is the smallest of the minimum cover, clear spacing between adjacent reinforcement, and $9d_b$ (mm); and f'_m is the specified compressive strength of the masonry assembly (MPa). Clauses 8.1.6.7.1 and 9.3.3.4 of TMS 402-13 (MSJC 2013a) states that the requirements for splice lengths are equal to the development length requirements calculated in accordance with Equation 2.7.

Equation 2.7 was first adopted in the 2008 edition of the Masonry Standards Joint Committee (MSJC 2008) *Building Code Requirements for Masonry Structures* (TMS 402/ACI 530/ASCE 5) and included in all subsequent editions of this standard (MSJC 2011, MSJC 2013). Figure 2.5 shows a comparison of the requirements in TMS 402-95 (MSJC 1995) and TMS 402-13 (MSJC 2013a) graphically, for walls constructed with 200 mm blocks and Grade 400 reinforcement placed at the mid-depth of the block, without the use of transverse reinforcement. Significantly longer lap splices are required based on these new provisions for larger bar sizes. The required splice lengths for No. 6 (M#19), No. 7 (M#22), and No. 8 (M#25) bars increased by 20, 42, and 91 percent, respectively, with the adoption of Equation 2.7, as calculated for an assumed masonry compressive strength, f'_m, of 10 MPa.

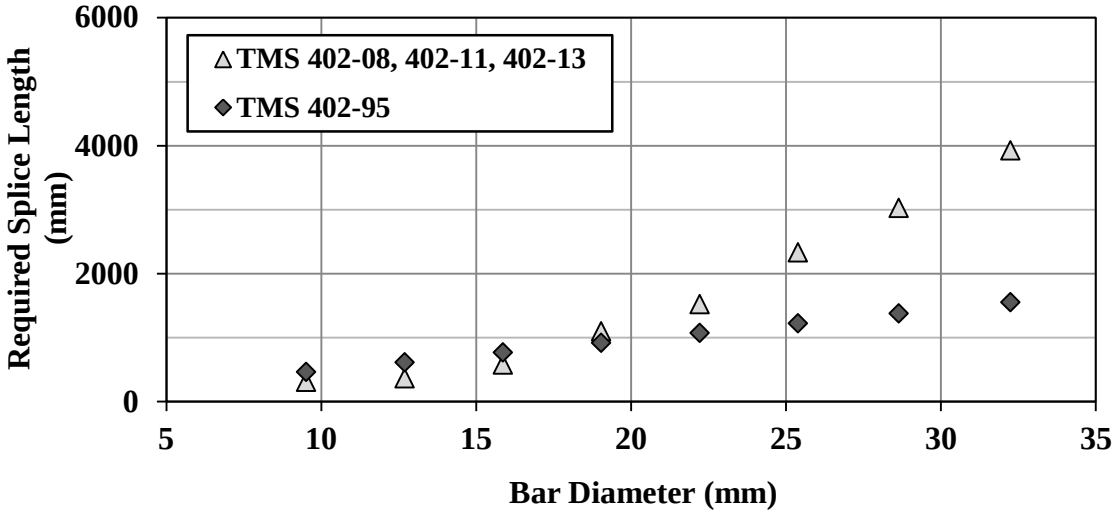

Figure 2.5. Comparison of required splice lengths in TMS 402-95 and TMS 402-13

2.6 Comparison of Provisions Presented in CSA S304.1-04 and TMS 402-13

Information presented in the previous two sections show that, in spite of the similarities in form and parameters, the splice length requirements presented in CSA S304.1-04 (CSA 2004a) and TMS 402-13 (MSJC 2013a) are substantially different. Figure 2.6 highlights these differences in a quantifiable manner and shows the required splice lengths as calculated using provisions in the two codes, presented in Equations 2.3b and 2.7, versus nominal bar diameter. The values shown in Figure 2.6 were calculated assuming that no transverse reinforcement was provided. Splice lengths were calculated for specimens with 200 mm wide blocks and Grade 400 reinforcement. Calculations were made assuming that the reinforcement was placed at the centre of the block, thus providing an effective depth of 95 mm. Therefore, the term $(d_{cs} + K_{tr})$ in the CSA S304.1-04 provisions presented in Equation 2.3a was set equal to its maximum value of $2.5d_b$, and Equation 2.3b was thus used. The in-situ compressive strength of grout was assumed to be 20 MPa, based on the typical in-situ grout strengths noted by Drysdale & Hamid (2005) and Hatzinikolas & Korany (2005). A corresponding specified compressive strength of the masonry assembly equal to 10 MPa was assumed based on the assumed f'_m value provided in TMS 602-13 (TMS 2013b). Both k_1 and k_2 were set equal to 1.0, and the bar size factors were used as prescribed in CSA S304.1-04 (CSA 2004a) and TMS 402-13 (MSJC 2013a).

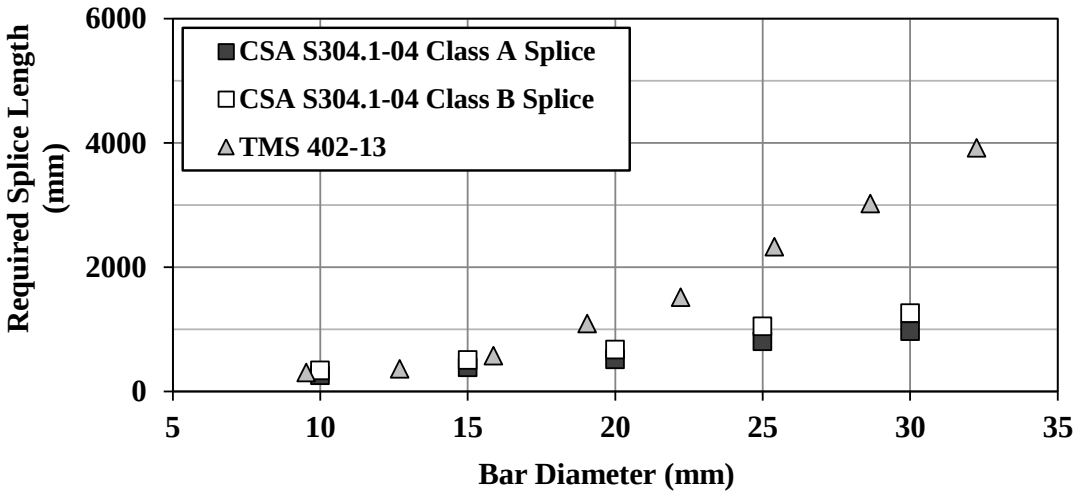

Figure 2.6: Splice requirements calculated from CSA S304.1-04 and TMS 402-13 provisions

Figure 2.6 shows that the splice length requirements of TMS 402-13 are greater than the requirements of CSA S304.1-04, particularly for large bar sizes. CSA S304.1-04 (CSA 2004a) requires 672 mm and 1049 mm splice lengths for No. 20 and 25 bars in Class B splices, which are used most often in masonry construction. TMS 402-13 (MSJC 2013a) requires splice lengths of 1093 mm and 2329 mm for No. 6 (M#19) and No. 8 (M#25) bars, respectively. Splice lengths shorter than 300 mm (12 inches) are not permitted for any bar size using either standard.

There are three key differences between the Canadian and American masonry standard provisions that each contribute to the differences seen in the splice length requirements of the two standards for larger bar sizes. These three differences are discussed herein.

The first noteworthy difference between the Canadian and American masonry standard provisions is the property used to reflect the compressive strength of the masonry assembly. The compressive strength of the grout, f'_{gr}, is used in CSA S304.1-04 (CSA 2004a). Suter and Fenton (1985) observed that minimum lap splice lengths calculated from CSA provisions at the time using f'_{gr} agreed more closely with their experimental results than splice lengths calculated using f'_m. TMS 402-13 (MSJC 2013a) instead uses the compressive strength of the masonry assembly, f'_m. NCMA (2009) chose the masonry assembly compressive strength for inclusion in their prediction and design

equations because they asserted that it better reflects of the composite action between the masonry block and grout.

Recent experimental results underscore the effect of poor bond between the masonry blocks and grout on splice performance and the relevance of using f'_m to represent the strength of the masonry assemblage, especially for the case when non-contact lap splices have been provided with the lap spliced bars located in adjacent cells (Ahmed & Feldman 2012). The poor bond between the masonry block and the grout due to grout shrinkage prevented the development of diagonal compressive struts. These compressive struts are required to develop an internal moment resistance sufficient to carry the applied external in-plane moment created by the lapped reinforcing bars. Failure of these specimens by masonry splitting, prior to the yielding of the reinforcement, therefore resulted.

The second noteworthy difference between the Canadian and American masonry code provisions is their respective dimensional coefficients for the equations used to calculate lap splice length requirements. The TMS 402-13 (MSJC 2013a) equation for development length in Metric units, as presented in Equation 2.7, simplifies as follows if the minimum cover is at least 2 d_b, as required in CSA S304.1-04 (CSA 2004a):

$$l_d = \frac{0.79 d_b f_y \gamma}{\sqrt{f'_m}} \quad (metric) \quad [mm] \qquad \{2.8\}$$

The dimensional coefficient in Equation 2.8 of 0.79 is then adjusted to reflect the differences between the compressive strength of the masonry assemblage and the compressive strength of the grout. The ratio of f'_m to f'_{gr} was calculated based on experimental data of the relationship between grout compressive strengths and resulting masonry compressive strengths for grout strengths ranging from 10 MPa to 40 MPa (Drysdale & Hamid 2004, Ahmed 2011). The resulting ratios of f'_m to f'_{gr} ranged from 0.9 to 0.4, and applying these ratios to Equation 2.8 results in the dimensional coefficient ranging from 0.85 to 1.23 in place of the 0.79 shown. The resulting range for the coefficient is noticeably greater than the coefficients of 0.36 and 0.47 for Class A and B splices, respectively, used in the CSA S304.1-04 (CSA 2004a) provisions presented in

Equation 2.3b. The difference in these coefficients contributes to the differences between the splice length requirements calculated for each standard.

The third significant difference between CSA S304.1-04 (CSA 2004a) and TMS 402-13 (MSJC 2013a) provisions is their respective bar size factors. The bar size factor k_3 in CSA S304.1-04 (CSA 2004a), set equal to 0.8 for No. 20 bars and smaller and 1.0 for bars larger than No. 20, is taken directly from CSA A23.3-04 (CSA 2004b). The CSA A23.3-04 provisions (CSA 2004b) for bond are nearly identical to those presented in ACI 318-11 (ACI 2011). Further work has identified concerns with the use of these bar size factors.

In their review of ACI 318 bond provisions, ACI Committee 408 (2012) noted the reduced bar size factor of 0.8 for No. 20 and smaller bars is potentially unconservative. ACI Committee 408 (2012) reports that ACI Committee 318 justified the reduced bar size factor for smaller bar sizes included in current provisions based on past code provisions and experimental results. However, this factor was derived based on the results of testing specimens with development or splice lengths less than 300 mm, shorter than permitted by Canadian and American concrete and masonry standards. Darwin (2005) reported that the inclusion of the 0.8 bar size factor results in a greater probability of failure in bond than in flexure. Furthermore, Scollard and Bartlett (2004) conducted a Monte Carlo simulation of model-simulated reinforced concrete beams to establish the resulting target reliability indices in flexure and bond based on provisions in the 1999 and 2002 editions of ACI 318. It was determined that the target reliability indices calculated for bond had more scatter than those obtained for flexure, and showed that bond failures were more likely to occur than flexural failures for beams reinforced with the smaller diameter bars that are subject to the 0.8 bar size factor (i.e. No. 20 bars and smaller). The simulation was repeated using a bar size factor of 0.85, and showed that the change in the resulting development lengths would increase the resulting target reliability index in bond sufficiently to ensure that a flexural failure would then govern. ACI Committee 408 (2012) recommended changes to current ACI 318-11 provisions, but no changes have been incorporated to date. These findings regarding the impact of the bar size factors on

target reliability indices in bond for reinforced concrete are relevant for the CSA S304.1-04 (CSA 2004a) provisions since these bar size factors were copied directly.

In contrast, the bar size factor γ in TMS 402-13 (MSJC 2013a) is set equal to 1.0 for No. 3 (M#10) to No. 5 (M#16) bars, 1.3 for No. 6 (M#19) to No. 7 (M#22) bars, and 1.5 for No. 8 (M#25) to No. 11 (M#36) bars. Instead of reducing required splice lengths for smaller bars, the required splice lengths for larger bars are increased to prevent the longitudinal splitting failure modes observed by NCMA (1999) for specimens with larger bar sizes. The bar size factors contribute to the longer splice requirements in TMS 402-13 (MSJC 2013a) as compared to CSA S304.1-04 (CSA 2004a).

The class factor for lap splices used in CSA S304.1-04 (CSA 2004a) provisions increases splice lengths by 30 percent for Class B splices. ACI Committee 408 (2012) stated this factor increases the target reliability index in bond for the resulting designs such that a flexural failure would then govern. However, the purpose of including the Class B splice factor was not primarily based on probabilities of bond failure. Rather, Darwin (2005) stated that the factor was incorporated into design provisions to encourage designers to stagger lap splices. A specific basis for the magnitude of the increase was not identified in the literature reviewed. As aforementioned, the staggering of lap splices is not practical or economical for masonry construction.

2.7 Comparison of Philosophies Used by Masonry and Concrete Researchers

A resolution of the differences between the approaches taken by researchers studying the behaviour of reinforced masonry and concrete, in terms of the specimen type used and the desired failure loads of test specimens, is needed. Resolving these differences will lead to a rationalization of the differences between the Canadian masonry code provisions (CSA 2004a), taken directly from the Canadian concrete code (CSA 2004b), and American masonry code provisions (MSJC 2013a), derived from experimental pullout specimen results, as presented in Section 2.6.

Recent reinforced concrete research has been based on the testing of beam end and splice specimens that better capture the stress state in the concrete surrounding the

reinforcement, as compared to pullout-type specimens (ACI Committee 408 2012, Pillai et al. 2008, MacGregor & Bartlett 2000). The ACI 10-2001 database, formally established in 1997, contains these test results exclusively, and has been used for the calibration of ACI 318 code provisions for development and lap splices (ACI Committee 408 2012). In contrast, a standard specimen type for masonry bond research has not yet been established. Only a select number of studies (Kisin & Feldman 2013, Sanchez & Feldman 2013, Ahmed & Feldman 2012, Ahmadi 2001, Uniat 1983) have included flexural masonry elements, so there is currently insufficient reliable data resulting from those specimen types from which splice length provisions can be established.

In addition, the research used to establish and calibrate TMS 402-13 (MSJC 2013a) provisions is based on double pullout specimens with tensile resistances of the spliced reinforcement well in excess of the yield strength of the reinforcement. NCMA's regression analysis (1999) included tests of double pullout specimens with lap splice lengths that were generally $48d_b$ at minimum. Consequently, the specimens that remained in the test database for the regression analysis used to establish the TMS 402-13 (MSJC 2013a) provisions generally achieved tensile resistances exceeding the yield strength of the reinforcement.

The approach taken by researchers studying the behaviour of reinforced concrete contrasts the approach taken by NCMA (1999, 2009) in that they have typically tested specimens with shorter lap splice lengths such that a bond failure occurred prior to yielding of the reinforcement (Darwin et al. 1996, Canbay & Frosch 2006, Orangun et al. 1977). Since the purpose of their study was to evaluate bond strength rather than ductility, Orangun et al. (1977) excluded specimens from their analysis in which the reinforcement reached its yield strength prior to failure. This study is significant because it forms the basis of provisions in ACI 318-11 (ACI 2011) and CSA A23.3 (CSA 2004b). Testing specimens that fail in bond allows for a determination of the relationship between splice length and the tensile resistance of spliced reinforcement, since these parameters are known to vary in a linear but non-proportional manner when the forces in the reinforcement are below those corresponding to yield (ACI Committee 408 2012). Further increases in splice length beyond those sufficiently long for the development of

the reinforcement yield strength will not result in proportional increases in tensile resistances due to the strain hardening behaviour of the reinforcement.

2.7.1 Resolution of Specimen Type and Failure Modes for Bond Research

Hammons et al. (1994) identified four primary failure modes that have been observed during investigations of lap splices in reinforced masonry:

1. Reinforcement yielding,
2. Reinforcement pullout,
3. Reinforcement rupture, and
4. Masonry longitudinal splitting.

Hammons et al. (1994) noted that splitting failures are most probable when limited cover, large bar sizes, or inadequate splice lengths are used. Hammons et al. (1994) also stated that reinforcement yielding is the preferred failure mode for design since it provides both the most efficient use of the reinforcement and sufficient ductility. A flexural failure will occur in masonry elements provided that the lap splice is sufficiently long.

NCMA (1999, 2009) observed the latter three failure modes in their experimental work. NCMA (1999) observed a handful of specimens that failed by rupture of the reinforcement with a stress ranging from 1.56 to 1.69 times its nominal yield strength. Achieving stresses well in excess of the yield strength of the reinforcement can only be expected to occur in double splice pullout tests. In elements such as concrete beams or masonry walls, a flexural failure is dependent on both the compressive strength and limited tensile strength of the concrete or masonry. Specimen failure would therefore occur in flexure prior to rupture of the reinforcement. As such, this failure mode would not be observed in the testing of flexural specimens such as wall splice specimens.

NCMA stated in their subsequent 2009 study that the new bond provisions first incorporated in TMS 402-08 (MSJC 2008) specifically consider the longitudinal splitting failure mode for lap splices and the potential for reinforcement pullout failure. Data from specimens that failed by longitudinal splitting was used exclusively for the calibration of these design provisions. However, the majority of these specimens achieved capacities

exceeding the yield strength of the reinforcement, with the target splice capacity set equal to 1.25 times the yield strength of the reinforcement. Regardless of the failure mode, the splice capacity observed in the testing of these double pullout specimens is likely conservative if compared to the splice capacity that would be observed in comparable wall splice specimens, given the results of Ahmed & Feldman's work (2012). The choice of using double pullout test specimens is the most probable reason for the increased splice length requirements first presented in TMS 402-08 (MSJC 2008).

Failure in bond occurs without warning, making bond failure an undesirable limit state. The probability of a bond failure should therefore be less than the probability of a flexural failure (ACI Committee 408 2012). However, for the purpose of designing an effective experimental investigation with the aim of rationalizing design provisions for the development and lap splice length of reinforcement, specimens must be designed to fail in bond prior to the yielding of the reinforcement.

2.7.2 Development of Design Expressions for Splice Length Requirements

As discussed in Section 2.7, researchers studying the behaviour of reinforced concrete have typically tested specimens with shorter lap splice lengths designed to fail in bond prior to yielding of the reinforcement such that the relationship between splice length and splice capacity could be determined. Consequently, various methods have been used to determine predictive equations for splice capacity, from which design expressions were then developed. Design expressions for splice length requirements must ensure that the full yield strength of the reinforcement can be achieved along the splice length with a certain level of reliability. Empirical equations derived from experimental data are the basis for predictive and design equations since the complexity of bond behaviour prevents the use of first principles to develop such expressions.

Regression analysis is typically used to derive a predictive equation for the tensile resistance of spliced reinforcement as a function of the parameters of interest in each study, including lap splice length, bar diameter, clear cover, or other parameters considered by the researchers. The predictive equations for splice capacity are typically then solved for the splice length by setting a target splice capacity corresponding to the

nominal yield strength of the reinforcement, equal to $A_s f_y$, such that required splice lengths can be calculated for given parameters (e.g. Darwin et al. 1996).

Predictive equations developed from regression analyses cannot be used directly for design expressions, however, as they reflect average best-fit values (Darwin et al. 1996). Approximately half of all structural elements with spliced reinforcement would have capacities that are less than the best-fit value if the predictive equations were used directly.

Researchers studying reinforced concrete have used various methods to provide a margin of safety. Canbay & Frosch (2006) applied a factor of safety of 1.2 to shift their experimental curves derived from tests of concrete beams, such that only 10 percent of their specimens (with no transverse reinforcement) would contain spliced reinforcement without sufficient tensile resistance to achieve the yield strength of the reinforcement. However, the use of a nominal value of the factor of safety does not consider any statistical measures associated with experimental data. Darwin et al. (1996) applied a strength reduction factor of 0.9 to their predictive equation relating the tensile resistance of a splice to the splice length, bar diameter, and other factors. The tensile resistance in this expression was divided by the strength reduction factor. The factor of 0.9 was chosen such that the resulting reliability index in bond was equal to 3.5 and thus a bond failure was approximately one-fifth as probable as a flexural failure. Hosney et al. (2012) reduced the constant of their equation by one standard deviation to provide a greater factor of safety. Chun et al. (2011) used a five percent fractile approach in determining design expressions for compression lap splices in concrete. The five percent fractile value was calculated based on the coefficient of variation and number of observations in the data set, and was then used to provide a margin of safety. Chun et al. (2011) calculated a five percent fractile value of 0.82 for their data. The tensile resistance term in their predictive equation was divided by the five percent fractile to incorporate a margin of safety. These methods all adjust predictive equations to incorporate a level of safety such that they can be used for design purposes. The splice lengths corresponding to the yield strength of the reinforcement can then be calculated using the adjusted predictive equation, extrapolating beyond the range of the data set.

In contrast, the NCMA (1999, 2009) targeted a splice capacity stress equal to 1.25 times the yield strength of the reinforcement, as discussed in Section 2.4. Orangun et al. (1977) noted in their seminal work on bond in reinforced concrete that such an increase in the target capacity proportionately increased the required splice lengths. This increase does not directly consider the stress-strain behaviour of the steel reinforcement, as the strain hardening in the reinforcement when loaded beyond the yield point results in a non-proportional increase of stress with strain. Instead, Orangun et al. (1977) recommended a capacity reduction factor be applied to the calculated development length, as this factor would account for variances in material and geometric properties of concrete members. Further, a change to the splice length provisions in ACI 318-11 (ACI 2011) has been recommended by ACI Committee 408 (2012), which would incorporate a strength reduction factor to provide a reliability index of 3.5 and thus ensure a bond failure is approximately one fifth as probable as a flexural failure.

A strength reduction factor applied to a splice length calculated using the nominal yield strength of the reinforcement would be a more logical approach for bond provisions in reinforced masonry as it would be consistent with the limit states design methodology already used in CSA S304.1-04 (CSA 2004a). A probability-based approach could be used to reliably establish this strength reduction factor for masonry, if a database of test results with a standardized and representative specimen type is created.

2.8 Lap Splice Length Selection

As discussed in Section 2.7, the choice of lap splice lengths shorter than those resulting in the yielding of the reinforcement in experimental specimens tested in flexure is important to determine the relationship between splice lengths and splice capacity. As such, a discussion of the findings of previous researchers in terms of splice lengths selected, predictive equations derived, and design recommendations provided is presented herein.

Masonry researchers have provided recommendations in terms of development length. Baynit (1980) provided expressions for splice length based on the bar diameter. Without a strength reduction factor, Baynit's expression results in splice lengths of 720 mm and 1100 mm for No. 20 and No. 25 bars respectively. Uniat (1984) recommended a 425 mm

design splice length for No. 20 bars, citing code provisions at the time as overly conservative. Based on Uniat's results (1984), Suter & Fenton (1985) recommended a slightly more conservative splice length value of 500 mm for No. 20 bars. Watanabe (1985) reported that for No. 6 (M#19) bars, a splice length of $14d_b$ (266 mm) was sufficient to develop the yield strength in the reinforcement.

Table 2.1 presents selected results of double pullout splice specimens from NCMA's 1999 and 2009 studies. Shown are results for specimens reinforced with imperial bar sizes No. 6 (M#19) and No. 8 (M#25), as they provide the closest comparison for metric No. 20 and No. 25 bars experimentally evaluated in this study. The values shown in Table 2.1 are the averages of three replicates of each specimen configuration listed. The samples constructed with No. 8 bars with 813 mm lap splices had an average splice capacity equal to 1.06 times the yield strength of the reinforcement, while the specimens constructed with No. 8 bars with 610 mm lap splices had an average splice capacity equal to 0.69 times the yield strength of the bars, given masonry prism compressive strengths and grout compressive strengths of 22.0 MPa and 20.1 MPa, respectively. The tensile resistance of the spliced reinforcement in the specimen constructed with 610 mm splice length is less than that corresponding to the yield strength of the reinforcement, indicating that a bond failure occurred prior to yielding of the reinforcement.

Table 2.1. Selected Results from NCMA (1999, 2009) Studies

Study	Reinforcement Size	Lap Splice Length (mm)	Masonry Compressive Strength (MPa)	Ratio of Splice Tensile Resistance to Reinforcement Yield Strength[1]
NCMA 1999	No. 6 (M#19)	915 mm	11.7	1.15
	No. 8 (M#25)	1219 mm	11.7	0.81
		1626 mm	11.7	1.09
NCMA 2009	No. 6 (M#19)	915 mm	15.0	1.45
	No. 8 (M#25)	610 mm	22.0	0.69
		813 mm	22.0	1.06
		1016 mm	22.0	1.25
		1219 mm	22.0	1.35

[1]Values reported are the average of three replicate specimens of each configuration.

Results from previous and ongoing research at the U of S using specimens reinforced with No. 15 reinforcement were also reviewed in determining the splice lengths to select for this investigation. Ahmed & Feldman (2012) used 300 mm lap splices for wall splice and double pullout splice specimens and observed all specimens of both types with lap spliced bars in contact developed the yield strength of the reinforcement. Sanchez & Feldman (2013) tested contact lap splices with 150 mm, 200 mm, and 250 mm lengths in wall splice specimens. The specimens with 150 mm and 200 mm contact lap splices consistently failed in bond without yielding of the reinforcement, while the specimens with 250 mm splice lengths did not consistently fail in bond.

The predictive equation developed by NCMA (1999), as presented previously in Equation 2.6, indicates that splice lengths of 505 mm and 1450 mm for No. 20 and No. 25 bars, respectively, will result in the development of the yield strength for the specimens to be used in this research. As such, all specimens in this study have been designed with lesser values of lap splice length, as discussed in detail in Section 3.2.

2.9 Summary

This chapter presented a review of literature related to development and splice length research in masonry. Splice length requirements in CSA S304.1-04 (CSA 2004a) do not account for parameters unique to masonry construction since these provisions are taken directly from CSA A23.3 (CSA 2004b). Double pullout specimens, as were used to calibrate TMS 402-13 (MSJC 2013a), do not replicate the stress state in the cementitious material surrounding the reinforcement as would occur in masonry walls subject to out-of-plane loads. As such, a re-evaluation of current Canadian and American development and splice length based on experimental testing of wall splice specimens in flexure is needed.

Flexural wall splice specimens are recommended as the specimen type for all future research, including the experimental work of this study, since these specimens are able to capture the stress state in the cementitious materials surrounding the reinforcement. Tests to establish and calibrate code provisions for masonry should be conducted with specimens designed to fail in bond (as indicated by bar pullout or longitudinal masonry

splitting) prior to reinforcement yielding. The relationship between splice length and splice capacity should be examined using the empirical methods employed by researchers studying the behaviour of reinforced concrete. Researchers studying reinforced concrete have typically developed prediction equations for splice capacity and then established design expressions by incorporating a margin of safety. These methods have been applied in the experimental design for this study, as is discussed further in Chapter 3.

CHAPTER 3 EXPERIMENTAL DESIGN, CONSTRUCTION, AND TESTING

A large scale experimental program was conducted to address the deficiencies in reinforced masonry bond and development length research as identified in Chapter 2. Achieving the objective of evaluating lap splice length requirements involved the construction of multiple wall splice specimens, tested horizontally under four-point loading, along with selected double pullout specimens for comparison, tested in direct tension.

Table 3.1 details the experimental design, including the bar sizes, specimen dimensions, splice lengths, and number of replicates selected. No. 20 and 25 reinforcing bars were tested in this study, with the database for this research bolstered by the inclusion of data for No. 15 bars from previous research at the University of Saskatchewan (U of S) (Sanchez & Feldman 2013). Three splice lengths for each bar size were tested. The effect of an increase in specimen width was explored with the samples constructed with No. 20 bars and 200 mm splice lengths, since the specimens reinforced with No. 25 bars were constructed with an increased width, as discussed further in Section 3.1.1. The construction and testing of these specimens occurred over two phases, due to space constraints in the laboratory.

Table 3.1. Experimental Design

Specimen Type	Bar Size [mm]	Specimen Width [blocks]	Specimen Height [Courses]	Lap Splice Length [mm]	Number of Replicates
Wall Splice	No. 20	2.5	13	200 [b]	6
		3.5	13	200 [b]	6
		2.5	13	250 [b]	3
		2.5	13	350 [b]	3
	No. 25	3.5	15	400 [b]	3
		3.5	15	600 [b]	3
		3.5	15	800 [b]	3
Double Pullout	No. 25	2.5	4	600[a]	6
		2.5	4	600[b]	6

[a]With lapped bars tied together, as discussed in Section 3.1.2.
[b]With lapped bars remaining untied, as discussed in Section 3.1.1 and 3.1.2.

Double pullout specimens reinforced with No. 25 bars and 600 mm tied and untied lap splices were tested as a point of comparison with the results obtained by the NCMA (1999, 2009). Three replicates of all but two specimen configurations were constructed to provide a reasonable estimate of variability. Six replicates for all double pullout specimens and the two widths of wall splice specimens reinforced with No. 20 bars spliced with 200 mm lap splices were constructed to allow for a statistical analysis of these test results.

3.1 Specimen Descriptions

Both wall splice and double pullout specimens were constructed in running bond by an experienced mason, with two spliced reinforcing bars placed symmetrically to minimize in-plane eccentricities. All cells in all specimens were fully grouted, to simplify all subsequent analysis. Wall splice specimens were constructed with widths of 2.5 and 3.5 blocks and were either 13 or 15 courses tall. Double pullout specimens were 2.5 blocks wide and 4 courses tall. Provided herein is a description of both specimen types and their geometries.

3.1.1 Wall Splice Specimens

Figure 3.1 shows the elevations of the 13 course high by 3.5 block (Figure 3.1 (a)) and 2.5 block (Figure 3.1 (b)) wide walls specimens reinforced with No. 20 bars. Similarly, Figure 3.2 shows the elevations of the 15 course high and 3.5 block wide walls reinforced with No. 25 bars. The 13 course height was adequate for the specimens reinforced with No. 20 bars since the required development length calculated in accordance with CSA S304.1-04 (CSA 2004a) was provided for the reinforcement between the end anchorage and the splice region. Also, this specimen height was consistent with previous masonry bond research conducted at the U of S (Ahmed & Feldman 2012, Sanchez & Feldman 2013, Kisin & Feldman 2013). The height was increased to 15 courses for the specimens reinforced with No. 25 bars to provide a longer development length for the reinforcement between the end anchorage and the splice region. This specimen height was the longest length for which the moment created by the self-weight of the wall would not exceed the theoretical cracking moment, as calculated in accordance with Clause 10.14 of CSA

S304.1-04 (CSA 2004a). This ensured cracking in the specimen did not occur when the specimen was rotated from its vertical construction position to its horizontal testing position.

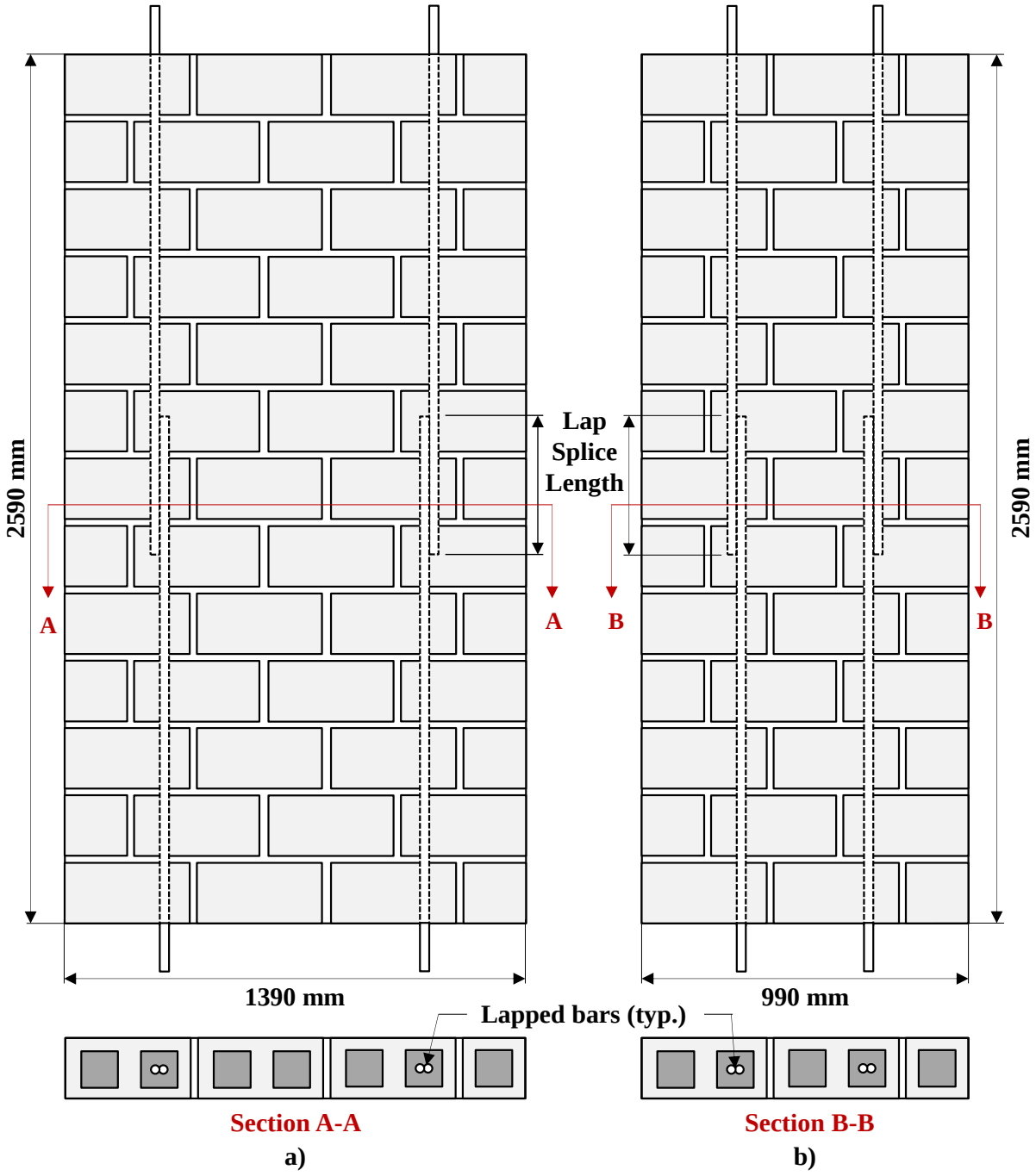

Figure 3.1. Wall splice specimens with spliced No. 20 reinforcement: a) 3.5 blocks wide, and b) 2.5 blocks wide

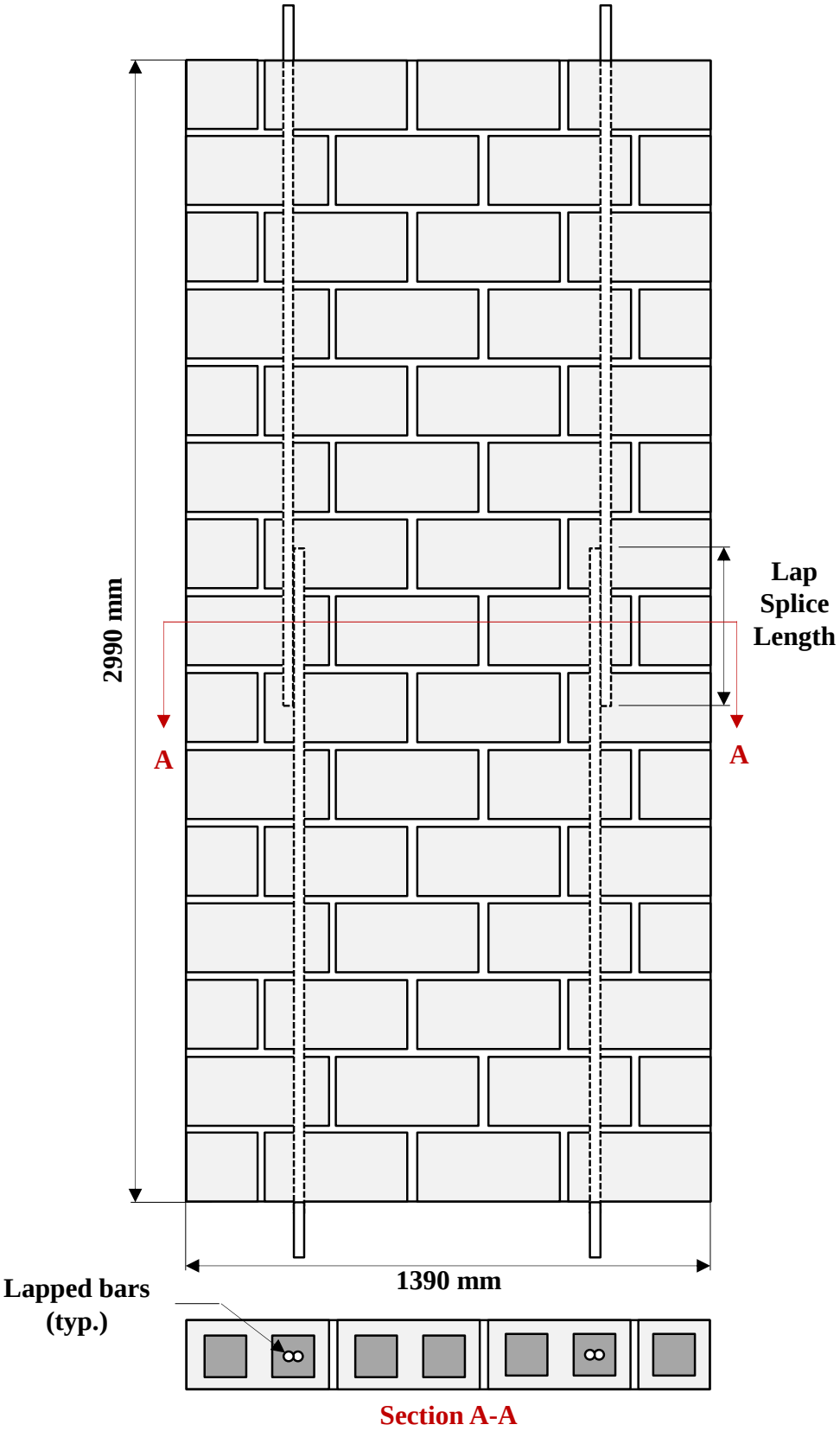

Figure 3.2. Wall splice specimens with spliced No. 25 reinforcement

The 2.5 block wide specimens with No. 20 bars were under-reinforced in flexure when checked in accordance with the provisions of CSA S304.1-04 (CSA 2004a). However, the same specimen width reinforced with No. 25 bars resulted in an over-reinforced section, with grout and masonry crushing anticipated prior to yielding of the reinforcement. This flexural failure mode was undesirable due to the difficulty of differentiating it from a bond failure as both result in crushing in the cementitious materials surrounding the reinforcement. Consequently, the width for specimens reinforced with No. 25 bars was increased to 3.5 blocks. It was expected that this increase in width would not significantly impact comparisons of results for the two bar sizes. Nonetheless, a comparison of two specimen widths with the same splice configuration was included to ascertain the validity of this assumption. Specimens reinforced with No. 20 bars and 200 mm splice lengths that were 3.5 blocks wide were built and tested as the means to make this comparison.

The shear resistance of all wall splice specimens was calculated in accordance with Clause 10.10 of CSA S304.1-04 (CSA 2004a), and was determined to be adequate assuming yielding of the reinforcement is attained. Therefore, no transverse reinforcement was provided.

Figures 3.1 and 3.2 also show the placement of the spliced reinforcement. All wall splice specimens were constructed with the lapped reinforcing bars placed in contact but not tied together, as is typical of local construction practices. Reinforcing bars were placed one cell in from the side faces for all specimens. Within the cell, the reinforcement was placed in the centre of the common 84 mm grout width between two vertically adjacent blocks. The reinforcement was placed mid-depth within the block such that the effective depth of the reinforcement was 95 mm for all specimens. The reinforcement extended beyond each end of the specimens by 190 mm to accommodate mechanical couplers applied prior to testing. These mechanical couplers provided additional anchorage for the reinforcement at the ends of the specimen and so ensured that failure occurred within the lap splice length during testing.

3.1.2 Double Pullout Specimens

Figure 3.3 shows the elevation of the 2.5 block wide double pullout specimens. The cross-sectional geometry of these specimens is consistent with specimens tested by the NCMA (1999, 2009) and Ahmed & Feldman (2012). The motivation for constructing and testing double pullout specimens in this program was to compare these results to those obtained by the NCMA (1999, 2009). Double pullout specimens were constructed with No. 25 bars only, as this bar size is the best point of comparison to the Imperial bar sizes used in the NCMA studies (1999, 2009). Specimens were four courses high, thus accommodating the 600 mm lap splice length. Six double pullout specimens were constructed with the lapped reinforcing bars tied together, such that true contact lap splices resulted. The other six double pullout specimens were constructed with the lapped reinforcing bars placed in contact but not tied together, as is typical of local construction practices. Plastic sheaths were used to debond the excess length of reinforcement beyond the splice region within the specimen. The reinforcement extended beyond each end of the specimen for anchoring to the test frame, as described in Section 3.6.2.

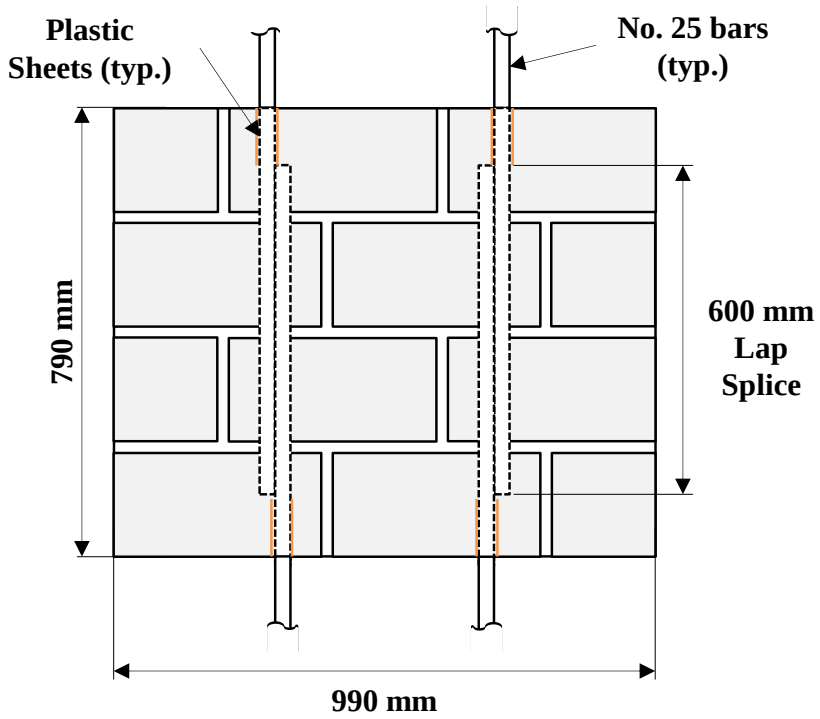

Figure 3.3. Double pullout specimen with 600 mm splice length

3.1.3 Abbreviated Specimen Designations

All wall splice specimens and double pullout specimens were assigned abbreviations to indicate the specimen type, splice length, bar size, specimen width, and replicate number. Wall splice specimen designations, which begin with W to indicate their specimen type, are of the form W*xxx*(No.*yy*)-*z.z*-*n*, where *xxx* denotes the lap splice length in mm, *yy* denotes the nominal bar size in mm, *z.z* denotes the specimen width in blocks (2.5 or 3.5), and *n* denotes the replicate number. Double pullout specimen designations begin with DP to indicate their specimen type. Designations for the double pullout specimens with the lap spliced bars tied together are of the form DP-T-*n* and double pullout specimens for which the lap spliced bars were not tied together have designations of the form DP-NT-*n*, where *n* denotes the replicate number.

3.2 Splice Length Selection

The various splice lengths used in the specimens were selected after careful consideration of previous studies, as presented in Section 2.8. The splice lengths for this research were chosen such that bond failures would be achieved in all specimens.

Three splice lengths per bar size were selected for the wall splice specimens to provide a sufficient range from which to develop expressions through regression analysis relating splice length and bar size to tensile resistance. Splice lengths of 200 mm, 250 mm, and 350 mm were selected for specimens constructed with No. 20 bars. These splice lengths were selected based on the results of previous work by Sanchez & Feldman (2013), as presented in Section 2.8. Splice lengths of 400 mm, 600 mm, and 800 mm were selected for specimens constructed with No. 25 bars. The largest splice length was selected based on the results of NCMA's studies (1999, 2009), as presented in Table 2.1.

One splice length was selected for all double pullout specimens, since the main purpose of the double pullout specimens was to offer a point of comparison to the results of the NCMA (1999, 2009); producing six replicates of an individual configuration was important to allow for statistical analysis of the resulting splice capacities. A splice length of 600 mm was chosen for the double pullout specimens, as it offers a close comparison to the 24 inch (610 mm) lap splices tested by the NCMA in their 2009 study,

which failed in bond prior to the forces on the bars reaching forces corresponding to the yielding of the reinforcement.

3.3 Selection of Number of Replicate Specimens

Three replicates of all specimen configurations were constructed, with the exception of the two double pullout specimen configurations and W200(No.20)-2.5 and W200(No.20)-3.5 configurations. The construction and testing of three replicate specimens matched that used in the NCMA testing programs (1999, 2009) and provided an indication of variability.

A statistical analysis of results was desired for specific specimen configurations, which necessitated the construction and testing of more replicates of these specimen configurations. As such, six replicates of the W200(No.20)-2.5 and W200(No.20)-3.5 configurations and each double pullout specimen configuration were constructed and tested to determine whether the resulting mean tensile resistance of the reinforcement was statistically different between the two specimen widths and two double pullout specimen configurations. Using six replicate specimens also allowed for the identification of statistical outliers, as outlined in ASTM E178 (ASTM 2012a).

3.4 Materials

Materials for this investigation were obtained from local suppliers and producers to match those used in typical local construction. The materials were ordered separately for the two construction phases, on account of limitations in storage room in the laboratory. Relevant material properties were obtained by tests of companion specimens, as described herein.

3.4.1 Masonry Units

Figure 3.4 shows the standard 200 mm wide two-cell lightweight concrete blocks with actual dimensions of 190 mm x 190 mm x 390 mm and nominal compressive strength of 15 MPa that were used. Interior blocks had frogged ends (Figure 3.4(a)), while exterior

blocks had flat ends (Figure 3.4(b)). Half blocks were cut from full blocks in the laboratory to ensure all blocks used in each specimen had consistent material properties.

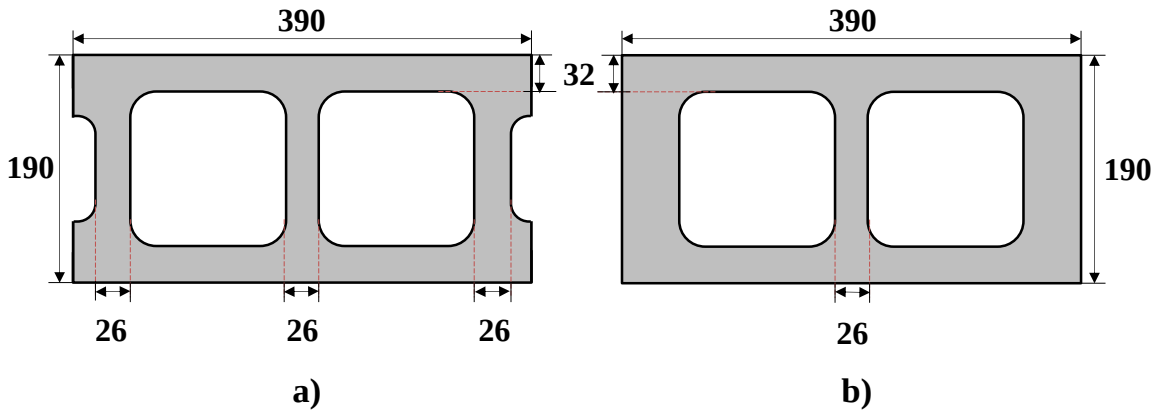

Figure 3.4. Plan view of masonry block units used, including minimum web and face shell thicknesses: a) frogged-ended full blocks, and b) flat-ended full blocks

Blocks used in the construction of specimens in Phase 1 were received in two shipments, and each shipment contained blocks from a single, but separate, production batch. Blocks from the second batch were used to construct the three replicates of the W200(No.20)-3.5 specimens. All other wall splice specimens in Phase 1 were constructed from blocks received in the first batch. Blocks for the second phase of construction were received in a single shipment.

Blocks were set aside throughout construction for testing of block properties in accordance with CSA A165-04 (CSA 2004c). Block dimensions, compressive strength, and absorption were tested using the procedures in ASTM C140 (ASTM 2012b), as prescribed by CSA A165-04 (CSA 2004c).

3.4.2 Mortar

Type S mortar was used as per the CSA S304.1-04 (CSA 2004a) requirements for structural masonry. The Type S mortar cement was supplied by Lafarge in 20 kg bags and stored in the laboratory prior to construction. Sand aggregate meeting the gradation requirements of CSA A179-04 (CSA 2004d) was procured from a local supplier. The aggregate was stored in bins in the laboratory. The gradation of the supplied mortar

aggregate was tested using the procedures outlined in CSA Test Method A23.2-2A (CSA 2009).

The mix design used in this experimental program matched that used by Ahmed (2011), Sanchez (2014), and Kisin (2014), to provide comparisons with specimens included in these past works. The water-to-cement ratio of the mix design was 0.7, and the cement-to-aggregate ratio was 1:3 by weight. Test trials performed and reported by Ahmed (2011) showed initial flow rates of 100 to 115 percent and 28-day compressive strengths in excess of 12.5 MPa, as required by CSA A179-04 (CSA 2004d).

The consistency of each batch of mortar was approved by an experienced mason prior to block placement. Retempering of mortar to compensate for evaporative moisture loss was done to maintain the mortar's workability during construction. Such retempering was done in accordance with CSA A179-04 (CSA 2004d).

3.4.3 Grout

All cells in the masonry blocks were filled with high slump grout. Lafarge Type GU cement was used to prepare the grout, which was supplied in 20 kg bags and stored in the laboratory until construction. A pre-blended aggregate meeting the 2:3 fine to coarse aggregate ratio recommendation of CSA A179-04 (CSA 2004d) was provided by a local supplier. Aggregate was stored on the laboratory floor or in aggregate bins. The aggregate for the first phase was provided in one batch, while aggregate for the second phase of construction was received in two batches. The gradation of the supplied grout aggregate for each phase of construction was established using the procedures outlined in CSA Test Method A23.2-2A (CSA 2009).

The mix design employed in this experimental program matched that used by Ahmed (2011), Sanchez (2014), and Kisin (2014). The water-to-cement ratio of the mix design was 1.0, and the cement-to-aggregate ratio was 1:5 by weight. A 250 mm slump was targeted as was a minimum compressive strength of 12.5 MPa.

3.4.4 Reinforcing Steel

Grade 400 deformed steel bars were used in this experimental program. No. 20 and 25 reinforcing bars were ordered in 6 m lengths from a local manufacturer and cut into the lengths required for each specimen using a band saw in the laboratory. All reinforcement of a given bar size and construction phase were obtained from the same heat batch.

3.5 Specimen Construction

The specimens were constructed in two phases due to space limitations in the laboratory. An experienced mason from Gracom Construction, provided courtesy of the Saskatchewan Masonry Institute (SMI), constructed all specimens. Specimens in the first and second construction phases were built between February 13 and 27, 2013, and September 4 and 19, 2013, respectively. Wall splice specimen construction was divided between the two construction phases, while the double pullout specimens were all constructed in the second construction phase.

3.5.1 Specimen Bases

Figures 3.5 and 3.6 show the plywood bases used for the construction of the wall splice and double pullout specimens, respectively. The bases were cut from sheets of 12.7 mm (½ inch) thick plywood. Bases for the 2.5 block wide specimens consisted of one layer of plywood, while those used for the 3.5 block wide specimens were two layers thick, with the plywood glued together and then fastened with wood screws to accommodate the increased weight of these specimens.

Holes were drilled in the plywood bases to allow the reinforcement to extend beyond the specimens as needed for testing. One block tall and five block tall staying platforms were used for the wall splice and double pullout specimens, respectively, to allow for these reinforcing bar extensions. The reasoning for the longer extensions for the double pullout specimens is provided in detail in Section 3.6.2, and was needed for the testing of the double pullout specimens.

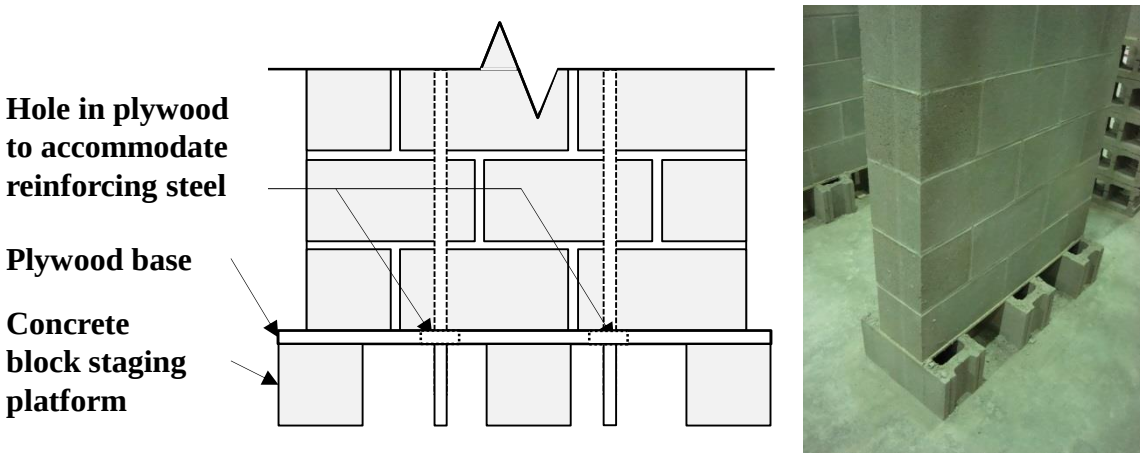

Figure 3.5. Wall splice specimen bases: a) illustration, and b) as-built photo (Note: Base for 2.5 block wide specimen shown)

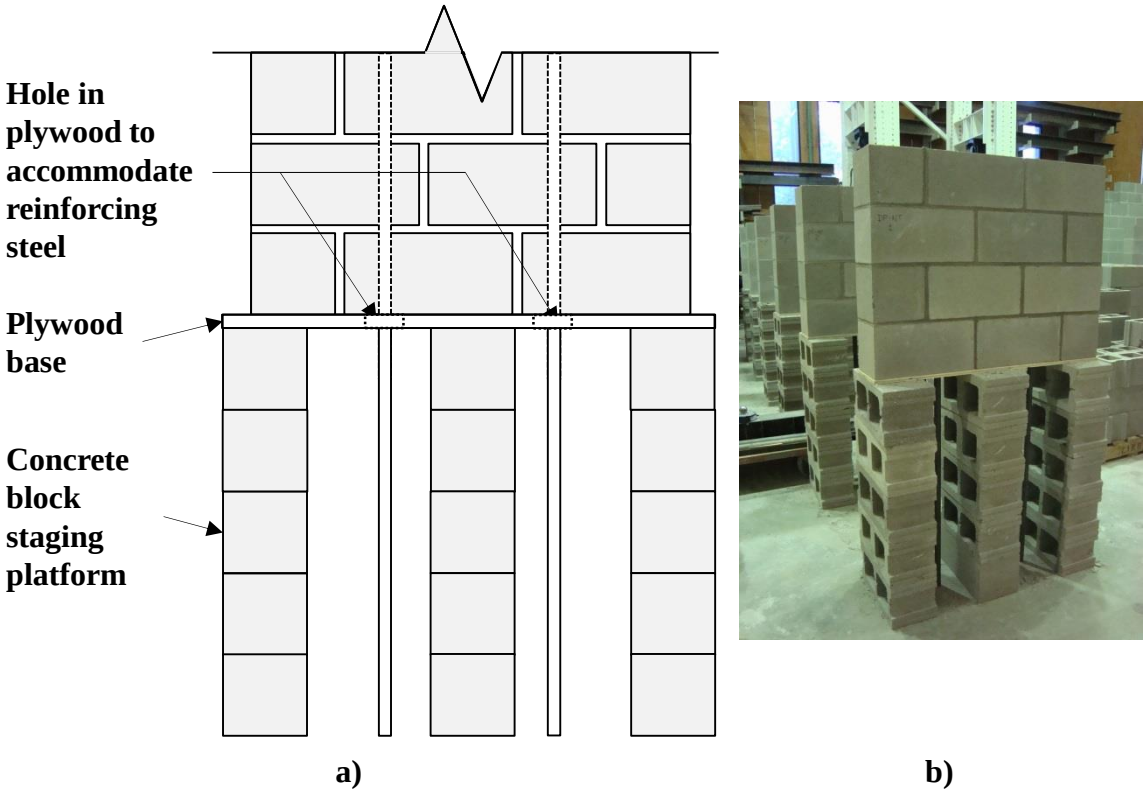

Figure 3.6. Double pullout specimen bases: a) illustration, and b) as-built photo

3.5.2 Reinforcement Preparation

Figure 3.7 shows the band saw used to cut the reinforcement into the appropriate lengths needed for the construction of each specimen, as described in Section 3.4.4. The lengths needed for each specimen were measured to the nearest millimeter, and the band saw was used for its accuracy in cutting the reinforcement and its ability to safely cut the larger bar sizes used. Excess lengths of each size of bar were saved and later tested to determine the stress versus strain characteristics of the reinforcement, as discussed further in Section 3.6.1.

Figure 3.7. Cutting of reinforcing bars with band saw

3.5.3 Block Preparation

Blocks were received from a local supplier in standard mixed pallets, each with 60 frogged end blocks and 30 flat ended blocks, at least one week in advance of construction. Once received, the shrink-wrapping on each pallet was removed and the blocks were stored for a minimum of one week so that they could equilibrate with the temperature and humidity conditions of the laboratory prior to construction. During this time, some pallets were sorted into flat- and frogged-ended blocks, since flat-ended blocks were used exclusively for half blocks. Flat-ended blocks were cut to create the half blocks since the half blocks were all placed on the exterior ends of specimens.

Figure 3.8 shows the masonry table saw used to wet-cut half blocks from the supplied flat-ended blocks in the laboratory.

Figure 3.8. Masonry table saw used to cut half blocks

3.5.4 Mortar Preparation

Multiple batches of mortar were prepared using Type S mortar cement and fine aggregate, as described in Section 3.4.2. Figure 3.9 shows the mixer used to prepare the mortar batches. The mixer featured three mixing heads and a rotating drum. The mortar was mixed by first placing half of the water and one third of the aggregate in the mixing drum. The mortar cement was then added, followed by another third of the aggregate, while the mixer was still stationary. The mixer was then started, and the last third of the aggregate was added while the drum rotated. The remaining water was also added, until the mortar reached the desired consistency. The mason confirmed that the consistency of each mortar batch was sufficient prior to placement, and retempered the mortar when needed. The mortar was transported by wheelbarrow from the mixer to the construction staging area.

Figure 3.10 shows the mortar cubes that were prepared during construction. One set of six 50 mm mortar cubes, cast in brass moulds, were prepared for each batch of mortar produced, following the procedures outlined in CSA A179-04 (CSA 2004d). The mortar cubes were then covered with plastic sheets and allowed to cure for 24 to 48 hours in the

mold, after which time they were removed from the mold and stored in the laboratory to cure.

Figure 3.9. Mixer used for mortar preparation

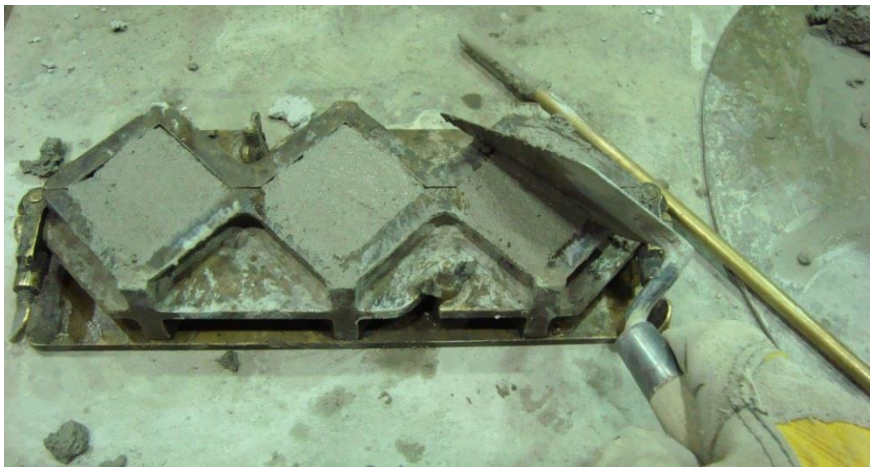

Figure 3.10. Mortar cube preparation

3.5.5 Grout Preparation and Placement

Grout was prepared in multiple batches over the course of construction. Type GU cement and pre-blended grout aggregate obtained from a local supplier were used, as detailed in Section 3.4.3. Figure 3.11 shows the concrete mixer used to prepare the grout. For each batch of grout, the first third of the aggregate was added to the mixer while it was in motion, followed by half of the water. Then, another third of the aggregate was added to the mixer. Next, the cement was added, followed by the remaining third of the aggregate. The remaining water was finally added, with slight adjustments made based on the moisture content of the aggregate such that the desired consistency was reached. The slump of each batch of grout was determined, and typically ranged from 245 mm to 255 mm. The grout was transported from the mixer to the construction staging area using wheelbarrows. The same batch of grout that was used to fill the reinforced cells in the splice region was also used to fill the masonry prism associated with every specimen.

Figure 3.11. Grout mixing

Figure 3.12 shows the grout prisms and cylinders that were prepared during construction. Three non-absorbent grout specimens, cast as per CSA A179-04 (CSA 2004d), and one absorbent grout prism, cast as per ASTM C1019 (ASTM 2012c), were prepared for each batch of grout. The companion specimens were allowed to cure in their respective

moulds for 24 to 48 hours with a plastic cover placed over their exposed surface to prevent moisture loss, after which point they were removed from their moulds.

Figure 3.12. Preparation of grout companion specimens

3.5.6 Companion Masonry Prisms Construction

Masonry prisms were constructed in conjunction with each wall splice and double pullout specimen in order to obtain the compressive strength of the masonry assembly. These prisms were constructed with frogged-end block units only. The gross cross-sectional area of the frogged-ended blocks is slightly less than that of the flat-ended blocks, thus the compressive strength of the frogged-ended blocks is most likely slightly less, and so will yield more conservative results.

Figure 3.13 shows the masonry prisms. Three course tall, fully grouted prisms were used, as per previous studies at the University of Saskatchewan (Ahmed & Feldman 2012, Sanchez & Feldman 2013, Kisin & Feldman 2013).

Figure 3.13. Masonry prisms

3.5.7 Construction Staging for Wall Splice Specimens

Construction of the wall splice specimens was staged in multiple lifts to allow for the placement of the spliced reinforcement with a continuous layer of grout encapsulating the lap splice region. Low lift grouting procedures, as described in CSA A371-04 (CSA 2004e), were followed such that clean-out holes were not required. Figure 3.14 shows the pencil vibrating of grout in the specimens after placement to ensure adequate compaction and consolidation.

Figure 3.14. Pencil vibration of grout

Figure 3.15 (a) and (b) shows the staging of construction and grout placement for the 13 course and 15 course high wall splice specimens, respectively. The lift heights were selected to ensure that the lap splices were encapsulated by a continuous layer of grout. All 13 course high specimens were grouted in two lifts, with the lower lift consisting of eight courses and the upper lift consisting of five courses. The 15 course high specimens were grouted in three lifts consisting of five courses each.

The reinforcement for all wall splice specimens was placed with the lapped bars in contact but not tied together, in order to replicate common construction practices used in Western Canada. The actual transverse spacing between the lap-spliced bars was expected to be within the ±13 mm tolerance specified in CSA A371-04 (CSA 2004e), and was measured after testing.

The bottom bars were placed after block construction and prior to grouting of the first lift, with the holes drilled in the plywood base acting as a guide. The top bars were placed during the grout placement of the first lift for the 13 course high specimens and during the grout placement of the second lift for the 15 course high specimens. The top bars were placed after filling the reinforcing cells with grout but before compacting the grout, since this represents typical construction practice. Placement of the bars in the centre of the common 84 mm grout width between two vertically adjacent blocks and at an effective depth of 95 mm was ensured by visual inspection. A hand level was used to ensure the bars were vertical after grout placement. The bars were adjusted after vibrating to best achieve their intended placement.

Figure 3.16 (a) shows the placement of the top bars. Plywood pieces that were 50 mm by 200 mm were used as a template to ensure correct placement of the top bars. Wire templates created from 1 inch (25.4 mm) grid stucco wire were used to aid in the placement of top and bottom reinforcing bars for the wall splice specimens reinforced with No. 20 bars. These wire templates were built into mortar joints above the sixth and seventh courses. Wire templates were not used for specimens reinforced with No. 25 bars because guide wires with an adequate grid size for the larger bar diameter were not available. Figure 3.16 (b) shows the placement of the wire templates.

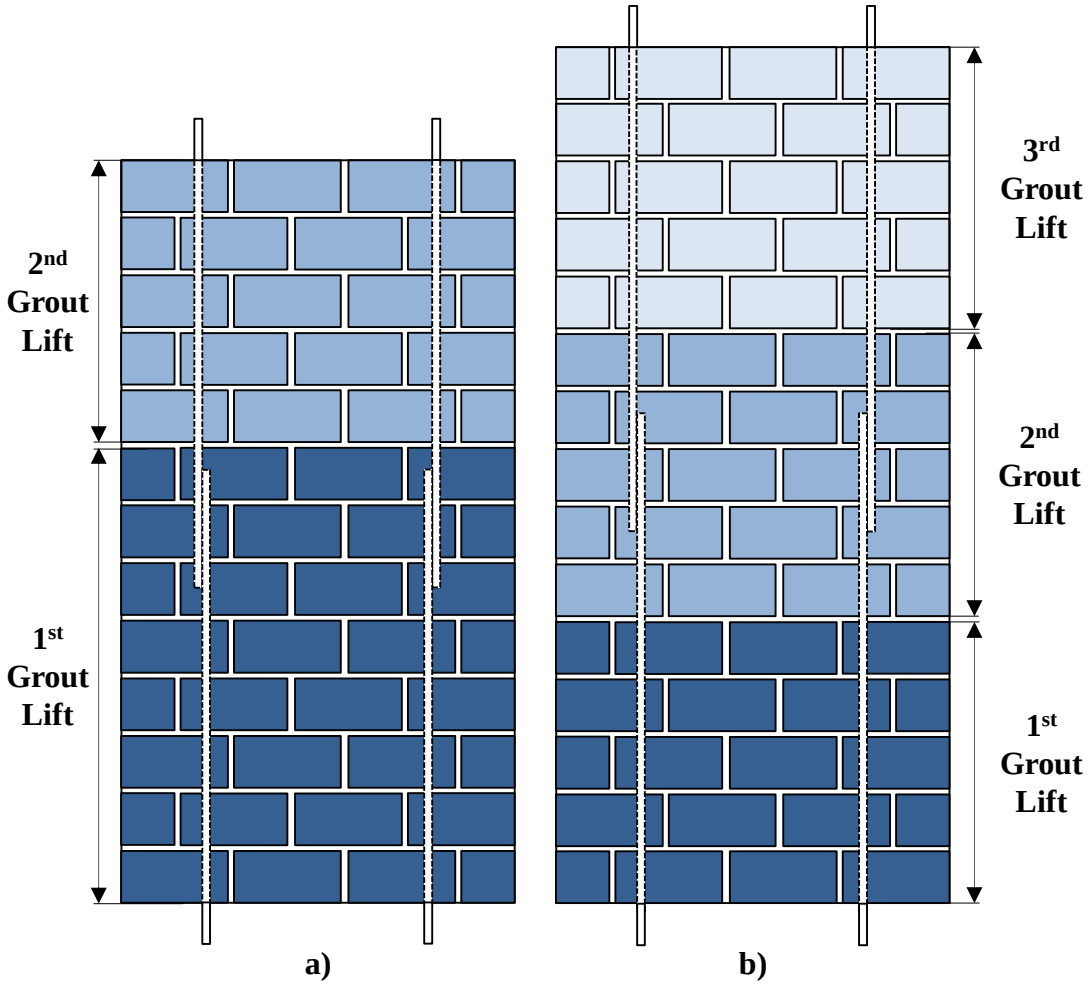

Figure 3.15. Grouting lifts: a) 13 course, and b) 15 course high specimens

a) **b)**

Figure 3.16. Placement of top bars: a) use of plywood and tie wires, and b) guide wire used to place No. 20 reinforcing bars in specimens

3.5.8 Construction Staging of Double Pullout Specimens

All double pullout specimens were constructed in a single lift. Figure 3.17 shows the plastic sheaths placed below (Figure 3.17(a)) and above (Figure 3.17(b)) the lap splice length to debond the remaining portions of these bars from the surrounding grout. These sheaths were made from 1½ inch (38.1 mm) diameter, 1/16 inch (1.6 mm) thick polyvinyl chloride (PVC) pipe, cut to the required length using a chop saw. The plastic sheaths for the bottom bars were glued onto the plywood bases, and those for the top bars were attached to the plywood support used to position the top bars on the top block of the specimen.

Figure 3.18 shows the lap spliced reinforcement used in the DP-T specimens, where the bars were held together using tie wire. The bars were placed through the hole in the plywood base once the blocks were erected. The reinforcement for the double pullout specimens with untied spliced reinforcement was placed in the same manner as for the wall splice specimens, as described in Section 3.5.7.

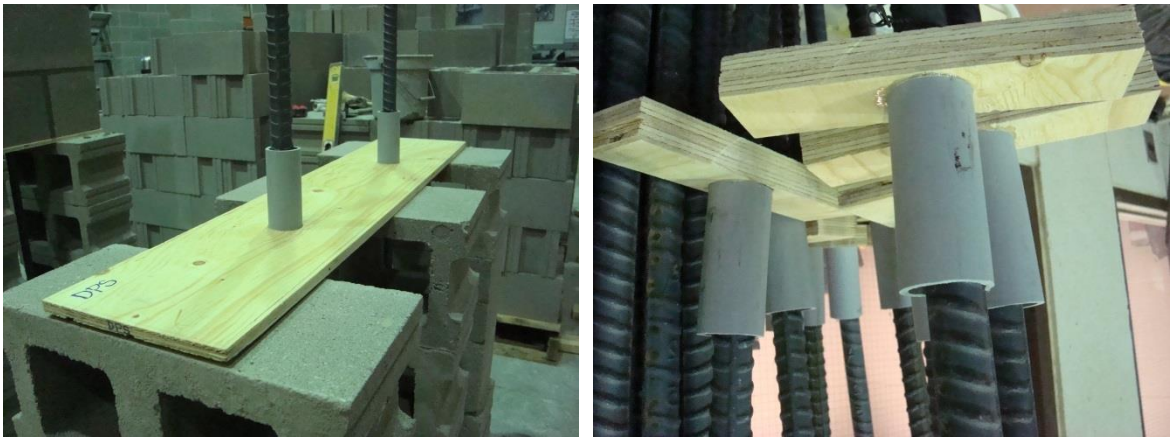

a) **b)**

Figure 3.17. Plastic sheaths used to debond the reinforcement in the double pullout specimens: a) sheaths for bottom bars attached to plywood base, and b) sheaths for tops bars attached to plywood

Figure 3.18. Lap spliced reinforcement connected using tie wire

3.6 Specimen Testing

Specimens were allowed to cure for a minimum of 28 days in the laboratory prior to testing. Testing for each phase commenced shortly after the conclusion of the 28-day curing period. Phase 1 testing took place between April 5 and June 21, 2013, while Phase 2 specimens were tested between October 21, 2013 and February 4, 2014. Detailed herein are the procedures followed for the testing of all specimens.

3.6.1 Companion Specimen Testing

The mortar, grout, masonry block, and masonry prism companion specimens were tested to determine their compressive strengths and stress-strain characteristics. The details of the testing for each of these specimen types are discussed herein.

Masonry Blocks

Masonry blocks were tested using the Amsler beam bending machine in the Structures Laboratory to determine their compressive strengths. A load cell was used to measure the applied loads during testing, and a National Instruments data acquisition system was used to record load data throughout testing on a laptop computer. The dimensions of the masonry blocks were determined using calipers. The web and face shell thicknesses, height, width, and length were measured for each block, in accordance with ASTM C140

(ASTM 2012b). The absorption properties of the masonry blocks were also tested, using the procedure outlined in ASTM C140 (ASTM 2012b). Three samples from each batch of blocks and phase of construction were tested for absorption and dimension properties, while six samples from each batch were tested for compressive strength, in accordance with ASTM C140 (ASTM 2012b).

Mortar Cube Testing

Mortar cubes were tested in accordance with CSA A179-04 (CSA 2004d). Figure 3.19(a) shows the testing of a mortar cube. Prior to testing, the width, length, and height of each mortar cube were measured using calipers to determine the exact dimensions of each specimen. Mortar cubes were tested in the Instron 600DX Universal Testing Machine (UTM) in load control mode with the load applied at a constant rate of 1 kN/min. The mortar cube was placed in the UTM such that the bearing surfaces were those cast against the brass molds and, hence, smooth. The applied load and corresponding displacement of the machine's crosshead were monitored and recorded by the data acquisition system attached to the UTM.

Grout Cylinders

Grout cylinders were tested in accordance with CSA A179-04 (CSA 2004d). Figure 3.19(b) shows the testing of a grout cylinder. Prior to testing, the diameter of the cylinder was measured at the top, middle, and bottom of the specimen. The average value was used to calculate the cross-sectional area of the cylinder. A sulphur compound was used to cap the tops and bottoms of all cylinders, thus creating uniform loading surfaces for testing. The cylinders were then tested in a stress-control mode, where the stress was applied at a rate of 15 MPa/min. The applied load and corresponding displacement were recorded by the data acquisition system attached to the Instron 600DX UTM. The stress versus strain profiles were then calculated from the acquired data.

Grout Prisms

Grout prisms were tested in accordance with ASTM C1019 (ASTM 2012c). Figure 3.19(c) shows the testing of a grout prism. The actual grout prism dimensions were

measured and recorded prior to testing. Square pieces of fibre board were placed at the top and bottom of the grout prism to provide an even bearing surface for the application of the load when testing in the UTM. The grout prisms were tested in a stress-controlled mode, with the stress applied at a constant rate of 15 MPa/min. The applied load and displacement were monitored and recorded by the data acquisition system attached to the UTM. The stress versus strain profiles were then calculated from the acquired data.

a) **b)** **c)**

Figure 3.19. Companion specimen testing: a) mortar cube, b) grout cylinder, and c) grout prism

Masonry Prisms

Masonry prisms were tested in accordance with CSA S304.1-04 Annex D (CSA 2004a). The top surface of each masonry prism was prepared prior to testing to create a level surface. To do so, excess grout on the bedding surface of the blocks was filed away and mortar was used to fill the tops of the cells of the prism to compensate for the grout shrinkage that occurred during specimen curing. Two steel angles were then attached to each masonry prism at a distance of 95 mm from the top and bottom of the prism using fast-setting, clear epoxy. These angles were used to seat the LVDTs used to measure the deflection of the prism during testing, as described herein.

Figure 3.20 shows the test set-up for the masonry prisms. The Amsler beam bending machine was used to test the masonry prisms. Each masonry prism was lifted onto the

beam bender using the overhead crane in the laboratory. Fibre board was placed below and above the masonry prism during testing to ensure an even loading surface. A steel beam and steel plate were used to distribute the load from the beam bender's crosshead uniformly across the surface of the masonry prism. A load cell was used to record the applied load during testing. Two LVDTs, each with a 50 mm stroke, were attached to a magnetic LVDT stand using LVDT holders. The magnetic stand was then attached to the base of the beam bender, and the LVDTs were positioned such that they were seated on the steel angles attached to the masonry prism.

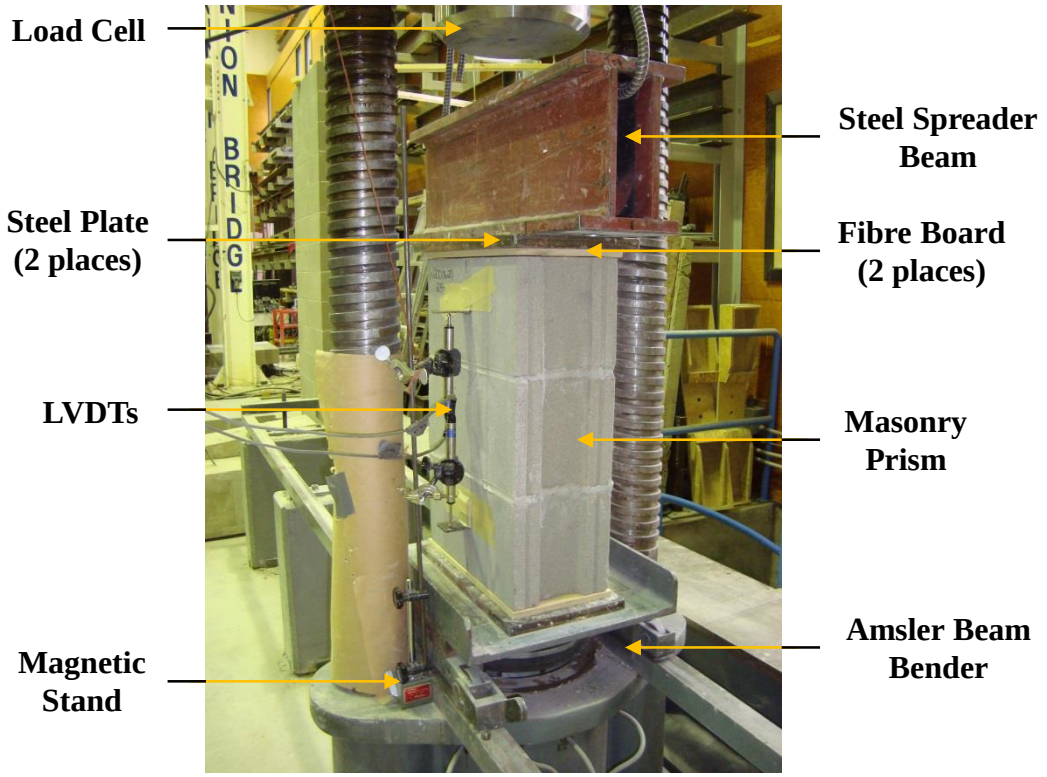

Figure 3.20. Masonry prism testing

Load was applied to the masonry prisms in accordance with CSA S304.1-04 Annex D (CSA 2004a). The loading rate was adjusted during the first half of the test until a load rate meeting the aforementioned criteria was achieved. The load during the second half of the test was applied at a constant rate until failure, such that the prism failed within the next 60 to 90 seconds.

A National Instruments data acquisition system was used to collect load and deflection data simultaneously throughout testing using a laptop computer. The deflection of the masonry prism was obtained by determining the difference in the displacements between the two LVDTs. The stress versus strain profile for each masonry prism was then calculated.

Reinforcing Steel Testing

Reinforcing steel samples were tested in accordance with ASTM A370 (ASTM 2012d) using the Instron 600DX UTM to determine their stress-strain characteristics. A minimum of three samples were tested for each bar size from each phase of construction.

Figure 3.21 shows the test set-up used for the reinforcing bar specimen tests. The test was conducted in a load controlled mode, with the load applied at a rate of 0.2 kN/s. The applied load and deflection of the crosshead of the Instron 600DX UTM were measured during testing. However, the deflection of the machine's crosshead included slippage of the grips of the machine because, in accordance with ASTM A370 (ASTM 2012d), the bar specimens could not be machined to provide better anchorage. To compensate, an LVDT with a 20 mm stroke was attached to the reinforcing bar specimen in order to obtain deformation measurements, particularly in the linear elastic and yield plateau regions. A 203 mm (8 in) gauge length, in accordance with ASTM A370 (ASTM 2012d), was marked on the bar prior to testing, and the LVDT holder was attached to the lower end of the gauge length. An aluminum rod and holder were attached to the upper end of the gauge length, thus measuring the bar's elongation over the gauge length. The LVDT set-up often fell off prior to the initiation of strain hardening, because necking could occur at any point within the 203 mm gauge length and often occurred close to the top or bottom of the gauge length. As such, data following this were not recorded. The stress versus strain profile for each reinforcing bar sample was calculated using the load and displacement data from the LVDT and the data acquisition system attached to the Instron 600DX UTM.

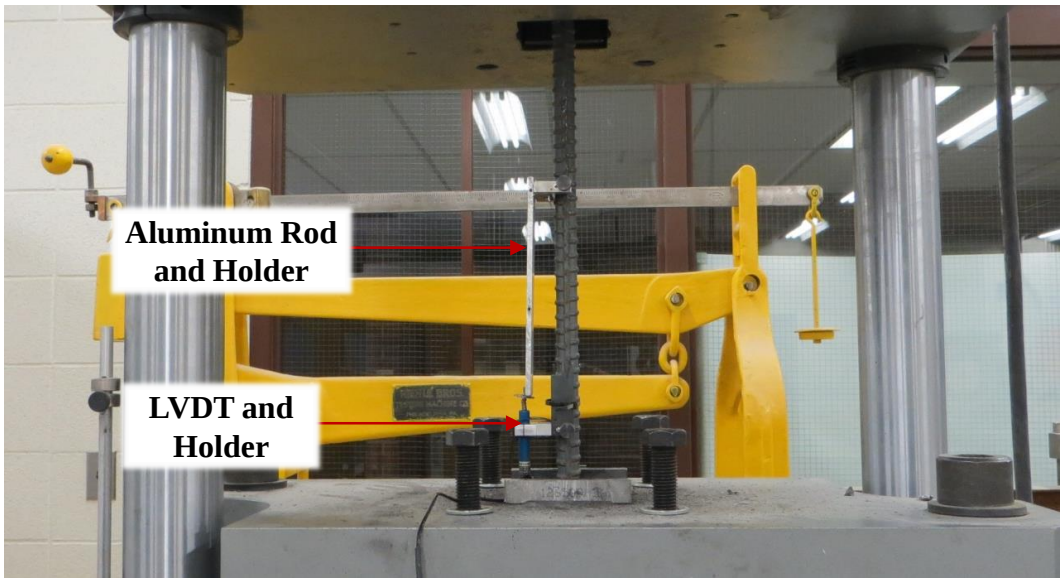

Figure 3.21. Test set-up for reinforcing bar tests

3.6.2 Double Pullout Specimen Testing

Figure 3.22 shows the frame used to test the double pullout specimens. Two beams formed from built-up C250x23 channel sections and two W310x74 columns were connected using high strength bolts. The two beams were originally designed by Ahmed (2011) and also used by Sanchez (2014). These beams were created from two C250x23 sections, 2400 mm in length, welded together back-to-back by 12 mm plates at five locations. The 65 mm gap between the backs of the channels allowed sufficient room for the reinforcing bars protruding from the double pullout specimens to extend beyond the frame. Steel plates that were 8 mm thick (shown in Figure 3.22) were welded to each channel web to stiffen them for the magnitudes of loads expected. Steel plates that were 12 mm thick (not shown in Figure 3.22) were also welded in the 65 mm gap between the back of the channels to stiffen them. These additional stiffeners were added to prevent buckling of the beams in the frame during testing.

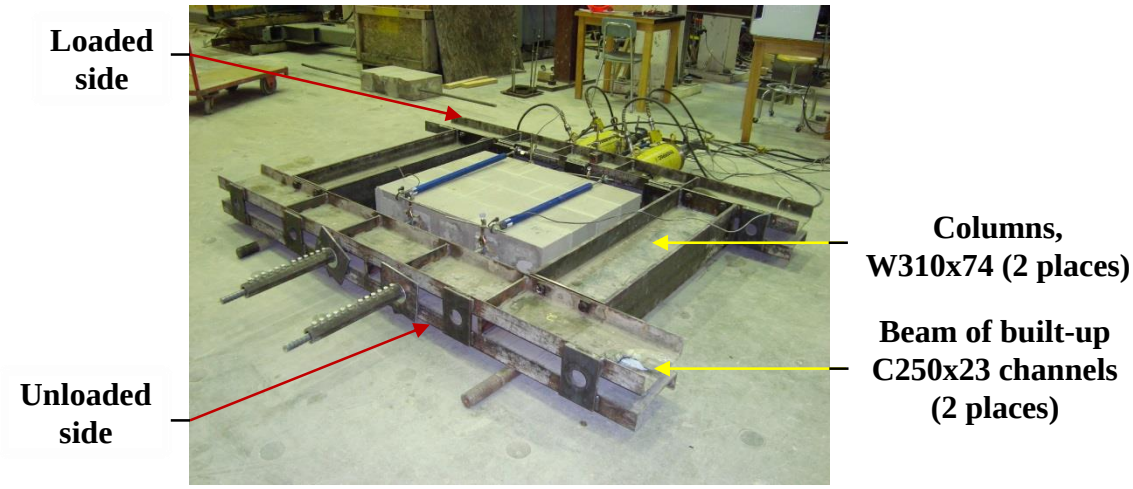

Figure 3.22. Double pullout specimen test frame

Each double pullout specimens was translated from its constructed position and rotated to the testing area on the floor of the Structures Lab using the overhead crane. The specimen was placed on two steel rollers to reduce friction during testing. The beam on the unloaded side of the test frame (shown in Figure 3.22) was attached to the columns of the test frame after the specimen was positioned. Three steel plates and one coupler were applied to each protruding bar on the unloaded side to anchor the specimen in the test frame.

Figure 3.23 shows a detailed view of the loaded side of the test frame. One hydraulic cylinder, one 12 mm steel plate, one Interface load cell with a 250 kN capacity, and one coupler were applied to each protruding bar on the loaded side of the frame. The first specimen tested, DP-T-1, was tested using Enerpac RCH 606 hydraulic cylinders, each with a 576 kN capacity. These cylinders were also used in Ahmed's (2011) work. However, it was found after testing the first specimen that larger hydraulic cylinders were needed due to constraints of the safe operating pressures for the pump in the Structures Lab. As such, Enerpac RH10010 hydraulic cylinders, each with a 1027 kN capacity, were used for the remaining 11 specimens. The load cell on each bar measured the applied load throughout testing. One LVDT with a 300 mm stroke was attached to a steel angle, which was then clamped to each coupler. This LVDT was used to measure the displacement of the bars on the loaded side of the frame. The hydraulic cylinder on each

bar applied a tensile force to the bar during testing by pushing against the test frame. The rate of extension of each hydraulic cylinder was controlled by a National Instruments data acquisition system. The valve to one cylinder was opened to apply an incremental displacement to that bar and then closed, after which the valve to the other cylinder was opened to apply a similar incremental displacement. The loading then proceeded in this fashion with alternating incremental displacements to each bar. The displacement of the LVDT attached to the couplers was used to control the load application rate and thus achieve an average loading rate of 0.025 mm/s.

Two modules programmed using LabVIEW software and a National Instruments data acquisition system on a laptop computer were used during testing, as was done in Ahmed's (2011) work. The first module controlled the load application rate, as described above. The second module recorded the applied loads as measured by the two load cells throughout testing at a rate of 2 Hz. The loading was thus computer-controlled.

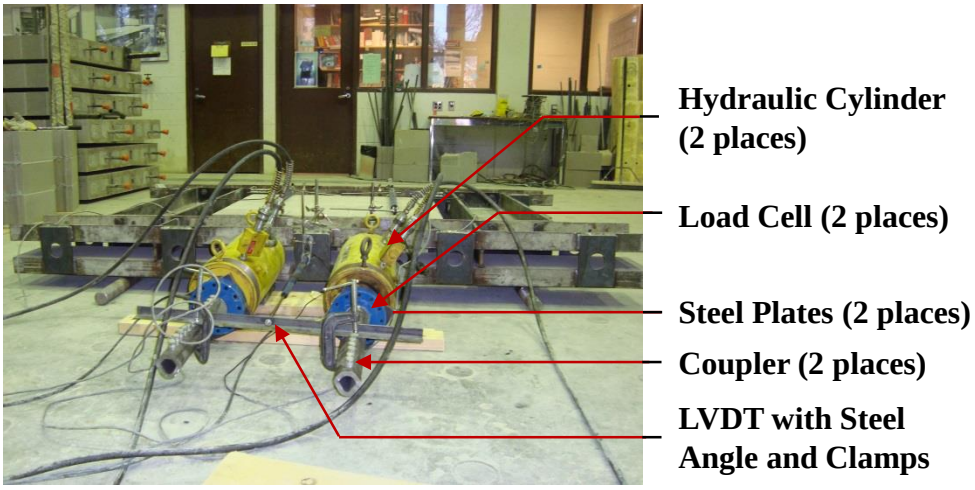

Figure 3.23. Setup of loaded side of test frame

3.6.3 Wall Splice Specimen Testing

The procedures for specimen transportation, testing, and instrumentation described herein are similar to those from past works at the University of Saskatchewan by Ahmed (2011), Sanchez (2014), and Kisin (2014). Wall splice specimens required transportation and rotation from the location where they were constructed to the testing bed. A steel moving

frame consisting of built-up steel beams and threaded high strength steel rods was used for this purpose, to prevent damage to the specimens. The frame was originally designed by Ahmed (2011), and was modified by Kisin (2014) to accommodate specimens that were 2.5 and 3.5 blocks wide. The frame consisted of two beams made from built-up structural steel channel sections and four threaded high strength rods, used to connect the two beams together.

Figure 3.24 shows the steel moving frame, including the two beams (at the top and bottom of the specimen, as shown in the illustration) and the 4 high strength rods. Each beam of the frame consisted of two C250x300 structural steel channels, connected at each end by two 12 mm steel plates welded to either side of the channels. The transverse spacing between the channels was 250 mm, to accommodate the 190 mm width of the wall. The channels themselves were stiffened with 6 mm plates welded to the channels at 12 locations along their length. Both beams had pivot bars that were used for lifting the frame and rotating the wall to the horizontal testing position. The lower horizontal beam had 25 mm diameter holes located on the flange to accommodate end plates that bolted onto the beam to secure the wall while it was in the vertical position. Inserts, built from the same steel channel sections used to construct the original frame, were added at the midspan of the frame using bolts. These inserts could be added for transporting the 3.5 block wide specimens or removed for transporting the 2.5 block wide specimens. Additional 25 mm holes were drilled to accommodate the placement of the reinforcement for the 3.5 block wide specimens. No additional adjustments of the frame were needed to accommodate the 15 course high specimens.

Securing a wall splice specimen in the moving frame entailed positioning the top and bottom beams over the specimen and then attaching the top and bottom beams to each other using the high strength steel rods. First, the lower beam of the moving frame was placed over the wall using the overhead crane such that the beam sat at the base of the wall. The end plates were then positioned underneath the wall and bolted to the lower beam. The upper beam, with the four steel rods attached, was then lowered over the wall to a position where it was centred over the twelfth mortar joint of the wall, which was the top mortar joint for 13 course high walls and the third mortar joint from the top for 15

course high walls. The threaded steel rods were then attached to the lower beam of the moving frame, to connect the upper and lower beams and thus secure the specimen.

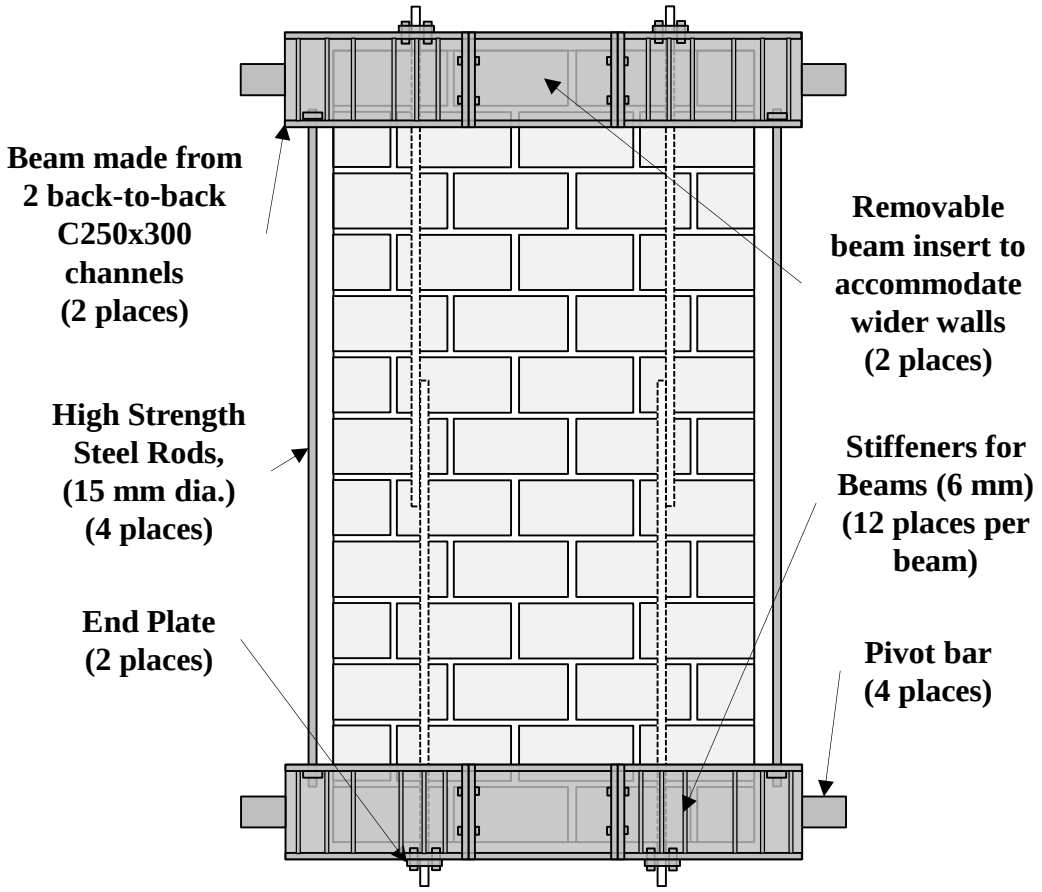

Figure 3.24. Built-up horizontal beams for steel moving frame

Figure 3.25 shows the transportation and rotation of a wall splice specimen. Figure 3.25(a) shows the lifting of the secured wall splice specimen, using the pivot bars at either end of the upper beam of the moving frame as a loading point for the lifting straps. The pivot bars on the lower beam were positioned on four spare concrete blocks (two at each side) in an open area of the laboratory, allowing the wall to slowly rotate on the pivot bars. Figure 3.25(b) shows the rotation of the wall. Spare blocks were placed underneath the wall to allow the wall to rest in its horizontal position while the moving frame was removed and the lifting straps were placed on the wall. Finally, the wall was moved into the test frame in its horizontal position using the overhead crane and lifting straps. Figure 3.25(c) shows the horizontal transport of the wall into the test frame.

a) **b)** **c)**

Figure 3.25. Transportation of wall splice specimens: a) specimen translation, b) rotating of specimen, and c) positioning of specimen in test frame

Figures 3.26 and 3.27 show the setup used for the testing of wall splice specimens. Two MTS actuators simultaneously applied the load to the specimen at a rate of 0.5 mm/min, to match the procedure used by Ahmed (2011), Sanchez (2014), and Kisin (2014). The load from the actuators was transferred to the upper transverse spreader beam to reduce the effect of any differences in applied load between them. A load cell placed between the upper transverse spreader beam, oriented perpendicular to the wall, and the lower spreader beam, oriented parallel to the wall and thus perpendicular to the upper transverse spreader beam, was used to measure the applied load on the specimen. The lower spreader beam was used to create the four-point loading on the specimen, with load points for the distributed loads located at the third points of the simply supported specimen.

Supports were located at the midpoint of the end courses. Each support featured a roller that was the same width as the wall. The rotation of one roller was prevented by screws in the support, creating a pinned support. The other support was free to rotate and so was effectively a roller support. ZAP Screwlok Type 2 mechanical couplers and steel plates were affixed to the bars protruding at both ends of the wall to provide end anchorage and so ensure that failure occurred in the splice region.

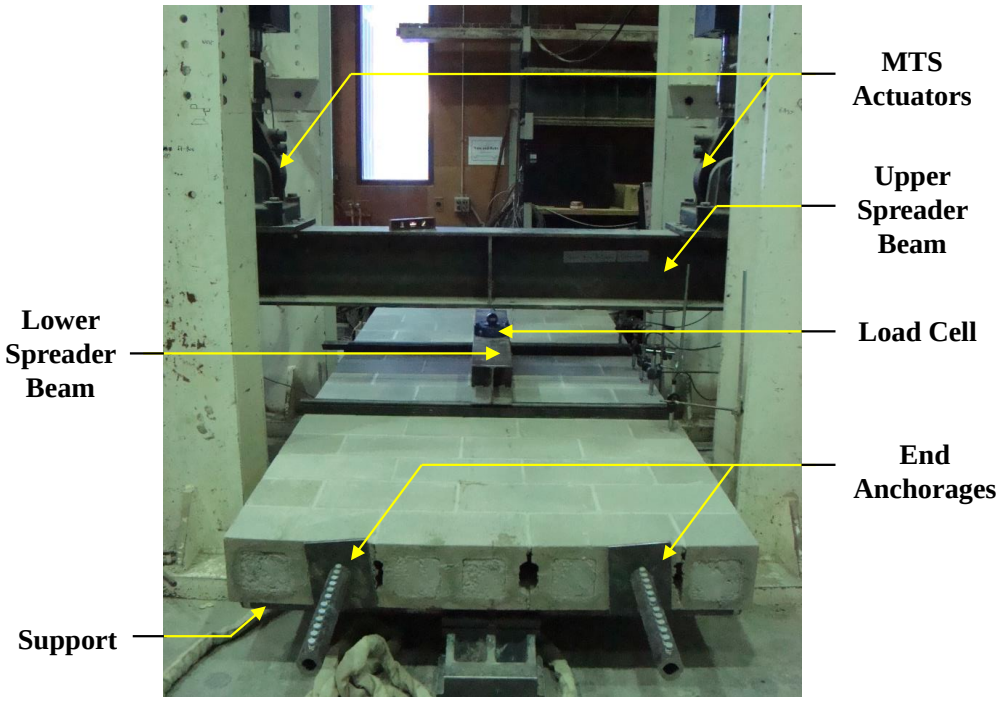

Figure 3.26. Test setup for wall splice specimens

Figure 3.27 shows the location of the LVDTs used to instrument the 13 course tall and 15 course tall specimens. Linear variable differential transducers (LVDTs), each with a range of 50 mm, were used to measure deflections during testing. Midspan deflections were measured on each side (East and West) of the wall. Deflections at four other locations along the length of the specimens were measured by four LVDTs placed along one side (the East side) of the wall.

Cracks were marked as the testing progressed on the non-instrumented side face (i.e. West side face). A National Instruments LabVIEW data acquisition system was used to collect load and deflection data simultaneously throughout the test on a laptop computer at a rate of 2 Hz.

Wall splice specimens were tested in displacement-control. As such, failure for each wall splice specimen was defined as the point when the applied load, which decreased continuously after the attainment of the maximum load, was equal to 40 percent of the maximum applied load. The test was then stopped.

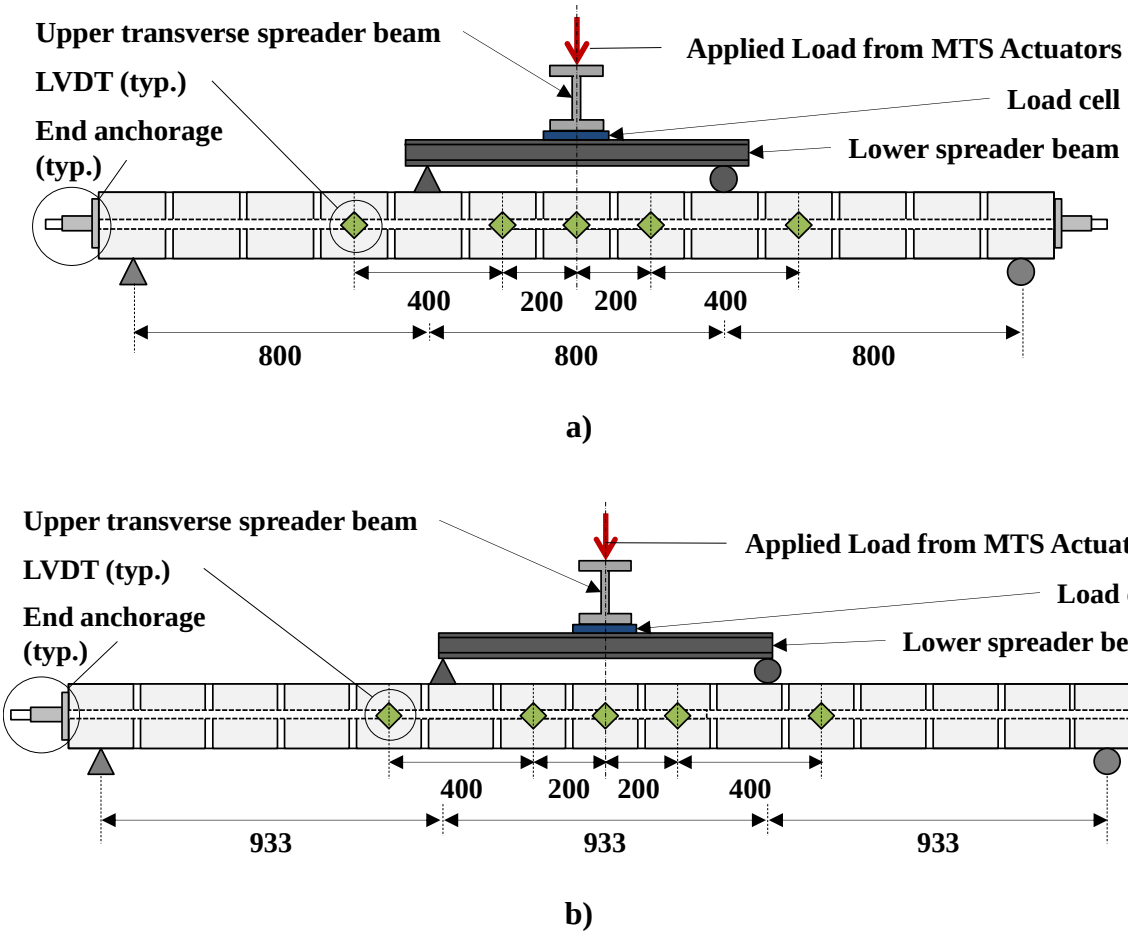

Figure 3.27. LVDT locations for wall splice specimen testing: a) 13 course high walls, and b) 15 course high walls

3.7 Summary

This chapter detailed the experimental design, construction, and testing for this research. The rationale behind the selection of the types of specimens included in the experimental program, as well as the dimensions of these specimens and the lap splice lengths selected, was discussed. The many facets of preparation and construction in the laboratory were detailed. Finally, the procedures used to test the wall splice specimens, double pullout specimens, and the accompanying companion specimens were discussed. The results from the testing of companion specimens, wall splice specimens, and double pullout specimens are presented in Chapter 4.

CHAPTER 4 RESULTS AND ANALYSIS

Presented in this chapter are the test results and analysis of the specimens included in the experimental program. The findings from the testing of the companion, wall splice, and double pullout specimens are discussed. The material properties determined from the testing of companion block, mortar, grout, masonry prism, and reinforcement specimens are presented. Qualitative observations of the failure modes and quantitative observations of the failure loads from the testing of the double pullout specimens are provided. Observations of load-deflection behaviour, deflection profiles, external cracking, and internal damage for the wall splice specimens are detailed. The numerical model used to calculate the tensile resistance of the lap spliced bars in the wall splice specimens is described. A relationship describing the tensile resistance of the spliced reinforcement as a function of splice length and bar size for the wall splice specimens is also provided. Finally, comparisons to current Canadian and American code provisions are offered.

4.1 Companion Specimen Testing and Material Properties

The properties of the materials used to construct the wall splice and double pullout specimens were determined by testing various types of companion specimens. Masonry blocks, mortar, grout, masonry prisms, and reinforcement specimens were tested in accordance with standards relevant to each, as are described in Section 3.6.1.

Table 4.1 shows the summarized results of block, mortar, and grout compressive strength testing, with further discussion of these tests presented in Sections 4.1.1 through 4.1.5. The results of the masonry prism compressive strength testing are presented in Section 4.1.6. The results of reinforcement testing are discussed in Section 4.1.7.

Full results of all material testing are presented in Appendices 4A through 4E, as noted in the following subsections. Statistical outliers were identified using the procedures outlined in ASTM E178 (ASTM 2012a), based on a selected 95 percent confidence interval. The test criterion, T_n, used for identifying outliers is:

$$T_n = \frac{|x_n - \bar{x}|}{s_s} \quad \{4.1\}$$

where x_n is the observation or data point of interest, $\bar{x}$ is the average value for all specimens in the sample set, and s_s is the standard deviation of the sample set. This test criterion was compared to critical t-values for a two-sided test at the 5 percent confidence level. If the calculated value of T_n for a specimen was greater than the critical t value, it was considered an outlier. This statistical test assumes the data is normally distributed.

Table 4.1. Summary of Results for Block, Mortar, Grout, and Masonry Prism Companion Specimen Testing

Companion Specimen	Phase	Number of Specimens Tested	Mean Compressive Strength (MPa)	COV (%)
Blocks	1 (Batch1)	12	19.7	10.6
	1 (Batch 2)	12	23.6	11.0
	2	12	27.4	5.12
Mortar cubes	1	107[1]	20.7[1]	21.6[1]
	2	96	22.8	14.7
Grout cylinders (non-absorbent)	1	93[2]	11.7[2]	12.3[2]
	2	93[3]	16.9[3]	22.0[3]
Grout prisms (absorbent)	1	33[4]	12.3[4]	13.5[4]
	2	32	19.0	17.6

[1]Data for one mortar cube was not recorded, and was thus excluded.
[2]Five cylinders identified as physical outliers and three cylinders identified as statistical outliers were excluded. Data for one cylinder was not recorded, and was thus also excluded.
[3]Three cylinders were not tested due to damage to specimen prior to testing, and were excluded.
[4]One grout prism identified as a statistical outlier was excluded.

4.1.1 Masonry Blocks

Masonry block companion specimens were tested in accordance with ASTM C140 (ASTM 2012b), with specimens tested for dimensional, absorption, and compressive strength properties. The results for dimensional and absorption testing are presented in

Appendix 4A. The dimensional properties met the minimum requirements as described by the Canadian Concrete Masonry Producers' Association (CCMPA 2012). The compressive strength of blocks from the two batches in Phase 1 and one batch in Phase 2 were 19.7 MPa, 23.6 MPa, and 27.4 MPa, respectively. The compressive strength of all units tested exceeded the nominal compressive strength of the blocks of 15 MPa. A summary of the compressive strength results are presented in Table 4.1, while individual results are presented in Appendix 4A. No physical or statistical outliers were identified for any of the masonry blocks tested. The differences between the two batches from Phase 1, and each Phase 1 batch and the Phase 2 blocks, were statistically significant at a 95 percent confidence interval. The higher block strength for the Phase 2 blocks likely contributed to the higher masonry prism strengths that resulted for the second construction phase.

4.1.2 Aggregate for Mortar and Grout

The gradation of sand aggregate for mortar and pre-blended aggregate for grout was tested in accordance with CSA Test Method A23.2-2A (CSA 2009). Figure 4.1 shows the gradation of the sand aggregate used in both phases of construction relative to the fine aggregate specifications provided in CSA A179-04 (CSA 2004d). Mortar aggregate used in both phases met these specifications since the percent finer than values for each sieve size were between the limits specified in CSA A179-04 (CSA 2004d).

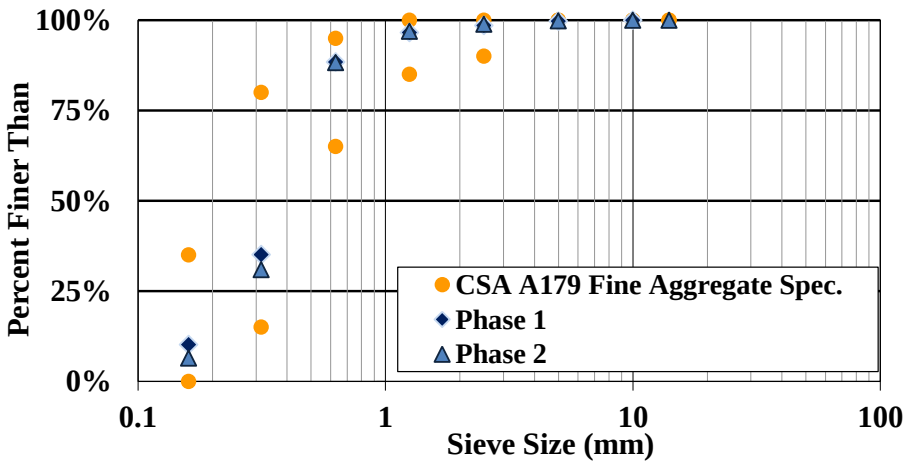

Figure 4.1. Mortar aggregate gradations

Figure 4.2 shows the gradation of the grout aggregate used in both phases of construction and the gradation of a 2:3 fine-to-coarse aggregate blend as is recommended by CSA A179-04 (CSA 2004d). The aggregate for the second phase of construction was received in two batches, as discussed in Section 3.4.3, and the gradation of both batches is shown. Grout aggregate used in Phase 1 was finer (i.e. had more material passing) than the CSA A179-04 (CSA 2004d) recommended 2:3 fine to coarse aggregate blend for grain sizes between 630 μm and 5 mm. This aggregate had some large particles, most of which had only one to two fracture faces, but was otherwise quite sandy. The first batch of aggregate used in the second phase of construction was very similar. However, the second batch of aggregate procured for the second construction phase was closer to the CSA A179 (CSA 2004d) recommended 2:3 fine to coarse aggregate blend, as seen in Figure 4.2. This batch of aggregate had more medium-sized particles with multiple fracture faces, which would likely contribute to higher grout strengths as compared to grout produced from the first batch used in the second phase of construction. Neither batch was rejected since the 2:3 fine to coarse aggregate blend is a recommendation, and since Clause 5.6 of CSA A179-04 (CSA 2004d) permits the use of any aggregate meeting the relevant property specifications for grout. CSA A179-04 (CSA 2004d) specifies a minimum grout compressive strength of 10 MPa when fine aggregate is used, and the results of grout cylinder and prism testing, presented in Table 4.1, show that the grout produced in both phases met this requirement. Additionally, this aggregate was also accepted because it represents that typically used in local construction in the area.

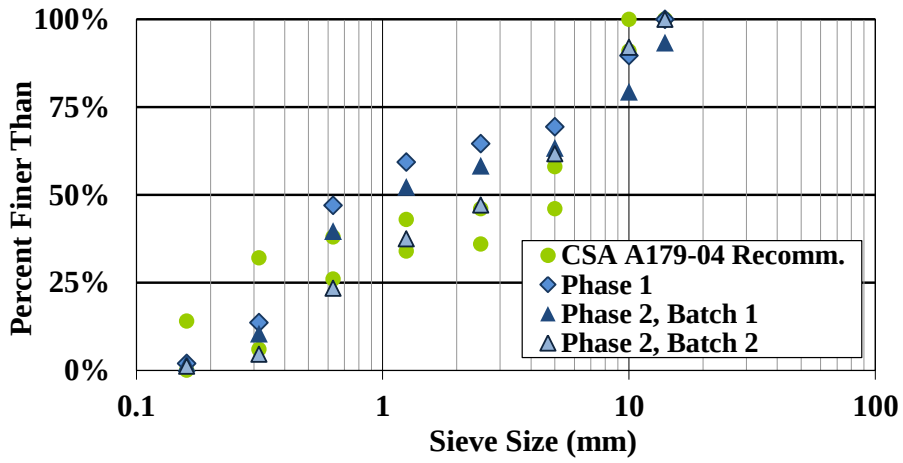

Figure 4.2. Grout aggregate gradations

4.1.3 Mortar Cubes

Table 4.1 presents the summarized results of the mortar cube testing, conducted in accordance with CSA A179-04 (CSA 2004d). Six mortar cubes were tested for each batch of mortar produced in the first and second phases of construction. Results for all individual specimens are provided in Appendix 4B. No physical or statistical outliers were identified amongst the specimens from either phase of construction. Data for one mortar cube from Phase 1 was not recorded, and thus it was excluded from the calculation of the average compressive strength. The difference in the compressive strengths of the mortar cubes between Phases 1 and 2 was not statistically significant. CSA A179-04 (CSA 2004d) specifies a minimum compressive strength of 12.5 MPa for mortar, and the results of mortar cube testing, presented in Table 4.1, show that the mortar produced in both phases met this requirement.

4.1.4 Non-Absorbent Grout Cylinders

Table 4.1 presents the results of the non-absorbent grout cylinder testing, conducted in accordance with CSA A179-04 (CSA 2004d). Three cylinders were tested for each batch of grout produced in the first and second phases of construction. Results for all individual specimens are provided in Appendix 4C. The average compressive strengths of grout cylinders from Phase 1 and 2 were 11.7 MPa and 16.9 MPa, respectively. These values met the minimum grout compressive strength requirement of 10 MPa for fine aggregate specified in CSA A179-04 (CSA 2004d).

Five cylinders from Phase 1 were identified as physical outliers due to sulphur caps that were either slanted or not fully bonded to the cylinder. Three additional cylinders from Phase 1 were identified as statistical outliers using the procedures outlined in ASTM E178 (ASTM 2012a). Data was not saved for one cylinder in Phase 1, and thus it was excluded from the calculation of the average compressive strength. Three cylinders (each from different batches) from Phase 2 were not tested because they were damaged prior to testing. These cylinders were thus excluded from the calculation of the mean compressive strength values reported in Table 4.1. No statistical outliers were identified for cylinders tested during the second construction phase.

One batch of grout from Phase 2 had a higher cement content due to a batching error on this particular grout batch. This batch of grout was placed in a shear span (i.e. outside of the splice region) in specimen W600(No. 25)-3.5-2, and so was expected to have a minimal effect on the tensile resistance of the spliced reinforcement for this specimen. The compressive strengths of the three cylinders from this batch were included in the calculation of the mean compressive strength value for Phase 2 grout cylinders since this batch of grout was placed in a test specimen.

The difference in mean values of compressive strengths between the two construction phases was found to be statistically significant at a 95 percent confidence interval, based on a student t-test. The main reason for this difference was likely the different aggregate sources used in each phase, as reported in Section 4.1.2. The higher grout strengths obtained for the grout cylinders constructed and tested in Phase 2, in combination with the higher block strengths that were also observed, likely contributed to the slightly higher masonry prism compressive strengths reported for this phase of construction.

4.1.5 Absorbent Grout Prisms

Table 4.1 presents the results of the absorbent grout prism testing, conducted in accordance with ASTM C1019 (ASTM 2012c). One prism was tested for each batch of grout produced in the first and second phases of construction. Results for all individual specimens are provided in Appendix 4D. The average compressive strengths for the grout prisms were greater than those for the grout cylinders. This result was expected, since the molds used in casting the grout prisms absorb excess water from the grout, thus increasing its strength. The average compressive strengths for the grout prisms also met the compressive strength requirements of CSA A179-04 (CSA 2004d).

No physical outliers were identified for the specimens tested during the first construction phase. One Phase 1 grout prism was identified as a statistical outlier using the procedures detailed in ASTM E178 (ASTM 2012a). No statistical outliers were identified for the grout prisms tested during the second construction phase. The identified statistical outlier was excluded from the calculation of the average compressive strength for Phase 1 as presented in Table 4.1.

The difference in mean values of compressive strength between the two phases was found to be statistically significant at a 95 percent confidence interval, as was the case for the grout cylinders, and was likely caused by the different aggregate sources used in each phase. As aforementioned in Section 4.1.4, the higher grout strengths reported in Phase 2, in combination with the higher block strengths in this phase, likely contributed to the slightly higher masonry prism compressive strength observed.

4.1.6 Masonry Prisms

Tables 4.2 and 4.3 present the results of the masonry prism testing for the masonry prisms associated with the wall splice specimens and double pullout specimens, respectively, conducted in accordance with CSA S304.1-04 Appendix D (CSA 2004a). Each masonry prism was tested on the same day as the wall splice or double pullout specimen with which it was associated. Section 3.1.3 includes a description of the abbreviated specimen designations, as used in these tables. No physical outliers were identified for specimens in either construction phase, and no statistical outliers were identified at the 95 percent confidence interval for either phase, using the procedures outlined in ASTM E178 (ASTM 2012a). The difference in mean values of the compressive strengths for masonry prisms associated with wall splice specimens between the two construction phases was found to be statistically significant at a 95 percent confidence interval, based on a student t-test, and likely resulted from the significant difference in the resulting grout strengths between the two phases, as described in Section 4.1.4 and 4.1.5.

The mean compressive strengths of the masonry prisms from both phases exceed the compressive strength value of 7.5 MPa provided in Table 4 of CSA S304.1-04 (CSA 2004a) for a specified compressive unit (block) strength of 15 MPa, Type S mortar, and grouted construction, as used in this study.

The compressive strength properties for the masonry prism associated with each wall were used in the numerical model, as will be described in Section 4.3.4. However, the differences in compressive strengths were not likely to have a significant impact on the calculated tensile resistances of the wall splice specimens. For instance, the tensile

resistance for a given curvature of 0.038 m^{-1} (the largest curvature observed among the wall splice specimens tested) calculated using the numerical model described in Section 4.3.4 for prism strengths of 12.5 MPa and 13.9 MPa (the average values from each construction phase) were 210 kN and 217 kN, respectively. The percent difference is thus 3 percent, indicating that the differences in the compressive strength of the masonry assembly are not substantial.

Table 4.2. Masonry Prism Compressive Strength Testing Results – Prisms Associated with Wall Splice Specimens

Phase	Associated Specimen	Compressive Strength (MPa)
1	W200(No. 20)-2.5-1	11.1
	W200(No. 20)-2.5-2	10.9
	W200(No. 20)-2.5-3	11.9
	W200(No. 20)-3.5-1	12.9
	W200(No. 20)-3.5-2	11.4
	W200(No. 20)-3.5-3	13.1
	W250(No. 20)-2.5-1	13.3
	W250(No. 20)-2.5-2	13.3
	W250(No. 20)-2.5-3	14.3
	W400(No. 25)-3.5-1	11.3
	W400(No. 25)-3.5-2	10.4
	W400(No. 25)-3.5-3	12.7
	W800(No. 25)-3.5-1	13.5
	W800(No. 25)-3.5-2	13.6
	W800(No. 25)-3.5-3	13.6
Average (MPa)		12.5
COV (%)		9.75%
2	W200(No. 20)-2.5-4	16.3
	W200(No. 20)-2.5-5	13.5
	W200(No. 20)-2.5-6	13.1
	W200(No. 20)-3.5-4	13.4
	W200(No. 20)-3.5-5	12.8
	W200(No. 20)-3.5-6	12.9
	W350(No. 20)-2.5-1	14.1
	W350(No. 20)-2.5-2	15.3
	W350(No. 20)-2.5-3	15.3
	W600(No.25)-3.5-1	13.3
	W600(No.25)-3.5-2	12.6
	W600(No.25)-3.5-3	14.0
Average (MPa)		13.9
COV (%)		8.40%

Table 4.3. Masonry Prism Compressive Strength Testing Results – Prisms Associated with Double Pullout Specimens

Phase	Associated Specimen	Compressive Strength (MPa)
2	DP-T-1	13.6
	DP-T-2	16.2
	DP-T-3	14.6
	DP-T-4	14.8
	DP-T-5	12.1
	DP-T-6	15.6
	DP-NT-1	13.9
	DP-NT-2	15.1
	DP-NT-3	16.1
	DP-NT-4	14.5
	DP-NT-5	16.0
	DP-NT-6	15.3
Average (MPa)		14.8
COV (%)		8.21%

Figure 4.3 shows the experimental stress versus strain curve for a representative masonry prism. Movement of LVDTs during testing, due to rubbing or bumping of LVDTs with the beam bender or due to slip of the LVDTs on the metal clips fastened to the masonry prism, impeded the recording of accurate displacement measurements. For instance, the vertical offset seen in Figure 4.3 was the result of LVDT movement at the start of the test. The theoretical stress versus strain curve is also shown, with the derivation of the theoretical curve described in detail in Section 4.3.4.

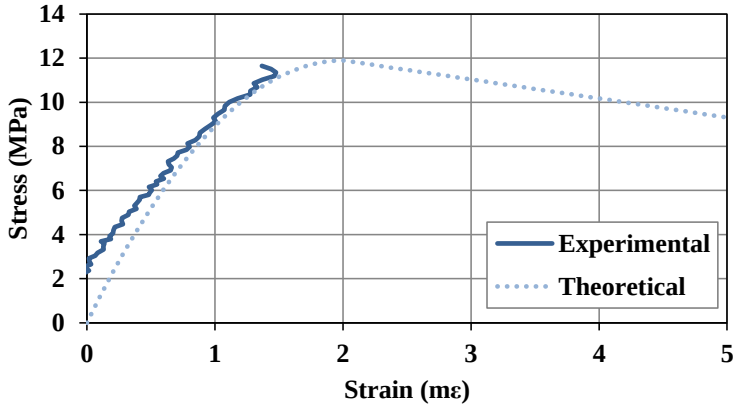

Figure 4.3. Stress versus strain curve for representative masonry prism (W200(No.20)-2.5-3)

4.1.7 Reinforcing Bar Test Results

Table 4.4 presents the results of reinforcement bar testing, which was conducted in accordance with ASTM A370 (ASTM 2012d). Results for all individual specimens are provided in Appendix 4E. A minimum of six specimens were tested for each bar size and heat batch. The strain at the initiation of strain-hardening (ε_{sh}) and the instantaneous slope at the initiation of strain-hardening strain (E_{sh}) were only calculated for specimens where LVDT displacement data was available through the strain hardening region of the test. Consequently, three additional specimens were tested for the No. 20 and 25 bar samples for Phase 1 to obtain LVDT displacement data. Displacement data as measured by the Instron testing machine was not considered due to grip slippage, as detailed in Section 3.6.1.

The values for strain-hardening strain as reported in Table 4.4 are comparable to those reported by Mirza & Skrabek (1991). The coefficient of variation is not reported for ε_{sh} and E_{sh} since this data was only obtained for two specimens for each of the No. 20 and No. 25 bars tested in Phase 1, and four and five specimens of the No. 20 and 25 bars, respectively, tested in Phase 2.

Table 4.4. Summary of Results for Reinforcement Companion Specimen Testing

Bar Size (mm)	Phase		Yield Strength, f_y (MPa)	Elastic Modulus, E_s (GPa)	Strain at Initiation of Strain-hardening, ε_{sh}	Slope at ε_{sh}, E_{sh} (MPa)	Ultimate Strength, f_{ult} (MPa)
No. 20	1[1]	*Average*	442	202	0.0135[3]	7080	602
		COV (%)	0.961	0.759	n/a	n/a	0.811
	2[1]	*Average*	429	204	0.0120[3]	4890	583
		COV (%)	0.406	2.50	n/a	n/a	0.412
No. 25	1[2]	*Average*	478	207	0.0168[4]	5620	640
		COV (%)	0.631	0.079	n/a	n/a	0.625
	2[2]	*Average*	468	201	0.0126[5]	4420	624
		COV (%)	0.320	5.36	n/a	n/a	0.357

[1]Nine replicate specimens were tested.
[2]Six replicate specimens were tested.
[3]Based on test results of 2 specimens for which LVDT displacement data was available.
[4]Based on test results of 4 specimens for which LVDT displacement data was available.
[5]Based on test results of 5 specimens for which LVDT displacement data was available.

Figure 4.4 shows the experimental stress versus strain curve for a representative reinforcement companion specimen. The theoretical stress versus strain curve is also shown, with the derivation of the theoretical curve described in detail in Section 4.3.4. The experimental and theoretical curves showed good agreement.

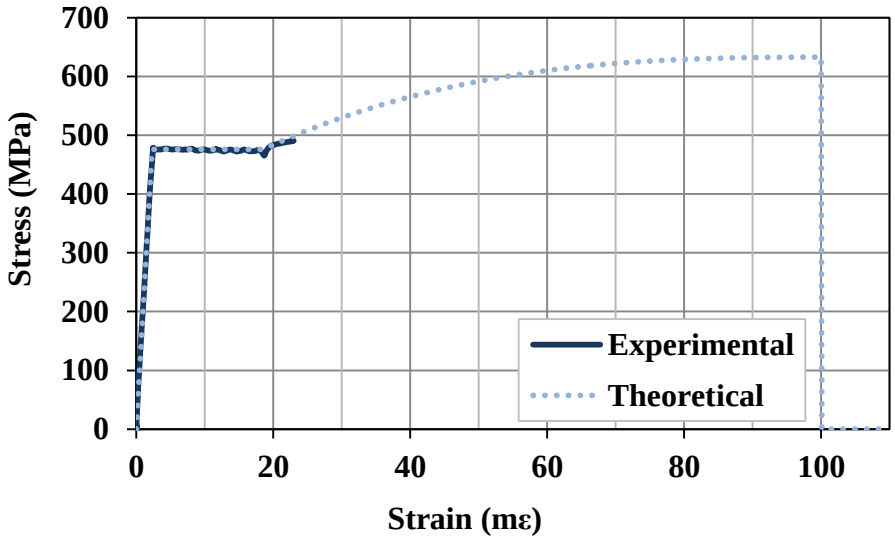

Figure 4.4. Stress versus strain curve for representative reinforcing bar sample

4.2 Double Pullout Specimens

Double pullout specimens were tested in this study to show that the construction and testing techniques used at both the University of Saskatchewan (U of S) and NCMA are reasonably similar, and thus the results from testing at the U of S can legitimately be used to assess the adequacy of current code provisions. Twelve double pullout specimens, each with splice lengths of 600 mm, were constructed and tested in this study. Six of these specimens were constructed with the lapped bars tied together, and six were constructed with the lapped bars placed in contact but not tied together. Problems with the application of similar loads between the two larger hydraulic cylinders impacted the results of the double pullout specimen testing. Detailed herein are the load histories and failure loads observed and the visual observations of damage made for the double pullout specimens.

4.2.1 Load Histories and Failure Loads of Double Pullout Specimens

Figures 4.5(a), (b), and (c) show the load versus time plots for DP-T-1 (tested with the small hydraulic cylinders, as described in Section 3.6.2), a representative DP-T specimen tested with the large hydraulic cylinders as described in Section 3.6.2 (DP-T-3), and a representative DP-NT specimen tested with the large hydraulic cylinders as described in Section 3.6.2 (DP-NT-1), respectively. The small hydraulic cylinders, used for testing DP-T-1, provided reasonable control in terms of applying approximately equal loads to the two bars throughout the test. The horizontal line segments seen in Figure 4.5(a) in which the applied load did not increase with time correspond to periods when the pump pressure had to be increased to apply additional load. Higher pressures could not safely be used for testing further specimens. The large hydraulic cylinders were thus used for all remaining tests because the larger area of these cylinders allowed for the generation of forces required to cause bar pullout without an increase to the pump operating pressure.

In contrast, the loads applied by the two hydraulic cylinders differed significantly throughout testing for all tests conducted with the large hydraulic cylinders, which created an in-plane bending moment on the specimen. When testing the DP-T specimens (Figure 4.5(b)), one hydraulic cylinder was initially not loading, but did then reach and surpass the load applied by the other hydraulic cylinder. The difference between the two cylinders was 34 kN on average. When testing the DP-NT specimens (Figure 4.5(c)), one hydraulic cylinder initially did not load, and then did not catch up to the other hydraulic cylinder once it started loading. The differences in applied loads in both cases were likely the result of differences between the two hydraulic cylinders in terms of their sensitivities to the voltages applied.

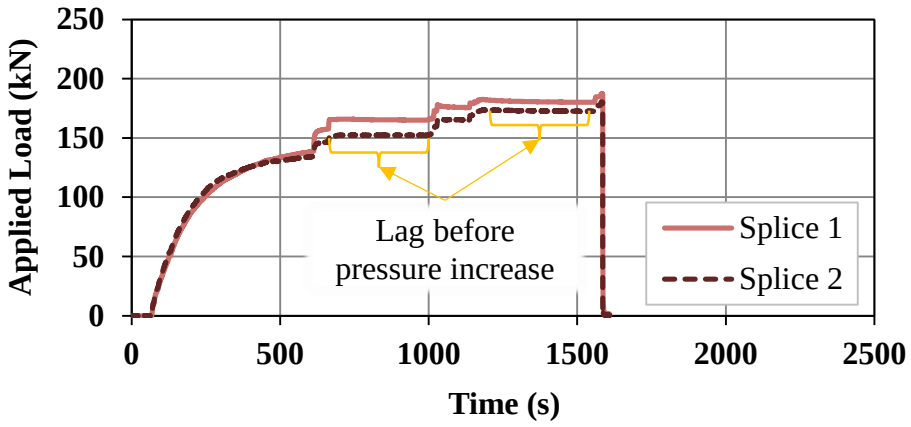

a)

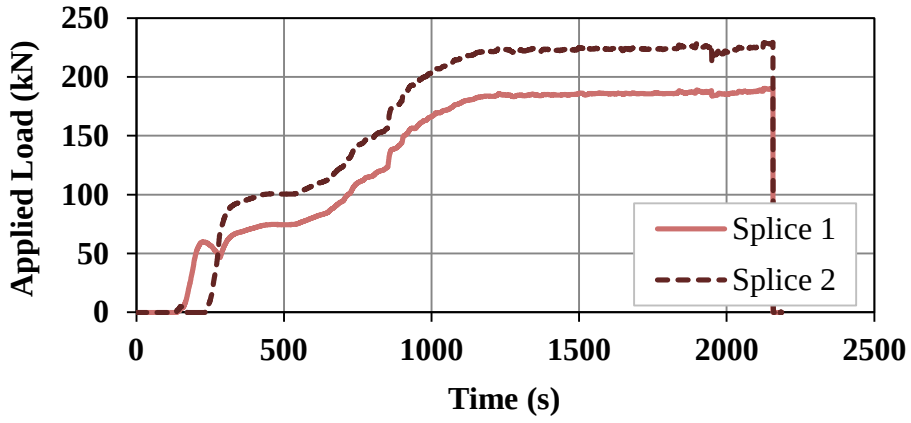

b)

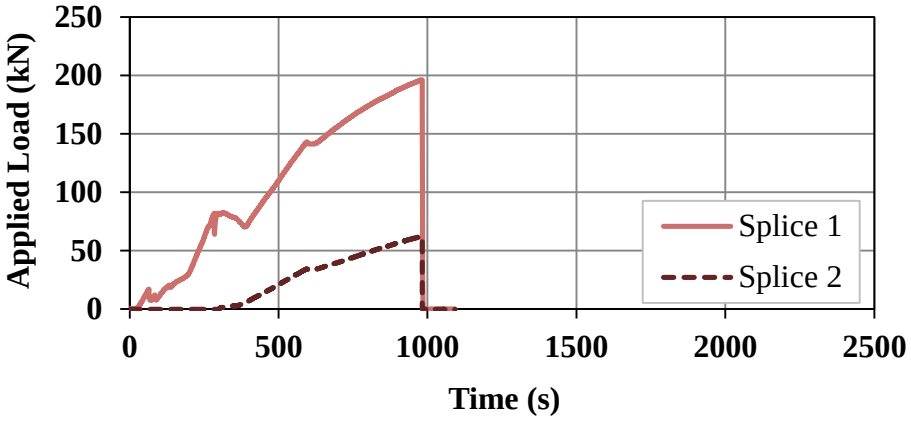

c)

Figure 4.5. Load-time histories of double pullout specimens: a) DP-T-1, tested with small hydraulic cylinders, b) representative DP-T specimen tested with large hydraulic cylinders (DP-T-3), and c) representative DP-NT specimen tested with large hydraulic cylinders (DP-NT-1)

Table 4.5 shows the loads on each splice at failure for the double pullout specimens, and identifies the splice whose splitting caused failure, as discussed further in Section 4.2.2. The failure loads on the two splices were substantially different for the DP-NT specimens, and were on average 15 percent lower than the failure loads for the DP-T specimens. This was expected, since the DP-T specimens contained splices with the lapped bars tied together with lugs in contact, thus requiring larger forces to cause the lugs to ride over each other. However, it should be noted that the greater disparity between the loads applied to each cylinder for the DP-NT specimens, caused by the differences in the sensitivities of each cylinder, created an in-plane bending moment acting simultaneously with the action of the applied loads. The magnitude of that in-plane bending moment was, on average, 22.3 kN·m, as calculated from basic principles of statics. It is likely that this in-plane moment created additional stresses in the cementitious materials, partially contributing to the lower failure loads recorded.

Table 4.5. Failure Loads for Double Pullout Specimens

Test Specimen	Max applied load on Splice 1 (kN)	Max applied load on Splice 2 (kN)	Failing Splice
DP-T-1	187	181	2
DP-T-2	155	100	1
DP-T-3	190	229	1
DP-T-4	208	248	1
DP-T-5	196	231	2
DP-T-6	223	222	2
Average (kN)	193	202	-
COV (%)	11.9	27.0	-
DP-NT-1	196	62.0	2
DP-NT-2	197	63.4	2
DP-NT-3	216	65.2	2
DP-NT-4	205	64.0	2
DP-NT-5	123	76.6	2
DP-NT-6	126	66.3	2
Average (kN)	178	66.2	-
COV (%)	23.4	7.97	-

Out-of-plane buckling of the test frame as evinced by the lifting of one corner of the double pullout test frame was noted in all tests, but most significantly in the DP-NT tests. The channel sections used to construct the test frame were relatively weak in out-of-plane buckling, and could not be restrained in the laboratory. Additionally, minor slack in the test frame set-up that resulted from slight misalignments of the reinforcement contributed to buckling since the members of the test frame were not completely flush with one another. This buckling likely influenced the results, causing the failure loads to be greater than expected (as described in Section 4.2.3) and, in the case of the DP-NT specimens, contributing to the disparity in loads between the two cylinders.

4.2.2 Qualitative External and Internal Damage Observation

Figures 4.6(a), (b), and (c) show specimen DP-T-1 (tested with small hydraulic cylinders), a representative DP-T specimen tested with large hydraulic cylinders (DP-T-3), and a representative DP-NT specimen (DP-NT-2), respectively. All specimens showed splitting through one of the reinforced cells.

The DP-T specimens, including DP-T-1, showed similar damage at failure. The cementitious material surrounding the reinforcement of the failing splice split over the entire splice length. The face shell and grout surrounding the reinforcement cracked diagonally. Additionally, the fragments of face shell and grout removed after testing showed evidence of the lugs of the reinforcement scraping against the grout. This evidence suggests that bar pullout was the cause of the failure for this specimen series. The DP-NT specimens exhibited similar damages at failure, although less scraping of the lugs was detected after testing.

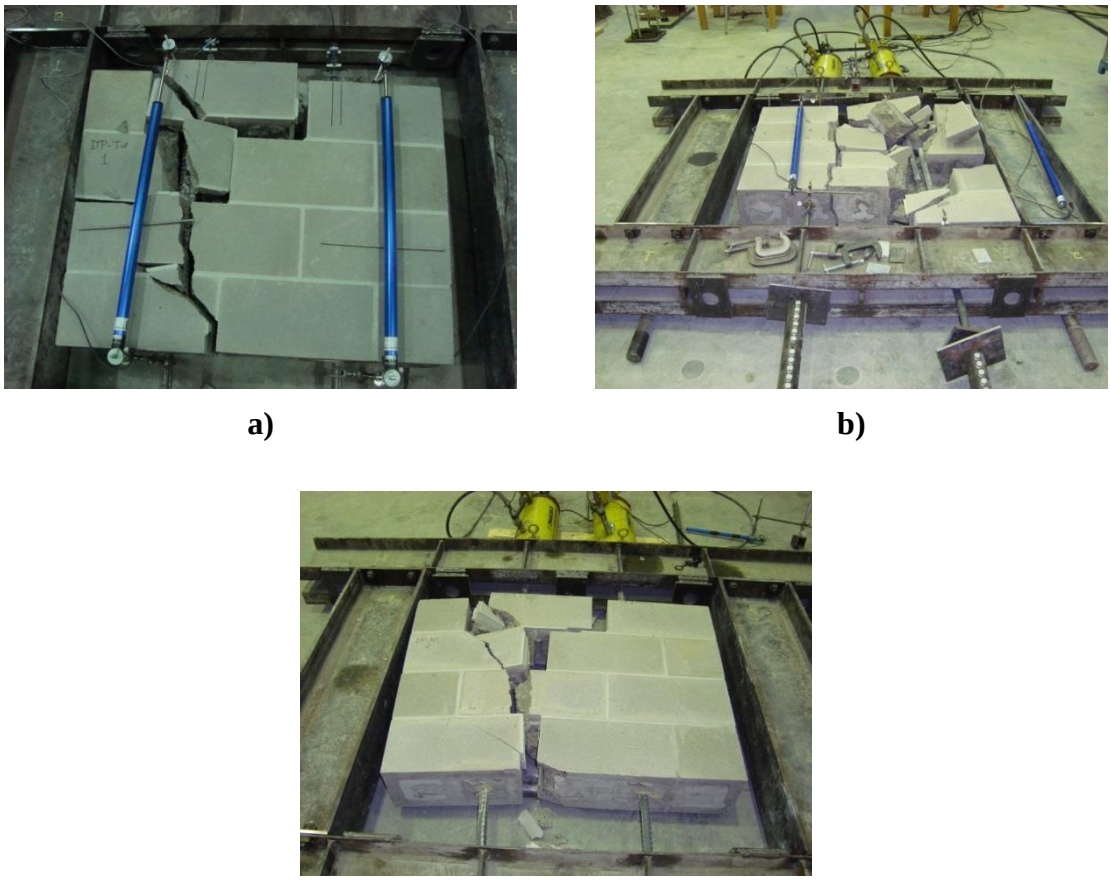

a) **b)**

c)

Figure 4.6. Failure of double pullout specimens: a) DP-T-1, tested with small cylinders, b) representative DP-T specimen tested with large cylinders (DP-T-3), and c) representative DP-NT specimen tested with large cylinders (DP-NT-2)

4.2.3 Comparison to NCMA (1999, 2009) Results and Prediction Equation

NCMA (1999) established a regression equation (Equation 2.6) to predict the tensile resistance of the spliced reinforcement for a double pullout specimen based on splice length, bar diameter, and masonry compressive strength. All specimens constructed in NCMA's studies (1999, 2009) were built with the lapped bars tied together. The predicted tensile resistance of the reinforcement for the double pullout specimens calculated using Equation 2.6 was 176 kN. This predicted capacity is representative of the DP-T specimens, since these were constructed with the lapped bars tied together, but not the DP-NT specimens, since they were constructed with the lapped bars not tied.

Specimen DP-T-1 failed at a load equal to 181 kN, which is 3 percent greater than the NCMA predicted value. Thus, when the small hydraulic cylinders were used, the experimental results agreed closely with the NCMA predicted values. Similarly, the average failure load of the specimens tested by Ahmed (2011) with contact lap splices was 89.7 kN. The failure load predicted by the NCMA regression equation for these specimens was 92.0 kN, which results in a 3 percent difference between the predicted and observed values. The close agreement between failure loads as recorded for specimen DP-T-1 and for the specimens constructed and tested by Ahmed (2011) and Equation 2.6 indicate that the construction and testing techniques used by the U of S and NCMA were reasonably similar.

4.3 Wall Splice Specimen Results and Analysis

Twenty-seven wall splice specimens, 18 of which were reinforced with No. 20 bars and 9 of which were reinforced with No. 25 bars, were tested in this study. The database for the subsequent analysis was then further bolstered by the inclusion of selected results of testing conducted on wall splice specimens reinforced with No. 15 bars by Sanchez & Feldman (2013). Load and deflection data were collected throughout the testing of each specimen, and visual observations of crack propagation were also recorded. Internal damage to the wall splice specimens was investigated after testing for select specimens to obtain further information on the resulting failure mode. A numerical moment-curvature analysis was used to calculate the tensile resistance of the lap splice for each wall splice specimen. A relationship for the tensile resistance of the lap splice as a function of splice length and bar diameter was established using a regression analysis. The resulting lap splice length to achieve yielding of the reinforcement was determined by extrapolating beyond the limits of the resulting equation. These test-based splice lengths were then compared to those calculated using current Canadian and American masonry code provisions to evaluate the adequacy of these provisions.

4.3.1 Load-Deflection Behaviour

Table 4.6 presents the experimentally- and theoretically-determined cracking loads, maximum load, and midspan deflection at the maximum load for the wall splice

specimens tested in this investigation. A description of the abbreviated specimen designations, as reported in Table 4.6, was presented in Section 3.1.3. The curvature at the maximum load, tensile resistance of the reinforcement in each specimen, and the average tensile resistance of the reinforcement for each configuration are also shown. The calculation of these parameters is discussed in detail in Sections 4.3.4 and 4.3.5.

Wall splice specimen W400(No.25)-3.5-2 could not be tested as the specimen was damaged prior to testing. A different loading program was erroneously used to apply the load to this specimen, resulting in cracks in all mortar joints surrounding one block in the splice region. As such, no test data was obtained for this wall, and it is not included in the results presented herein.

The cracking loads, as reported in Table 4.6, were determined based on the visual observation of first cracking on the non-instrumented side of the wall during testing and a review of the numerical load and deflection data. The cracking load was considered to be the load at which cracking was first observed on the non-instrumented side of the wall unless the load-deflection curve for the wall showed a distinct point at which the slope of the curve changed; this sudden slope change would indicate a change in the flexural rigidity of the specimen corresponding to the opening of the first crack on the specimen. In such cases, the cracking load was determined to be at the time when a sudden slope change was observed; this resulted for six of the 27 wall splice specimens. Cracking loads showed some variability, which is likely due to the complex nature of the initiation of cracking in masonry elements subject to out-of-plane bending and potential variability in construction. Cracks generally initiated at a mortar-block interface. The theoretical cracking loads, calculated in accordance with Clause 10.14 of CSA S304.1-04 (CSA 2004a) and adjusted to exclude the moment caused by the self-weight of the specimen, were typically less than the observed experimental cracking loads by 15 percent on average. These differences likely resulted from the additional rigidity in the system during testing due to friction inevitably present between the supports and the wall that would create a slight axial compression in the wall.

Table 4.6. Summary of Load and Deflection Results for Wall Splice Specimens

Test Specimen	Observed Cracking Load (kN)	Theor. Cracking Load (kN)	Maximum Load (kN)	Mean Displacement at Max. Load (mm)	Curvature at Maximum Load (1/m)	Tensile Resistance (kN)	Mean Tensile Resistance (kN)	COV (%)
W200(No. 20)-2.5-1	4.0	3.3	24.4	9.24	0.0139	48.6	56.9	8%
W200(No. 20)-2.5-2	2.7		23.4	11.5	0.0168	58.3		
W200(No. 20)-2.5-3	2.7		25.3	11.9	0.0165	58.4		
W200(No. 20)-2.5-4	5.6		20.7	10.6	0.0149	57.4		
W200(No. 20)-2.5-5	3.9		24.3	11.9	0.0153	56.4		
W200(No. 20)-2.5-6	4.5		23.1	11.6	0.0170	62.1		
W200(No. 20)-3.5-1	5.5	4.6	24.7	11.4	0.0164	63.9	58.3	16%
W200(No. 20)-3.5-2	2.0		23.7	9.08	0.0130	49.4		
W200(No. 20)-3.5-3	4.7		27.0	12.2	0.0172	67.0		
W200(No. 20)-3.5-4	11		25.4	12.1	0.0170	68.0		
W200(No. 20)-3.5-5	5.0		21.0	9.02	0.0115	45.2		
W200(No. 20)-3.5-6	5.1		19.1	9.58	0.0142	56.0		
W250(No. 20)-2.5-1	4.3	3.3	30.8	12.4	0.0199	72.3	70.8	6%
W250(No. 20)-2.5-2	2.7		28.1	12.1	0.0182	66.2		
W250(No. 20)-2.5-3	3.7		29.1	13.8	0.0201	74.0		
W350(No. 20)-2.5-1	0.9	3.3	42.4	18.9	0.0252	92.4	98.0	7%
W350(No. 20)-2.5-2	2.5		45.2	17.9	0.0283	105		
W350(No. 20)-2.5-3	1.7		41.1	18.8	0.0258	96.3		
W400(No. 25)-3.5-1	2.8	1.2[2]	51.6	22.1	0.0219	123	132[2]	9%[2]
W400(No. 25)-3.5-2[1]	n/a[1]		n/a[1]	n/a[1]	n/a[1]	n/a[1]		
W400(No. 25)-3.5-3	3.5		44.4	23.3	0.0243	140		
W600(No. 25)-3.5-1	3.4	1.2	57.1	23.6	0.0241	138	138	7%
W600(No. 25)-3.5-2	2.2		56.9	25.5	0.0299	129		
W600(No. 25)-3.5-3	2.0		58.9	23.2	0.0256	148		
W800(No. 25)-3.5-1	2.8	1.2	70.3	31.5	0.0336	193	196	10%
W800(No. 25)-3.5-2	0.5		74.4	33.9	0.0308	178		
W800(No. 25)-3.5-3	2.7		69.1	37.7	0.0380	216		

[1]Specimen damaged prior to testing, thus no results are available.
[2]Calculated based on the results of two replicate specimens.

Figure 4.7 shows the experimental and theoretical load versus midspan deflection curves for representative specimens (W350(No.20)-2.5 configuration). The calculation of the theoretical curve is detailed in Section 4.3.4. Appendix 4F presents the load-deflection curves for all specimens. A change in slope corresponding to the reduction in rigidity due to initiation of flexural cracking was observed for most wall splice specimens. All wall splice specimens failed prior to the yielding of the reinforcement, as evinced by the sudden drop in load shown in the experimental curves. The applied load decreased after the attainment of the maximum applied load with increasing deflection, since the test was conducted in displacement-control. One of the two splices in the wall failed first, at which point the wall did not have sufficient resistance to support the applied load. Thus, the decrease in load with increasing deflection to the point of failure occurred shortly after the failure of the first splice.

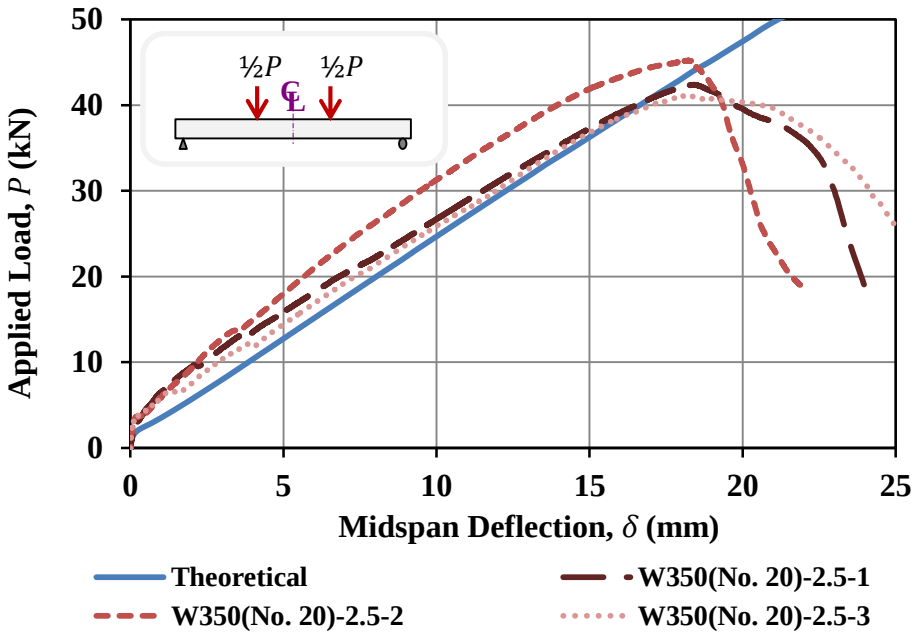

Figure 4.7. Load versus midspan deflection curve for representative wall splice specimens (shown for W350(No.20)-2.5 configuration)

4.3.2 External Damage Observations

Cracks were marked on the non-instrumented side of each wall splice specimen as testing progressed. Figure 4.8 shows the noted flexural cracking following the completion of

testing for a typical specimen. Cracking occurred at mortar bed joints exclusively, as expected for reinforced masonry. The crack patterns were consistent with those found by Sanchez & Feldman (2013) for their specimens reinforced with No. 15 bars and were consistent with those expected for masonry wall elements loaded in flexure.

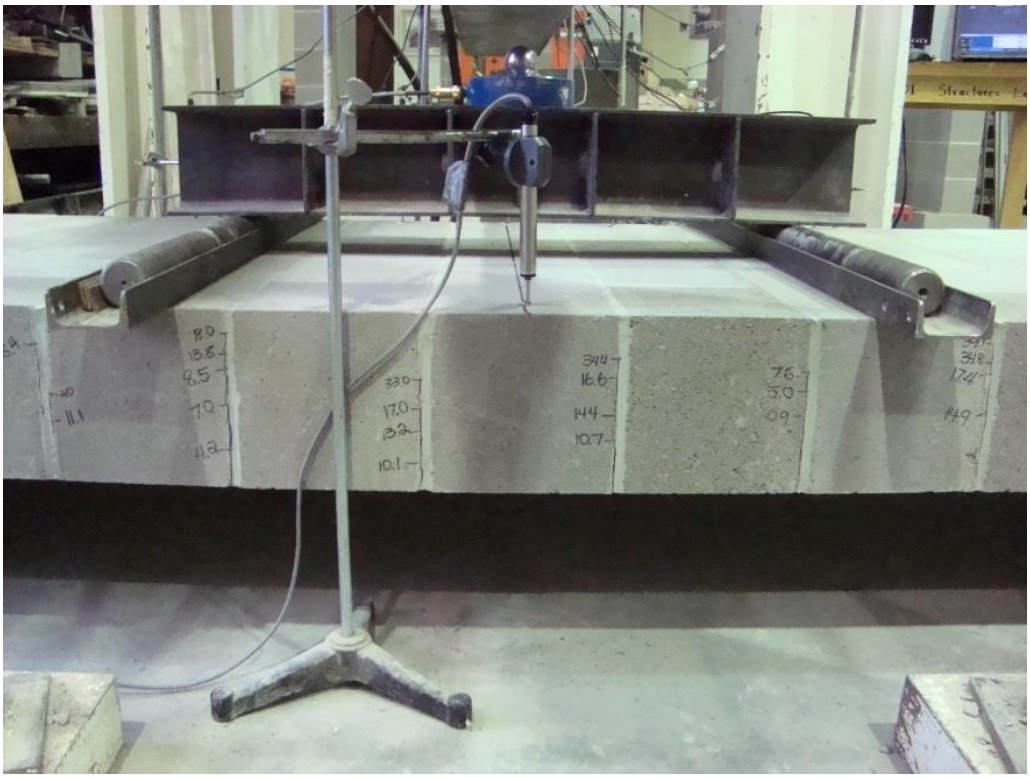

Figure 4.8. Flexural cracking of representative specimen (W350(No.20)-2.5-1)

Flexural cracking of the specimens reinforced with No. 20 bars occurred throughout the test until the maximum load of the wall was reached. Similar crack depths were observed at any given location for different specimens. The most prominent cracking occurred in the bed joints on either side of the central block for each specimen.

Flexural cracking of the W400(No.25)-3.5 specimens continued until the failure of the specimen at an average maximum load of 48.0 kN. Most of the crack initiation, lengthening, and widening for the W800(No.25)-3.5 specimens, which failed at an average maximum load of 71.3 kN, occurred prior to the application of approximately half to two-thirds of the maximum load. Similarly, most of the cracking for the W600(No.25)-3.5 specimens occurred prior to the application of approximately two-

thirds of the maximum load, thus at similar load levels at which the cracking ceased for the W800(No.25)-3.5 specimens.

The W600(No. 25)-3.5 and W800(No.25)-3.5 specimens displayed further top face cracking of the wall in addition to the flexural cracking noted above, which was not observed for any other specimens. Figure 4.9 shows the crack patterns on the top face of a representative W800(No.25)-3.5 specimen. Most notably, cracking occurred in the reinforced cells starting at the end of the specimen, and continued into the constant moment region between the two load points where the splice was located. The cracking propagated into the splice region as the specimen neared its maximum load. Figure 4.10 shows the additional splitting cracks observed at one end of a W800(No.25)-3.5 specimen once the mechanical couplers were removed after testing. The W600(No.25)-3.5 specimens exhibited cracking on the top face of the wall as well, but to a lesser extent than the W800(No.25)-3.5 specimens since the maximum loads were lower.

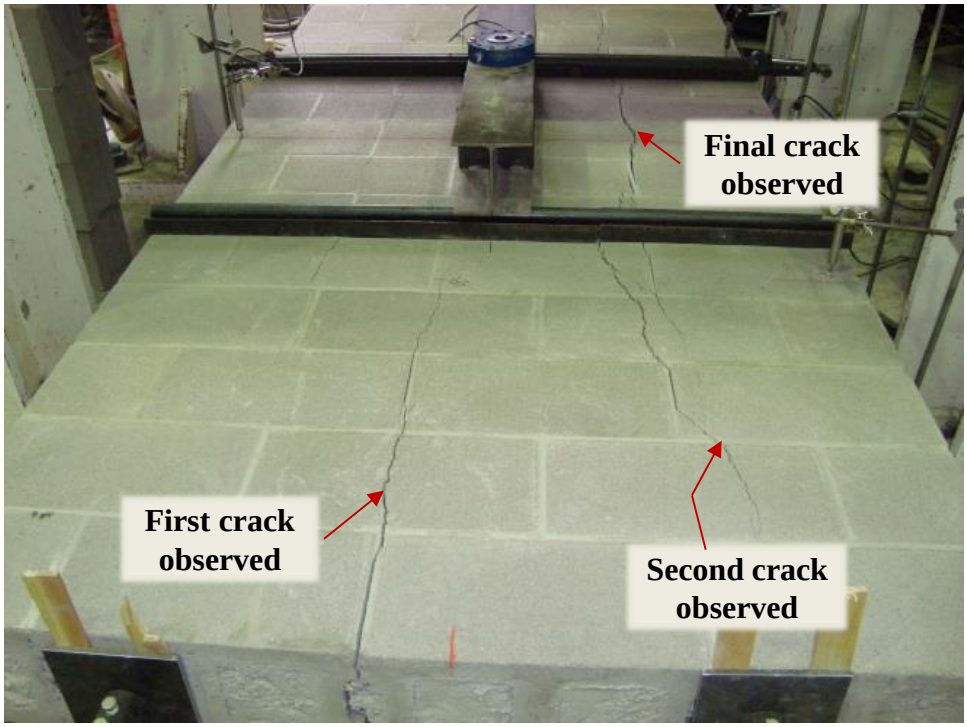

Figure 4.9. Cracking on top face of specimen W800(No.25)-3.5-3

Figure 4.10. Splitting of grout surrounding reinforcement on W800(No. 25)-3

The cracking observed in the W600(No. 25)-3.5 and W800(No.25)-3.5 specimens was likely the result of the reduced cover of the masonry given the larger bar size. Cracking on the top face was not observed on the specimens reinforced with No. 25 bars and 400 mm lap splices because the ultimate loads for these specimens were just below the load levels at which the cracking on the top face initiated for the W600(No. 25)-3.5 and W800(No.25)-3.5 specimens.

4.3.3 Observations of Internal Damage

Selected specimens of each configuration were saw-cut through the splice region to remove the face shell and grout to the depth of the reinforcement such that internal cracking and possible indicators of bond failure could be assessed. Observations of diagonal cracking and bar pullout in the splice region indicated that bond failures occurred in all specimen configurations. Figure 4.11(a) shows the observed diagonal cracking in the grout surrounding the spliced reinforcement in a representative wall splice specimen. ACI Committee 408 (2012) reports that the presence of such diagonal cracks indicates the failure of a lap splice in bond in reinforced concrete. Figure 4.11(b) shows the pullout of one of the bars in a representative wall splice specimen, as evinced by a gap between the bar end and the grout, in one of the lap splice bars in a representative wall splice specimen.

The face shell and grout were also removed to the depth of the reinforcement within one of the shear spans for the W800(No.25)-3.5 specimens, due to the additional cracking observed in these specimens. Figure 4.12 shows the diagonal cracking observed at the end of one W800(No.25)-3.5 specimen. This cracking propagated through the grout in the cell. The direction of this cracking, pointing downward and away from the splice region, is consistent with a bond failure in the splice region, since the direction indicates bar slip occurred in the splice region and this bar movement caused the cracking seen at the end of the specimen. The bars would have slipped in the opposite direction had a development failure in the anchorage region occurred. This indicates that the provided end anchorages worked as intended.

a) b)

Figure 4.11. Evidence of bond failures in wall splice specimens: a) diagonal cracking in grout surrounding splice reinforcement, and b) bar pullout in lap splice

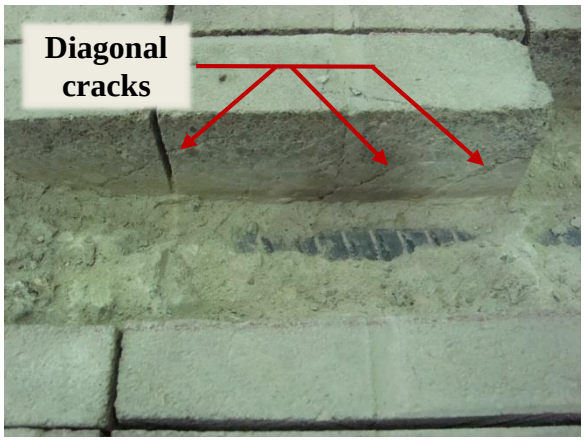

Figure 4.12. Diagonal cracking at end of W800(No.25)-3.5 representative sample

One half of specimen W800(No.25)-3.5-3 cracked significantly during testing, such that pieces of the face shell and grout surrounding the reinforcement could be easily removed by hand after testing. Figure 4.13 shows one such piece of the grout surrounding the reinforcement in this specimen. The pieces of grout surrounding the reinforcement from the splice region showed clear evidence of scraping of the lugs of the reinforcement on the grout that surrounded them, again indicating that the reinforcement slipped.

Figure 4.13. Scraping of reinforcement lugs on surrounding grout in splice region, specimen W800(No.25)-3.5-3

A jackhammer was used to remove the face shell and grout to the depth of the reinforcement for the remaining wall splice specimens to verify the actual splice length and transverse bar spacing within each lap splice. Appendix 4G presents this data. CSA A371-04 (CSA 2004e) specifies a tolerance of 13 mm when placing reinforcement in walls and flexural elements where the distance from the farthest masonry face to the reinforcement centreline is less than 200 mm, as was the case for these walls. The actual splice lengths all met this criteria, with the exception of W350(No.20)-2.5-3, where one lap splice was 15 mm shorter than designed, and W600(No.25)-3.5-1, where the two lap splices were 15 mm and 20 mm shorter than designed, respectively. The transverse

spacings of the bars met this criteria as well, with the exception of one splice in five wall splice specimens, where the transverse spacing was 15 mm (W200(No.20)-2.5-1, W200(No.20)-2.5-4, W350(No.20)-2.5-2, W400(No.25)-3.5-1, and W800(No.25)-3.5-3). However, it is also worth noting that CSA S304.1-04 (CSA 2004a) permits non-contact lap splices with spacings not more than one-fifth of the required lap splice length or 150 mm without further penalty, and this requirement was met for all wall splice specimens.

A comparison between actual splice length and transverse spacing and tensile resistance is presented in Appendix 4G. There was no consistent trend between the actual splice lengths and the tensile resistances of the spliced reinforcement, which was likely due to the effects of the variability in the actual transverse spacing in combination with the variability in the actual splice lengths. Thus, the nominal values of splice lengths were used in all further analysis.

4.3.4 Numerical Analysis Methods

The tensile resistances of the spliced reinforcement could not be determined through direct means. Strain gauges were not placed on the reinforcing bars, since doing so would have impacted the bond between the grout and the reinforcement. As such, a numerical model was needed to calculate the tensile resistances of splices in the wall splice specimens.

Furthermore, the equivalent rectangular stress block approach presented in CSA S304.1-04 (CSA 2004a) could not be used to calculate stresses, strains, moments, and curvatures of the wall splice specimens since this simplified approach is only valid when the strain in the masonry reaches its ultimate (crushing) value of 0.003. The numerical model used in this research instead considered the stress-strain relationship for the masonry and the reinforcement specifically, calculating the tensile resistance of the spliced reinforcement based on the curvature at the maximum load for each wall splice specimen. The numerical model used herein is similar to that used by Ahmed (2011), Sanchez (2014), and Kisin (2014). A detailed description of the equations used and a copy of the MathCAD code are provided in Appendix 4H.

First, the deflection profile of each wall splice specimen was used to determine the experimental curvature of the specimen at the maximum load. Figure 4.14 shows the deflection profile of a representative sample at various load levels, and the parabolic curve fit to this data at each load level determined using a regression analysis. The parabolic curve provided a good fit to the measured deflections, and the root-mean-square error (RMSE) values for the deflections were typically less than 5 percent of the midspan deflection at maximum load for each specimen. The experimental curvature was then calculated as the second derivative of the deflection profile at the ultimate load.

The tension in the reinforcement at maximum load, hereafter referred to as the tensile resistance of the spliced reinforcement, and theoretical moment-curvature curves for each wall splice specimen were determined using an iterative process whereby the distance to the neutral axis from the compression (top) face of the wall was calculated such that horizontal force equilibrium was achieved. The components and processes of the numerical model are detailed herein.

The stress-strain relationship for the masonry was modelled using a modified Kent-Park curve (Priestly & Elder 1983). This theoretical curve has been used successfully by Ahmed (2011), Sanchez (2014), and Kisin (2014), and has shown good agreement with experimental results when reliable LVDT data were obtained. The compressive strength of the masonry assembly, f'_m, as determined from the masonry prism tests associated with each wall splice specimen, was used in this model. The modified Kent-Park curve assumes a parabolic stress-strain relationship to the point when the maximum prism strength is reached, followed by a linear decreasing relationship between stress and strain. The expression is presented in detail in Appendix 4H.

The strain corresponding to the maximum stress was set equal to 0.0020 as originally proposed by Kent & Park (Priestly & Elder 1983), as Ahmed (2011) found good agreement between this value and his experimental results. Problems encountered during masonry prism testing in this study, as discussed in Section 4.1.6, prevented further assessment of the strain at maximum load from experimental data.

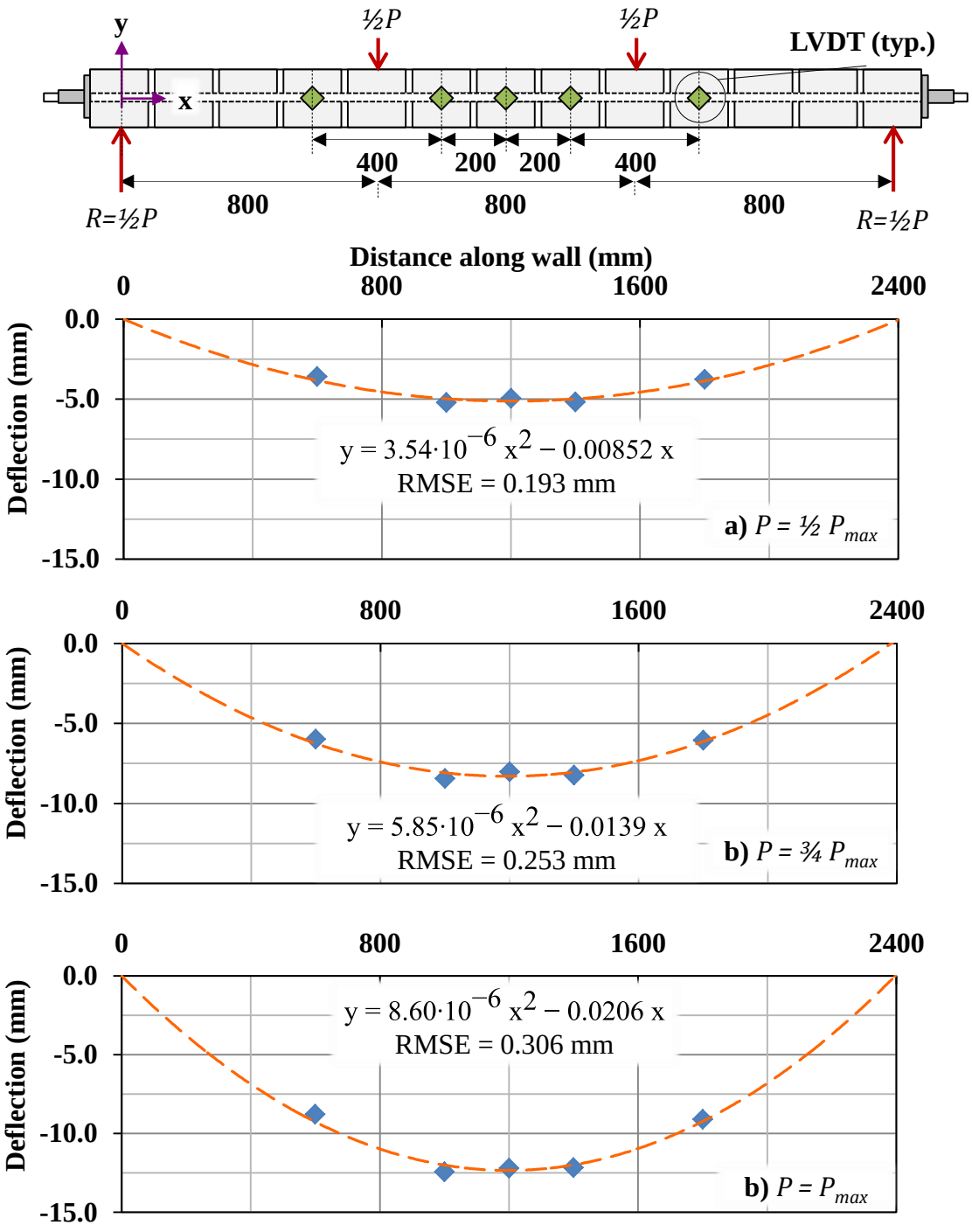

Figure 4.14. Experimental deflection profile at maximum load for representative wall splice specimen (W200(No.20)-3.5-3): a) P = ½ P_{max}, b) P = ¾ P_{max}, and c) P = P_{max}

The stress-strain relationship for the reinforcement was modelled assuming a linear rising segment to represent its elastic region, a straight line corresponding to the yield plateau, and a cubic equation corresponding to the strain hardening region for the reinforcement. The equation used is presented in detail in Appendix 4H. The tensile properties as measured during testing of companion specimens, as detailed in Section 4.1.7, were used as boundary conditions to establish the theoretical stress-strain curve. The elastic modulus, E_s, and actual yield strength, f_y, of the reinforcement were used to create the linear elastic portion of the curve. The strain at the initiation of strain hardening, ε_{sh}, was used to determine the point at which strain hardening and the parabolic curve started. The instantaneous slope at the initiation of strain hardening, E_{sh}, and the actual ultimate stress, f_{ult}, were used as boundary conditions for the cubic equation. It was assumed that the slope of the curve was equal to zero at the point of the ultimate stress. Figure 4.4 shows the theoretical stress-strain curve for a representative sample of reinforcement, which showed good agreement with the experimental data obtained.

Three further assumptions were used in the development of this model. First, it was assumed in the development of this model that plane sections remained plane. Second, contributions of the masonry block or grout to the tensile strength of the wall were neglected. Finally, any axial loads induced by friction at the supports were ignored, as they were assumed to be negligible.

Figure 4.15 shows the strain, stress, and force distributions on the cross-section of the wall splice specimens. The effective depth of the reinforcement, d_{eff}, width, b, and height, h, are shown in Figure 4.15(a). The depth to the neutral axis of the section, kd, was determined using an iterative analysis. A depth to the neutral axis was assumed, and the corresponding tensile force in the reinforcement and resultant compressive force in the masonry could be calculated. This calculation was conducted iteratively until the tensile force in the reinforcement and the compressive force in the masonry were within 0.5 percent of each other, for the given experimental curvature at the maximum applied load level. The strains in the reinforcement and masonry were calculated assuming a linear strain distribution, as shown in Figure 4.15(b). The compression area of the masonry was divided into 100 segments for the calculation of the strains, stresses, and

forces in the masonry. The strain was calculated at the mid-depth of each segment of the compression area based on the linear strain distribution, and the stress was then calculated for each segment based on the modified Kent-Park curve. The resultant compressive force for each segment was calculated by multiplying the stress by the area of the segment, and the total compressive force was then calculated by summating the compressive forces in each segment. The strain in the reinforcement was calculated using the linear strain distribution, and the stress was then calculated using the nominal bar area and the theoretical stress-strain curve described previously. Calculations in Appendix 4H show that the error associated with the choice of 100 segments of the compression area was 0.08 percent, based on the percent difference between the moment at a fixed curvature of 0.025 m^{-1} calculated for 100 segments and the approximate asymptotic value of the moment at a fixed curvature of 0.025 m^{-1}.

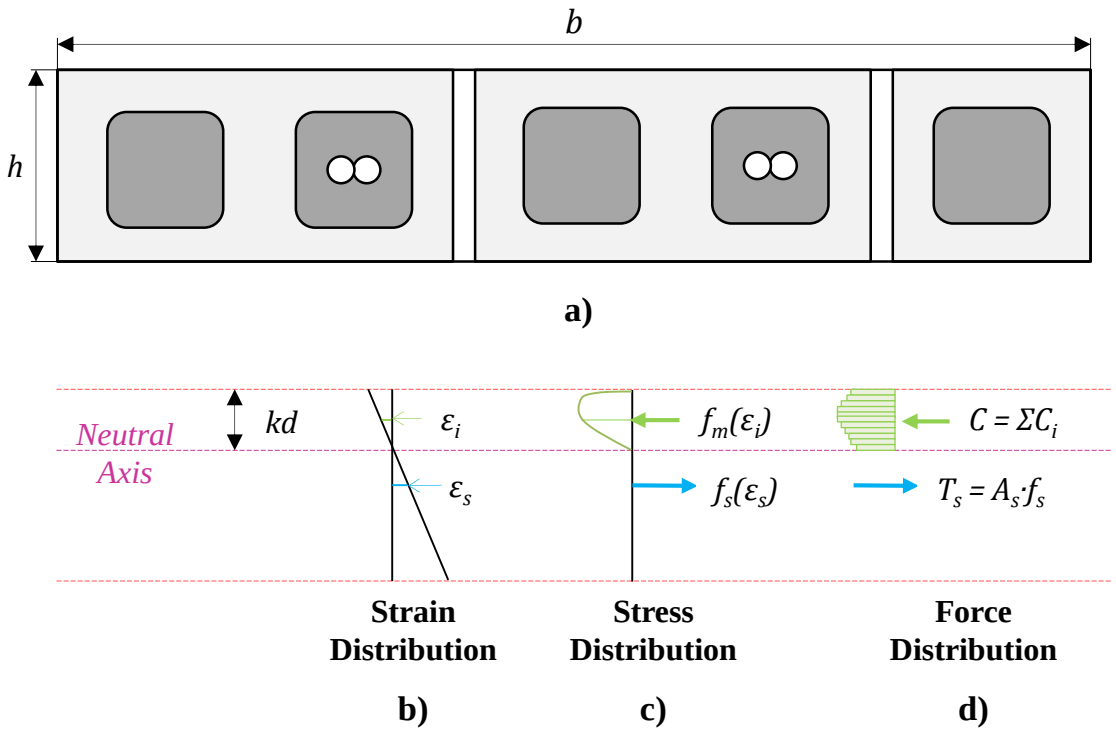

Figure 4.15. Illustration of the numerical moment-curvature model: a) specimen dimensions, b) strain distribution, c) stress distribution, and d) force distribution

The tensile force in the reinforcement at the curvature corresponding to the maximum applied load was calculated to find the tensile resistance of the spliced reinforcement for each wall splice specimen. The numerical model was also used to calculate the theoretical relationship between moment and curvature for each wall splice specimen. The moment was calculated as the summation of the force in each segment of the masonry above the neutral axis location multiplied by the distance between the centroid of each individual segment and the centroid of the reinforcement. The moment-curvature relationship for the uncracked section was calculated as the ratio of the applied moment, M_a, to the flexural rigidity of the gross cross section, $E_m I_g$, where E_m is the elastic modulus of the masonry and I_g is the moment of inertia of the gross section. E_m was calculated in accordance with CSA S304.1-04 (CSA 2004a) Clause 6.5.2, and so was equal to $850 \cdot f'_m$. Uncracked section properties were assumed until the cracking moment, M_{cr}, was reached, at which point the numerical model was used to calculate the moment-curvature relationship for the cracked section.

Figure 4.16 shows a comparison of the theoretical and experimental moment-curvature relationships for a representative wall splice specimen. The theoretical and experimental curves show good agreement, and were typical for all specimens. The experimental moment-curvature relationship showed a slightly greater moment at a given curvature, 2.41 percent on average, as compared to the theoretical curve. This difference may have resulted from frictional resistance at the supports or rigidity at the supports, which would have resulted in a small axial load in the wall splice specimen that would increase its moment capacity and hence increase the actual curve. The effects of axial loads were not considered in the numerical model.

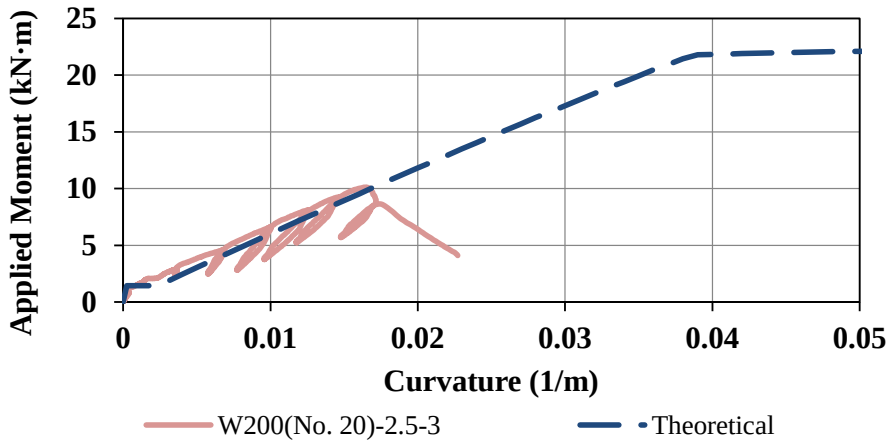

Figure 4.16. Theoretical and experimental moment-curvature relationship for a representative wall splice specimen (W200(No.20)-2.5-3)

The theoretical load-deflection curves were then developed based on the theoretical moment-curvature expressions using the conjugate beam method. The length of the wall splice specimen for these calculations was discretized into 10 mm segments (240 segments in total for the 13 course high walls, 290 segments for the 15 course high walls), as described in Appendix 4H. The error associated with the selection of 240 segments for the 13 course high walls was 0.002 percent, while the error associated with the selection of 280 segments for the 15 course high walls was 0.000 percent. As such, the calculated midspan deflection values were relatively insensitive to the number of segments selected.

The moment in each segment corresponding to any applied load was calculated using basic statics principles. The curvature corresponding to this moment was then calculated using the uncracked section properties for moments below the cracking moment, and cracked section properties using an effective moment of inertia for moments above the cracking moment.

Bischoff's (2005) equation was used to determine the effective moment of inertia. Bischoff (2005) demonstrated that his modifications to Branson's equation (Branson 1977) provide better estimates of the effective stiffness of reinforced concrete members with reinforcement ratios less than 1 percent. Bischoff's (2005) equation is also relevant for masonry since CSA S304.1-04 (CSA 2004a) uses Branson's equation (1977) for the

calculation of the effective moment of inertia of masonry elements, to which Bischoff (2005) proposed modifications. The reinforcement ratios of the wall splice specimens in this study ranged from 0.45 percent to 0.76 percent, and so Bischoff's equation (2005) was most appropriate for the determination of their effective stiffness.

The midspan deflection of the wall splice specimens was calculated using the conjugate beam method. It was assumed that the deflection of the real wall at both supports was equal to zero, hence the moment on the corresponding conjugate beam at both supports was equal to zero. It was also assumed that the maximum deflection of the real wall occurred at the midspan of the wall, thus the slope at the midspan of the real wall was equal to zero and consequently the shear on the corresponding conjugate beam at midspan was equal to zero. The sum of the curvature of each segment of the conjugate beam multiplied by the distance of that segment from one support results in the calculation of the midspan deflection.

The theoretical load-deflection curves were generated at 1 kN increments using the numerical model. Figure 4.7 shows the theoretical and experimental load-deflection curves for a representative specimen configuration, and the curves for all specimens are presented in Appendix 4F. The theoretical and experimental curves for all specimens showed good agreement.

4.3.5 Tensile Resistances of Wall Splice Specimens

Table 4.6 presents the calculated curvature at the maximum load level and the calculated tensile resistance of the spliced reinforcement of the wall splice specimens tested in this study, as well as the average tensile resistance of the spliced reinforcement for each wall splice specimen configuration as calculated using the moment-curvature analysis detailed in Section 4.3.4. The tensile resistances of the spliced reinforcement are reported for a single splice in each wall splice specimen, assuming both will have equal magnitudes. Reported coefficient of variation (COV) values of the tensile resistance of the spliced reinforcement were less than 10 percent for all but the W200(No.20)-3.5 configuration.

For each bar size, greater tensile resistances of the spliced reinforcement were observed for specimens with longer lap splice lengths, as was expected. Furthermore, the tensile

resistances of the spliced reinforcement for all specimens were less than that corresponding to the yield strength of the reinforcement, further suggesting that all specimens failed in bond.

4.3.6 Effect of Specimen Width

As discussed in Section 3.1.1, it was expected that the two specimen widths as used in this study would not significantly impact the tensile resistances of the spliced reinforcement observed for the wall splice specimens. The validity of this assumption was ascertained by comparing the tensile resistances of the spliced reinforcement reported for the W200(No.20)-2.5 and W200(No.20)-3.5 specimens; these specimens were reinforced with No. 20 bars with 200 mm lap splices in 2.5 and 3.5 block widths, respectively. A two-tailed student t-test was used to assess whether the difference in tensile resistances of the spliced reinforcement observed for these two specimen configurations was statistically significant using a 95 percent confidence interval. It was found that the difference was not significant. Therefore, it may be concluded that the increased specimen width used for the specimens reinforced with No. 25 bars did not significantly impact the tensile resistance values observed.

4.3.7 Comparison Between Wall Splice and Double Pullout Specimens

A comparison between the results of double pullout specimen and wall splice specimen testing in this study was originally desired. However, a comparison is not meaningful due to the problems encountered during double pullout specimen testing, including the application of non-equal loads by the two hydraulic cylinders and the out-of-plane bending of the test frame. Specifically, the one double pullout specimen tested with the small hydraulic cylinders for which the load application was well controlled contained tied lap splices, whereas all wall splice specimens constructed in this study had lap splices in which the bars were not tied together. Thus, the results of DP-T-1 cannot be compared to the results of the W600(No.25)-3.5 specimens.

A comparison of the test setups used for the double pullout specimens and the wall splice specimens can be made. The difficulties encountered in the double pullout specimen testing as related to the application of approximately equal loads by the two hydraulic

cylinders and the out-of-plane bending of the frame appear specific to the test frame itself. Results of double pullout tests are thus highly dependent on the design of the test frame. The testing of wall splice specimens does not involve a similar test frame for loading the specimens, and is thus less susceptible to such dependencies. Additionally, the results reported by Ahmed & Feldman (2012) indicate shortcomings with the use of double pullout specimens for the testing of the tensile resistances of spliced reinforcement. Ahmed & Feldman (2012) reported a statistically significant increase in the tensile resistance of the spliced reinforcement in the wall splice specimens as compared to the double pullout specimens, and the evidence of strain hardening of the reinforcing bars in the wall splice specimens, as discussed in Section 2.3. As such, wall splice specimens are recommended as the preferred test specimen type for masonry bond research.

4.4 Comparison to Current Code Provisions

A comparison between the resulting test data and current code provisions was desired to evaluate the adequacy of current splice length requirements. For this comparison, a regression analysis of the wall splice specimens was conducted to determine a predictive equation for tensile resistance as a function of splice length and bar size. A five percent quantile approach was then applied to this predictive equation to provide an adequate margin of safety such that splice lengths calculated using the adjusted predictive equations are appropriate for design purposes. An estimate of the splice length corresponding to the yield strength of the reinforcement for each bar size was extrapolated from the adjusted predictive equation. These splice lengths were then compared to the current Canadian and American code provisions, as presented in Equations 2.3 and 2.7, respectively. This comparison is used herein to provide recommendations for future research and code refinement.

For this comparison, specimens reinforced with No. 15 bars that were constructed and tested previously by Sanchez & Feldman (2013) were included to bolster the overall database and thus reflect the range of bar sizes typically used in Canadian masonry construction. Table 4.7 presents the results from the testing of specimens by Sanchez &

Feldman (2013). The specimen designations provided in Table 4.7 follow the format used for all specimens in this program, which is described in Section 3.1.3. These specimens included a 25 mm transverse spacing between the spliced bars and are the closest point of comparison to the wall splice specimens with bars in contact but not tied together as constructed in this study. Sanchez & Feldman (2013) found that the tensile resistances of spliced reinforcement was greater for bars tied together in contact than for bars with some transverse spacing provided between the spliced bars. Furthermore, Sanchez & Feldman (2013) report that the transverse spacing between spliced bars placed in the same cell did not significantly affect the tensile resistance of the reinforcement, based on the results from testing specimens including 25 mm and 50 mm transverse spacings between spliced bars. As such, the specimens constructed with a 25 mm transverse spacing are most comparable to the specimens constructed in this study where the bars were placed nominally in contact but not tied together.

Table 4.7. Tensile Resistances of Wall Splice Specimens Tested by Sanchez & Feldman (2013)

Test Specimen	Splice Length (mm)	Tensile Resistance (kN)
W150(No.15)-2.5-1	150	64.4
W150(No.15)-2.5-2	150	79.8
W150(No.15)-2.5-3	150	64.4
W200(No.15)-2.5-1	200	73.3
W200(No.15)-2.5-2	200	75.5
W200(No.15)-2.5-3	200	86.4
W250(No.15)-2.5-1	250	70.8
W250(No.15)-2.5-2	250	95.0
W250(No.15)-2.5-3	250	86.8

4.4.1 Determination of Predictive Equation

A regression analysis was conducted to derive a predictive equation for the tensile resistance of the reinforcement. The effects of lap splice length, l_s, and bar diameter, d_b, were found to be statistically significant at a five percent confidence level. The resulting equation for the tensile resistance, T_r, as a function of l_s and d_b was then:

$$T_r = 299 - 27.6d_b + 0.692{d_b}^2 + 0.189l_s \ \ [kN] \qquad \{4.2\}$$

The resulting root-mean-square-error (RMSE) for this equation was equal to 11.3 kN, which is equal to 14, 9, and 6 percent of the tensile resistance corresponding to the yield strength of the reinforcement for No. 15, 20, and 25 bars, respectively. The form of the equation is similar to that derived by NCMA (1999), as presented in Equation 2.6. Both linear and square terms accounting for the bar diameter, d_b and ${d_b}^2$, were included such that the effect of bar diameter was significant at a 5 percent confidence level.

Figure 4.17 shows a plot of tensile resistance versus splice length including both the tensile resistance of the spliced reinforcement obtained experimentally and those calculated using the predictive equation. Three parallel lines corresponding to each bar size are shown, although the line for the No. 15 bar size coincides with the line for the No. 25 bar size. It was observed that the line for the No. 20 bar size had the lowest intercept, and a reason for this lower intercept could not be identified. It was also observed that specimens with splice lengths resulting in the ends of the splice coinciding with mortar bed joints of the wall generally demonstrated lower tensile resistances than the lines of best fit, particularly for the No. 20 and No. 25 bar sizes. The difference between the experimental tensile resistance and the predicted tensile resistance of the spliced reinforcement, hereafter referred to as the residual, for the W600(No.25)-3.5 specimens ranged from -5.43 kN to -24.2 kN, with an average of -15.1 kN. The residuals for the W200(No.20)-2.5 specimens ranged from 1.91 to -11.6 kN, with an average of -3.33 kN. The residuals for the W200(No.20)-3.5 specimens ranged from 7.81 to -15.0 kN, with an average of -1.94 kN. The residuals for the W200(No.15)-2.5 specimens ranged from 9.02 kN to -4.08 kN, with an average of 1.02 kN. Kisin (2014) noted that the mortar bed joints are naturally a point of weakness for the wall splice specimens, since the bond between mortar and masonry block is limited. Furthermore, the ends of a lap splice are naturally the points where cracking will be induced due to the change in stiffness at these locations (MacGregor & Bartlett 2000). Consequently, these combined effects likely reduced the capacity of these specimens. These specimens were included in the analysis as the termination of splice ends at mortar joints cannot feasibly be avoided in masonry construction.

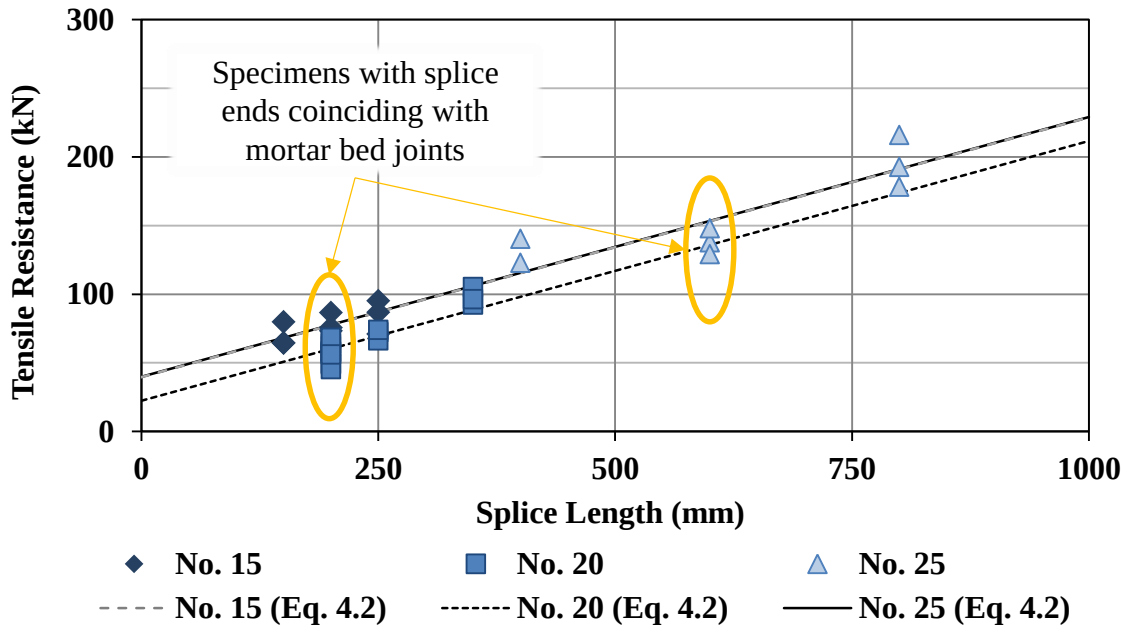

Figure 4.17. Relationship between splice length, bar size, and tensile resistance

It is worth noting that the precision of this equation is limited by the number of specimens available in the data set (Bickis 2014). The use of three parallel lines each corresponding to a bar size considered, by the inclusion of the bar diameter terms d_b and ${d_b}^2$, reduces the certainty with which the intercepts of each line are known. Additionally, the inclusion of d_b and ${d_b}^2$ in addition to the splice length, l_s, leaves fewer degrees of freedom in the residual for the expression. Finally, the effects of confounding between the splice length and bar size increase the errors of estimates made using the predictive equation. However, bar size and lap splice length are both known to be significant factors for the tensile resistance of spliced reinforcement (ACI Committee 408 2012). The use of three parallel lines results in a different intercept for each bar size. The physical significance of the different intercepts is that each bar size has a different resistance based on the bond strength developed from the bearing of one lug on the surrounding cementitious material. For these reasons, the terms accounting for the bar size of the reinforcement were included in the model despite the reduced precision resulting from their inclusion.

4.4.2 Adjusted Predictive Equation for Design Purposes

An adjustment to the predictive equation presented in Equation 4.2 was then needed to provide adequate safety for the calculation of required splice length values for design purposes. Methods used by other researchers were presented in Section 2.7.2. A five percent quantile approach was selected for this study, as the variability of the test results and the uncertainty associated with the predictive equation are both incorporated in such an approach (Bickis 2014, Ross 2009, Devore 2008). The five percent quantile value was used to reduce the intercept of the predictive equation such that values calculated using the resulting design expression represent the lower 95 percent tolerance limit for required splice lengths. Consequently, 95 percent of all future specimens are expected to have tensile resistances of the reinforcement that exceed the values predicted by the design expression.

The expression for the lower 95 percent tolerance value of tensile resistance, hereafter referred to as the adjusted predictive equation, is then (Bickis 2014):

$$T_r^{\,*} = T_r - \sqrt{kF_{2\alpha,k,n-k} \cdot s^2 \cdot \left(1 + \frac{1}{n_i} + \frac{\left(l_s - \overline{l_{s_i}}\right)^2}{\sum_{ij}\left(l_{s_{ij}} - \overline{l_{s_i}}\right)^2}\right)} \qquad \{4.3\}$$

where T_r is the tensile resistance of the spliced reinforcement calculated as a function of splice length, l_s, and bar diameter, d_b, from Equation 4.2; k is the number of bar sizes considered in the model and is equal to 3; n is the total number of specimens included in the data set, equal to 35; $F_{2\alpha,k,n-k}$ is the value of the F-distribution at the confidence level α with k and $n-k$ degrees of freedom, equal to 2.27; s^2 is the estimated residual variance of the predictive equation calculated using an analysis of variance table, equal to 127 kN^2; n_i is the number of specimens of the i^{th} bar size, equal to 9 for No. 15 bars, 18 for No. 20 bars, and 8 for No. 25 bars; $\overline{l_{s_i}}$ is the mean splice length of all specimens of the i^{th} bar size, equal to 200 mm, 233 mm, and 625 mm for No. 15, 20, and 25 bars, respectively; and $l_{s_{ij}}$ is the splice length for the i^{th} bar size and j^{th} splice length.

Figure 4.18 shows a plot of tensile resistance versus splice length including both the tensile resistance of the spliced reinforcement obtained experimentally and lines showing the predicted values for each bar size calculated using Equation 4.3. The experimental data points all fall above the adjusted predictive equation lines for each bar size, as is expected since the adjusted predictive equation was calibrated such that the tensile resistance of 95 percent of all specimens would exceed that predicted by the equation.

Equation 4.3 was then used to determine what design lap splice lengths correspond to the nominal yield strength of the reinforcement, including the 5 percent quantile to provide a margin of safety. These splice lengths were 390 mm, 740 mm, and 1060 mm for No. 15, 20, and 25 bars, respectively. These splice lengths are 44.7, 29.9, and 19.9 percent greater, respectively, than those required as calculated from Equation 4.2. The splice lengths corresponding to the nominal yield strength of the reinforcement determined from Equation 4.3 were used as the basis for comparison with provisions currently in the Canadian and American masonry standards.

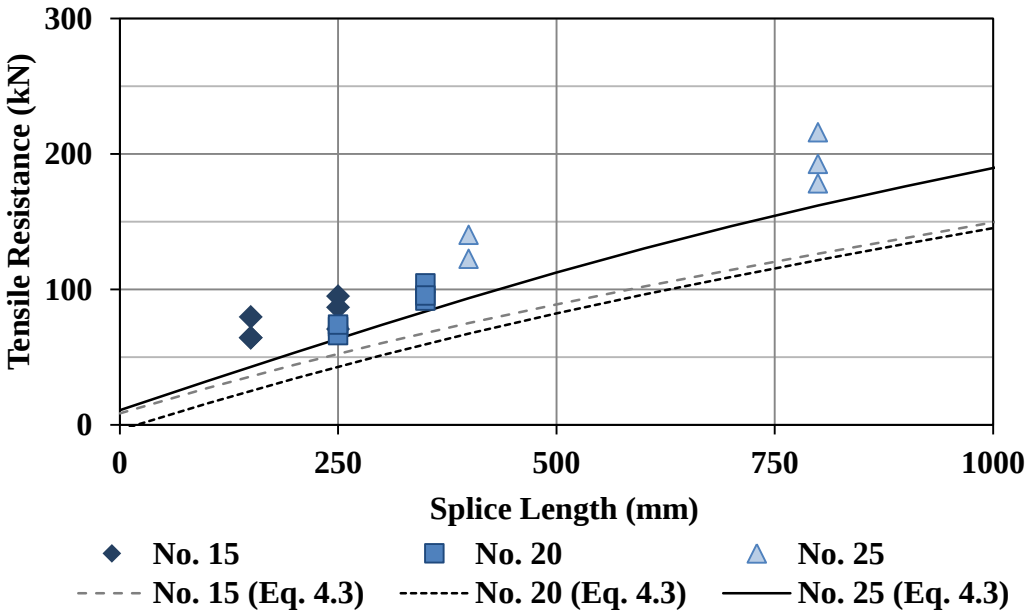

Figure 4.18. Adjusted predictive equation for tensile resistance

4.4.3 Resulting Code-to-test Ratios for Splice Lengths

Table 4.8 shows a comparison of the splice lengths calculated using Equation 4.3 corresponding to the nominal yield strength of the reinforcement, and the lap splice lengths requirements of CSA S304.1-04 (CSA 2004a) (Equation 2.3) and TMS 402-13 (MSJC 2013a) (Equation 2.7). Code-to-test calculated ratios are also provided, which were calculated by dividing the code-required splice length for each code by the splice length requirement from the adjusted equation. A code-to-test calculated ratio greater than one indicates that the splice length code requirement is conservative, whereas a code-to-test ratio less than one indicates that the splice length code requirement is unconservative.

Table 4.8. Comparison of Adjusted Prediction Equation to Current Code Provisions

Bar Size (mm)	Splice Length Calculated Using Equation 4.3 (mm)	Code Provision Splice Length Requirements (mm)			Code-to-test Calculated Ratios of Splice Lengths		
		CSA S304.1-04 Class A	CSA S304.1-04 Class B	TMS 402-13	CSA S304.1-04 Class A	CSA S304.1-04 Class B	TMS 402-13
No. 15	390	440	575	485	1.13	1.47	1.24
No. 20	740	590	765	1155	0.793	1.03	1.56
No. 25	1060	920	1195	2140	0.865	1.12	2.02

The in-situ compressive strength of the grout, f'_{gr}, when calculating splice lengths in accordance with CSA S304.1-04 (CSA 2004a) was taken as the average value of all absorptive grout prisms tested for both phases, equal to 15.5 MPa. The specified compressive strength of the masonry assembly, f'_m, when calculating splice lengths in accordance with TMS 402-13 (MSJC 2013a) was taken as the 75th percent confidence level of the 10-percentile value of the average masonry assembly compressive strength determined through masonry prism testing. TMS 602-13: *Specification for Masonry Structures* (MSJC 2013b), states that f'_m can be determined from masonry prism testing, and notes the work of Bennett (2010) in regards to calculating specified compressive

strength values based on the experimental results from testing masonry prisms. This value was calculated as follows:

$$f'_m = f_{av} - t' \cdot \frac{1}{\sqrt{n}} \cdot s \qquad \{4.4\}$$

where f_{av} is the average compressive strength of the masonry assembly of the masonry prisms tested; t' is the value of the non-central t-distribution at the 75th percent quantile, n is the number of masonry prisms tested, and s is the standard deviation of the compressive strength of the masonry assembly, as determined through masonry prism testing (Bennett 2010). The resulting specified compressive strength, f'_m, based on the compressive strengths of the 27 masonry prisms constructed in association with each wall splice specimen in this study, was equal to 11.1 MPa. This value was used for calculating the splice length requirements as provided in TMS 402-13 (MSJC 2013a). Bennett (2010) asserts that the use of the 75th percent confidence level of the 10-percentile value of the masonry assembly compressive strength based on masonry prism testing is reasonably consistent with the provisions of other codes, including CSA S304.1-04 (CSA 2004a).

The code-to-test ratios for the CSA S304.1-04 (CSA 2004a) Class A splice length requirements for No. 15 bars are greater than one and hence conservative, but are less than one and hence unconservative for No. 20 and 25 bars. The code-to-test ratios for Class A and B splices decreased by 29 percent between No. 15 and No. 20 bars, and 23 percent between No. 15 and No. 25 bars. The code-to-test ratios were the lowest for the No. 20 bars for both Class A and B splice length requirements.

The code-to-test ratios for the CSA S304.1-04 (CSA 2004a) Class B splice length requirements are greater than one and hence conservative for all three bar sizes. Splices in masonry construction in Canada are designed nearly exclusively as Class B splices, since staggering of reinforcement is not possible. Additionally, many designers use the simplified equation (provided in Equation 2.4) when calculating splice length requirements, which is more conservative than the original equation (Equation 2.3), which was used to calculate the splice length requirements presented in Table 4.8. As

such, the splices included in masonry construction to date designed to CSA S304.1-04 (CSA 2004a) standards are generally sufficient.

The code-to-test calculated ratios for the TMS 402-13 (MSJC 2013a) splice length requirements increase with increasing bar sizes. The increase in code-to-test ratios between the No. 15 and No. 20 bars of 25 percent is slightly less than the increase between the No. 20 and No. 25 bars of 30 percent. The code-to-test ratios for TMS 402-13 (MSJC 2013a) are all greater than one, and hence are all conservative.

The code-to-test calculated ratios of splice lengths, as presented in Table 4.8, should ideally be equal to one for each bar size in both CSA S304.1-04 (CSA 2004a) and TMS 402 (MSJC 2013a) to ensure the required splice lengths are sufficiently long that the tensile resistance of the splice corresponds to the yield strength of the reinforcement, with the included margin of safety, while also ensuring the provisions are not overly conservative and thus negatively impacting the ease of construction for masonry elements. As such, adjustments to each code are needed. Modifications to the current provisions of both codes are provided for walls subject to out of plane flexural loadings.

4.4.4 Recommended Changes to CSA S304.1-04

Two key changes are recommended for the CSA S304.1-04 (CSA 2004a) provisions, as discussed herein. These two changes pertain to the current distinction between classes of splices and the current bar size factor.

First, the CSA S304.1-04 (CSA 2004a) provisions should not include separate classes of splices. As discussed in Section 2.6, the rationale for the inclusion of Class A and Class B splices was not based on probabilities of bond failure, but to encourage designers to stagger lap splices (Darwin 2005). Since staggering lap splices is generally not feasible in masonry construction due to construction staging, no distinction should be made between classes of splices in revisions to the current provisions. As such, all further recommendations presented herein are based on the Class A requirements, such that the 1.3 factor for Class B splices can be removed and the provisions of CSA S304.1-04 (CSA 2004a) can be reworded to avoid making distinctions for different classes of lap splices.

Second, the bar size factor, k_3, then needs to be adjusted to increase the code-to-test calculated ratios for each bar size to unity. The current bar size factor of 0.8 for No. 15 bars is adequate, since the code-to-test ratio for No. 15 bars is 1.13. The current bar size factors for the No. 20 and 25 bars of 0.8 and 1.0, respectively, need to be increased since the code-to-test ratios for these bar sizes are less than one. An increase in the bar size factor to a value of 1.1 for the No. 20 bars results in an increase of the code-to-test ratio to 1.09. Setting the bar size factor for No. 25 bars to a value of 1.2 increases the code-to-test ratio to 1.04.

Based on these changes, the recommended expression for splice length requirements in CSA S304.1-04 (CSA 2004a) is:

$$l_d = 1.15 \frac{k_1 k_2 k_3}{(d_{cs} + K_{tr})} \frac{f_y}{\sqrt{f'_{gr}}} A_b \qquad \{4.5\}$$

$$k_3 = \begin{cases} 0.8 & \text{for No. 15 bars} \\ 1.1 & \text{for No. 20 bars} \\ 1.2 & \text{for No. 25 bars} \end{cases}$$

CSA S304.1-04 (CSA 2004a) provisions should be revised to include the specified compressive strength of the masonry assembly, f'_m, instead of the in-situ compressive strength of the grout, f'_{gr}, for the reasons stated in Section 2.6. However, further investigation is needed to establish the relationship between masonry assembly and grout compressive strengths for wall splice specimens. It is recommended that future research consider grout and masonry compressive strengths as factors for the tensile resistance of spliced reinforcement, similar to the approach taken by the NCMA (1999, 2009).

4.4.5 Recommended Changes to TMS 402-13

The code-to-test calculated ratios based on TMS 402-13 provisions (MSJC 2013a) for all three bar sizes are greater than unity, and hence are overly conservative. As such, an adjustment to the bar size factors was applied to set the code-to-test calculated ratios for all bar sizes equal to unity.

The current bar size factor, γ, in TMS 402-13 (MSJC 2013a) for the No. 15, 20, and 25 bar sizes are 1.0, 1.3, and 1.5, respectively. If these bar size factors are instead set equal

to 0.9 for No. 15 and 20 bars and 0.8 for No. 25 bars, the resulting code-to-test ratios for the No. 15, 20, and 25 bar sizes are then 1.12, 1.08, and 1.08, respectively. Consequently, the recommended expression for splice length requirements in TMS 402-13 (MSJC 2013a) is:

$$l_d = \frac{1.57 d_b^2 f_y \gamma}{K\sqrt{f'_m}} \quad (Metric) \qquad \{4.6\}$$

$$\gamma = \begin{cases} 0.9 & \text{for No. 15 bars} \\ 0.9 & \text{for No. 20 bars} \\ 0.8 & \text{for No. 25 bars} \end{cases}$$

4.4.6 Summary of Recommended Changes to Canadian and American Code Provisions

Figure 4.19 shows a comparison of the proposed revisions to CSA S304.1-04 (CSA 2004a) and TMS 402-13 (MSJC 2013a) and the current provisions of both of these codes. Notably, current CSA S304.1-04 (CSA 2004a) provisions require adjustments to the bar size factors for the No. 20 and 25 bar sizes based on the removal of splice classes, whereas the current TMS 402-13 (MSJC 2013a) provisions are too conservative for No. 20 and 25 bar sizes. The proposed revisions to TMS 402-13 (MSJC 2013a) result in shorter splice length requirements in comparison to the current requirements of this code. Decreases of 11.1, 44.4, and 87.5 percent for No. 15, 20, and 25 bars, respectively, result based on the proposed changes to TMS 402-13 (MSJC 2013a). The incorporation of the proposed changes to TMS 402-13 (MSJC 2013a) will greatly facilitate the construction of masonry walls with No. 20 and 25 reinforcement in particular. The proposed changes to CSA S304.1-04 (CSA 2004a) result in splice length requirements that are slightly less than the current Class B requirements, which are used almost exclusively for masonry construction.

The proposed revisions to both codes result in splice length requirements that are nearly identical, with percent differences of 0.981, 1.16, and 3.72 percent for No. 15, 20, and 25 bars, respectively. The slight percent differences between the proposed provisions are the result of rounding the proposed bar size factors for each bar size in each code, since all bar size factors were reported to one decimal place as is currently provided in each code.

It is expected that these provisions will provide splice lengths having tensile resistances of the reinforcement exceeding that corresponding to the nominal yield strength of the reinforcement for 95 percent of all splice lengths, on account of the five percent quantile approach used in the development of these revised code provisions.

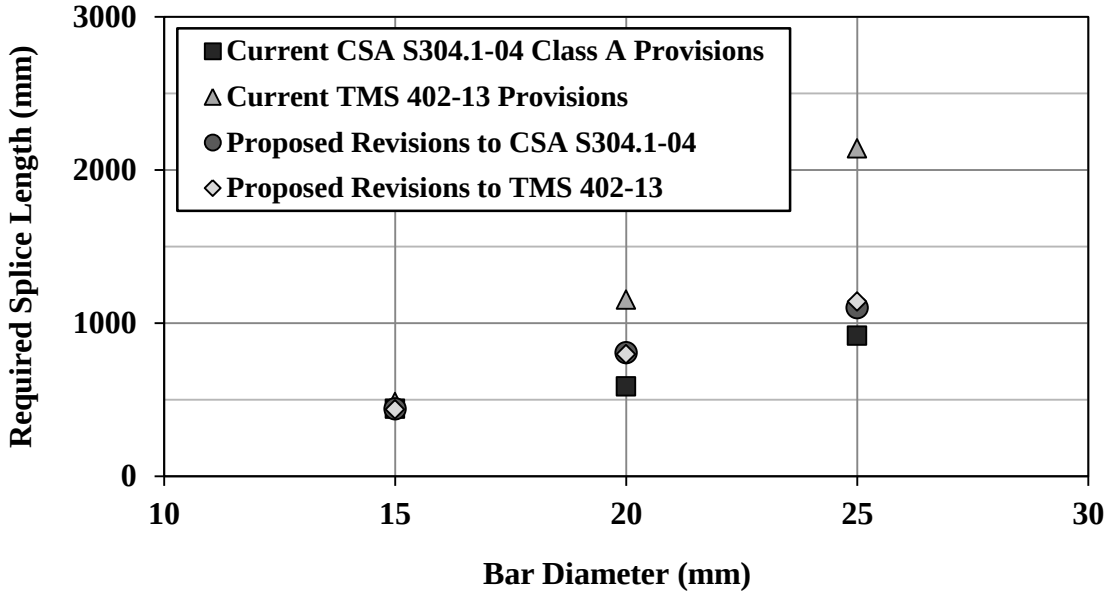

Figure 4.19: Splice requirements for recommended revisions to CSA S304.1-04 and TMS 402-13 provisions

4.5 Summary

This chapter described the test results and analysis of the companion specimens, wall splice specimens, and double pullout specimens constructed and tested in this study. Results from the testing of one DP-T specimen where approximately equal loads were applied by the hydraulic cylinders closely matched the failure load predicted by NCMA's (2009) equation, with a percent difference of 3 percent. The close agreement of the predicted and actual tensile resistance of the spliced reinforcement for this specimen suggests that the construction and testing techniques used at the U of S and NCMA are reasonably similar. Therefore, the test results from specimens constructed and tested at the U of S are valid for the assessment of code provisions, as presented in this chapter. It is also noted that the dependency of the test results for double pullout specimens on the

hydraulic cylinders and the test frame indicate that double pullout specimen testing is not easily repeatable, and is not recommended for future work for this reason.

The results from the testing of the wall splice specimens were presented in detail. The load-deflection behaviour, the visual assessment of crack propagation during testing, and the investigation of internal damage to the specimens after testing indicated that bond failures occurred for all wall splice specimens. The numerical model used to calculate the tensile resistance of the spliced reinforcement in the wall splice specimens was described. A regression analysis was then used to determine the tensile resistance of the spliced reinforcement as a function of splice length and bar size. This predictive equation was then adjusted to provide an adequate margin of safety using a five percent quantile approach, such that the resulting splice lengths calculated using this equation represent the lower 95 percent tolerance limit. This adjusted equation was then used to calculate the splice lengths that correspond to the yield strength of the reinforcement for each bar size. These splice lengths were then compared to those calculated using the relevant provisions included in current Canadian and American codes, and revisions to the splice length requirement equations in both codes were recommended.

CHAPTER 5 CONCLUSIONS AND RECOMMENDATIONS

In this study, 27 wall splice specimens and 12 double pullout specimens were constructed and tested. All specimens were constructed by a journeyman mason in the Structures Laboratory. Companion specimens of block, mortar, grout, masonry prisms, and reinforcing bar samples were tested in accordance with the standards relevant to each to determine the properties of these materials.

The double pullout specimens were tested in direct tension. The one double pullout specimen tested with approximately equal loads applied to both bars had a tensile resistance that was within 3 percent of the tensile resistance predicted by the NCMA equation (1999). Problems were encountered during the testing of the remaining double pullout specimens, however, as the loads applied by the two hydraulic cylinders differed substantially and out-of-plane buckling of the frame occurred.

Eighteen of the wall splice specimens were reinforced with No. 20 bars, and nine of the wall splice specimens were reinforced with No. 25 bars. The database for this research was bolstered by the inclusion of selected results of testing conducted by Sanchez & Feldman (2013) on wall splice specimens reinforced with No. 15 bars. The wall splice specimens were tested in four-point loading, with load and deflection data collected throughout the testing of each specimen. A numerical moment-curvature analysis was used to calculate the tensile resistance of the spliced reinforcement for each wall splice specimen. A predictive equation for the tensile resistance of the spliced reinforcement based on splice length and bar size was developed through regression analysis. This predictive equation was then adjusted using a five percent quantile approach to provide an adequate margin of safety for calculating design values of splice length requirements. This adjusted equation was extrapolated to find the design splice lengths corresponding to the nominal yield strength of the reinforcement. These splice lengths were then compared to current CSA S304.1-04 (CSA 2004a) and TMS 402-13 (MSJC 2013a) provisions for splice length requirements. Recommended changes to these current provisions were then presented.

Presented herein is a summary of the findings of this research.

5.1 Summary of Findings

The major findings of this study are presented herein, in response to each of the five specific objectives stated in Section 1.1.

5.1.1 Confirming U of S Construction and Testing Techniques are Reasonably Similar to Those of the NCMA

Double pullout specimens were tested in this study for the purpose of confirming that the construction and testing techniques at the University of Saskatchewan (U of S) and the NCMA are reasonably similar. The rationale for this comparison was to establish that results from testing at the U of S can legitimately be used to assess the adequacy of current code provisions that were based on NCMA (1999, 2009) results. The double pullout specimens constructed with lapped bars in contact and tied together are comparable to the specimens constructed by NCMA (1999, 2009), and thus the capacity for these specimens was compared to the predicted tensile capacity calculated based on NCMA's regression equation. The double pullout specimen constructed with bars tied together and tested with the small hydraulic cylinders that applied approximately equal loads to each bar had an experimental failure load of 181 kN. The predicted capacity was 176 kN, resulting in a 3 percent difference between the predicted and experimental capacities. Additionally, the average experimental failure load as reported for Ahmed's (2011) specimens constructed with contact lap splices was 89.7 kN while the predicted failure capacity was 92.0 kN. Similarly, a 3 percent difference resulted. The close agreement between these values indicates that construction and testing techniques used by the U of S and NCMA are reasonably similar.

5.1.2 Development of Empirical Predictive Equation for Tensile Resistance

A predictive equation for the tensile resistance of the spliced reinforcement was developed though a regression analysis of the results of wall splice specimen testing. It was determined that splice length and bar size were significant factors at the five percent confidence level. The form of the predictive equation is similar to that developed by the NCMA (2009). The inclusion of terms for the bar size resulted in a model with three parallel lines, one for each of the three bar sizes considered in this study. It was found

that the specimens with splice lengths resulting in the end of the splice coinciding with mortar bed joints of the wall demonstrated lower tensile resistances than the lines of best fit.

5.1.3 Quantifying Splice Lengths Needed to Develop Tensile Resistances Equal to the Yield Strength of the Reinforcement

The predictive equation discussed in Section 5.1.2 was then adjusted to provide an adequate margin of safety for determining design splice lengths. The adjustment was based on a five percent quantile approach, and considered both the variability of the test results themselves and the uncertainty associated with the predictive equation. The adjusted equation was then extrapolated to determine the splice lengths corresponding to the nominal yield strength of the reinforcement (with the inclusion of the aforementioned margin of safety). It was found that the splice lengths corresponding to the nominal yield strength of the reinforcement for No. 15, 20, and 25 bars were 390 mm, 740 mm, and 1060 mm, respectively.

5.1.4 Code-to-test Calculated Ratios of Splice Length

Code-to-test calculated ratios of splice lengths were calculated for CSA S304.1-04 (CSA 2004a) and TMS 402-13 (MSJC 2013a) by dividing the splice length requirements of each respective code by the required splice lengths calculated using the adjusted predictive equation. Code-to-test ratios less than one indicated code required splice lengths that are unconservative. It was found that the code-to-test calculated ratios for the CSA S304.1-04 (CSA 2004a) Class A provisions were 1.13, 0.793, and 0.865 for No. 15, 20, and 25 bars, respectively. The code-to-test ratio is greater than one and thus conservative for the No. 15 bars, but less than one and thus unconservative for No. 20 and 25 bars. The code-to-test calculated ratios for the CSA S304.1-04 (CSA 2004a) Class B provisions were 1.47, 1.03, and 1.12 for No. 15, 20, and 25 bars, respectively. The Class B provisions, which are used almost exclusively in the design of masonry elements, are thus conservative for all three bar sizes. The code-to-test ratios for the TMS 402-13 (MSJC 2013a) provisions were 1.24, 1.56, and 2.02 for No. 15, 20, and 25 bars, respectively. These provisions increase with increasing bar size, and are conservative since all ratios are greater than one.

5.1.5 Recommendations for Changes to Current Provisions

Changes were recommended for both the CSA S304.1-04 (CSA 2004a) and TMS 402-13 (MSJC 2013a) provisions for cases of masonry walls subject to out-of-plane flexural loading such that the resulting code-to-test ratios would be equal to one for all bar sizes. The bar size factors used in each code were adjusted for each bar size individually such that the code-to-test ratios were then equal to one, while leaving the current form of each equation intact. The recommended bar size factors for the CSA S304.1-04 (CSA 2004a) provisions, k_3, are 0.8, 1.1, and 1.2 for No. 15, 20, and 25 bar sizes, respectively. These recommendations are based on the current Class A provisions, such that the 1.3 factor for Class B splices can be eliminated and the provisions of CSA S304.1-04 can be reworded to avoid making distinctions for different classes of lap splices. The recommended bar size factors for the TMS 402-13 (MSJC 2013a) provisions, γ, are 0.9, 0.9, and 0.8 for No. 15, 20, and 25 bar sizes, respectively. These recommendations bring better consistency to the requirements of the two codes and thus ensure the safety, economy, and constructability of masonry walls.

Two additional recommendations were offered in regards to the CSA S304.1-04 (CSA 2004a) provisions. First, the provisions should not differentiate between Class A and B splices, since the staggering of lap splices is not practically feasible for masonry construction. As such, the recommendations made in this study were based on the current Class A requirements. Second, the provisions should be further revised to use the specified compressive strength of the masonry assembly, f'_m, instead of the in-situ compressive strength of the grout, f'_{gr}, as is currently used. Further investigation is needed to incorporate this modification.

5.2 Recommendations for Future Research

This study offered an initial investigation of the splice lengths required for the reinforcing bar sizes typically used in Canada. The following recommendations are offered for further research work exploring splice length requirements for reinforced masonry.

- All future experimental work examining splice length requirements for reinforced masonry should use wall splice specimens and not double pullout specimens. The double pullout specimens do not accurately replicate the stress state of the cementitious material surrounding the reinforcement for a wall in flexure. Additionally, the dependence of the results of double pullout specimen testing on the test frame, as seen in this study, limits the reliability of this test.

    - Further modifications to the test frame and test procedure would be needed to conduct any further investigations testing double pullout specimens. The beams that are formed from built-up channel sections should be replaced by steel I-beam sections for better resistance to bending and torsion during testing. Additionally, the test setup should incorporate a single actuator and spreader beam for applying loads to the two reinforcing bars protruding from the specimen, as opposed to the two cylinders applying loads independently as used in this study.

- The recommended changes to the current Canadian and American masonry code provisions are valid for flexural walls subject to out-of-plane loading. Further research should review the applicability of these recommendations for other masonry elements, particularly masonry shear walls. Tension uplift in shear walls is a concern in particular geographic locations where hurricanes and other such severe weather events occur. However, requirements for tension uplift should be considered a special case and evaluated separately due to the infrequent occurrence of this detail in most areas.

- Further investigation is needed to better capture the effects of splice ends coinciding with mortar bed joints on the tensile resistance of the reinforcement.
    - It was noted in this study that those specimens containing lap splices where the ends of the splice coincided with the mortar joints had lower tensile resistances than predicted by the best fit, predictive equation. However, the impact of this detail should be determined quantitatively such that recommendations for code provisions can be made.

- The possibility of testing wall splice specimens vertically should be considered. Testing specimens horizontally, as was done in this program, results in the self-weight of the specimen causing an additional moment on the specimen which would not otherwise be encountered by walls, which are built vertically. Testing wall splice specimens vertically would better represent walls constructed for real applications.

- The effect of transverse reinforcement was considered outside the scope of this study. The inclusion of transverse reinforcement, as used commonly in masonry construction, would likely improve the tensile resistance of the spliced reinforcement, as has been reported by others (NCMA 2009). As such, further testing investigating the effects of transverse reinforcement in wall splice specimens should be investigated.

- Most importantly, a full parametric investigation of splice length requirements is needed.
  - A future investigation should include a sufficient number of replicate specimens to establish the statistical significance of the reported tensile resistances of the spliced reinforcement. The inclusion of more replicate specimens will also improve the precision of the prediction and adjusted prediction equations used to compare the test results to current code provisions.
  - This study was limited in scope to one grout strength and one masonry assembly strength, one block strength and block density, one cover depth, and one block size. The effects of these three properties should be explored in a future investigation. Future studies should also consider the effects of partial grouting of the specimens, as is most common in masonry construction.
  - Testing of specimens with larger block sizes would be of particular significance for specimens reinforced with No. 25 bars. It was observed in this study that the specimens reinforced with No. 25 bars showed additional cracking patterns most likely resulting from the lower cover for these specimens. The recommended splice lengths provided based on this research may thus be conservative.

- Future studies should include No. 10 and No. 30 bar sizes, as both of these sizes are allowed by current code provisions, even if these bar sizes are used infrequently.

REFERENCES

Abrams, D.A. 1913. Tests of bond between concrete and steel. Bulletin No, 71, Engineering Experiment Station, University of Illinois, Urbana, IL.

Ahmadi, B.H. 2001. Effect of loss of bond in lap splices of flexurally loaded reinforced concrete masonry walls. Materials and Structures, **34**(8): 475-478.

Ahmed, K. 2011. Evaluation of contact and non-contact lap splices in concrete block masonry specimens. M.Sc. Thesis, Department of Civil and Geological Engineering, University of Saskatchewan, Saskatoon, SK.

Ahmed, K., & Feldman, L.R. 2012. Evaluation of contact and noncontact lap splices in concrete block masonry construction. Canadian Journal of Civil Engineering, **39**(5): 515-525.

American Concrete Institute (ACI). 2011. ACI 318-11: Building code requirements for structural concrete and commentary. ACI, Farmington Hills, MI.

American Concrete Institute (ACI) Committee 408. 2012. ACI 408R-03: Bond and development of straight reinforcing bars in tension. ACI, Farmington Hills, MI.

American Society for Testing and Materials (ASTM). 2012a. ASTM E178-08: Standard practice for dealing with outlying observations. ASTM International, West Conshohocken, PA.

American Society for Testing and Materials (ASTM). 2012b. ASTM C140-12a: Standard Test Methods for sampling and testing concrete masonry units and related units. ASTM International, West Conshokocken, PA.

American Society for Testing and Materials (ASTM). 2012c. ASTM C1019-11: Standard test method for sampling and testing grout. ASTM International, West Conshohocken, PA.

American Society for Testing and Materials (ASTM). 2012d. ASTM A370-12: Standard test methods and definitions for mechanical testing of steel products. ASTM International, West Conshohocken, PA.

Baynit, A.R. 1980. Bond and development length in reinforced concrete block masonry. M. Eng. thesis, Dept. of Civil and Environmental Engineering, Carleton University, Ottawa, ON.

Bischoff, P.H. 2005. Reevaluation of deflection prediction for concrete beams reinforced with steel and fibre reinforced polymer bars. ASCE Journal of Structural Engineering, **131**(5):752-767.

Bickis, M. 2014. Personal communication, April 8-21, 2014.

Branson, D.E. 1977. Deformation of concrete structures. McGraw-Hill, New York, NY.

Canadian Concrete Masonry Producers' Association (CCMPA). 2012. Physical properties of standard metric size block: size code 20. *In* CCMPA Metric Technical Manual. Available from http://www.ccmpa.ca/wp-content/uploads/2012/02/Final2013Sec4.pdf [accessed March 24, 2014].

Canadian Standards Association (CSA). 2009. CAN/CSA A23.2-09: Test methods and standard practices for concrete. CSA, Rexdale, ON, Canada.

Canadian Standards Association (CSA). 2004a. CAN/CSA S304.1-04: Design of masonry structures. CSA, Mississauga, ON, Canada.

Canadian Standards Association (CSA). 2004b. CAN/CSA A23.3-04: Design of concrete structures. CSA, Mississauga, ON, Canada.

Canadian Standards Association (CSA). 2004c. CAN/CSA A165-04: CSA standards on concrete masonry units. CSA, Mississauga, ON, Canada.

Canadian Standards Association (CSA). 2004d. CAN/CSA A179-04: Mortar and grout for unit masonry. CSA, Mississauga, ON, Canada.

Canadian Standards Association (CSA). 2004e. CAN/CSA A371-04: Masonry construction for buildings. CSA, Mississauga, ON, Canada.

Canbay, E., and Frosch, R.J. 2006. Design of lap-spliced bars: is simplification possible? ACI Structural Journal, **103**(3):444-451.

Chun, S.C., Lee, S.H., and Oh, B. 2011. Compression splices in high-strength concrete of 100 MPA (14,500 psi) and less. ACI Structural Journal, **108**(6):715-724.

Darwin, D. 2005. Tension development length and lap splice design for reinforced concrete members. Progress in Structural Engineering and Materials, **7**: 210-225.

Darwin, D., Zuo, J., Tholen, M.L., and Idun, E.K. 1996. Development length criteria for conventional and high relative rib area reinforcing bars. ACI Structural Journal, **93**(3):1-13.

Devore, J.L. 2008. Probability and statistics for engineering and the sciences (7th ed.). Thomson Brooks/Cole, Belmont, California.

Drysdale, R.G., and Hamid, A.A. 2005. Masonry structures: behaviour and design (Canadian edition). Canada Masonry Design Centre, Mississauga, ON.

Hammons, M.I., Atkinson, R.H., Schuller, M.P., & Tikalsky, P.J. 1994. Masonry research for limit states design. US Army Corps of Engineers Report CPAR-SL-94-1, Vicksburg, MI.

Hatzinikolas, M.A., and Korany, Y. 2005. Masonry design for engineers and architects. Canadian Masonry Publications, Edmonton, AB.

Hosney, A., Hatem, M.S., Rizkalla, S.H., and Zia, P. 2012. Development length of unconfined conventional and high-strength steel reinforcing bars. ACI Structural Journal, **109**(5):655-664.

Kisin, A. 2014. Evaluation of mitigative techniques for non-contact lap splices in concrete block construction. M.Sc. Thesis, Department of Civil and Geological Engineering, University of Saskatchewan, Saskatoon, SK.

Kisin, A., and Feldman, L.R. 2013. Construction solutions for non-contact lap splices in concrete block construction. *In* Proceedings of the 12th Canadian Masonry Symposium, Vancouver, British Columbia (electronic compendium), Vancouver, BC, 2-5 June 2013, 11 pp.

MacGregor, J.G., & Bartlett, F.M. 2000. Reinforced concrete: mechanics and design (1st Canadian edition). Prentice Hall Canada Inc., Toronto, ON.

Masonry Standards Joint Committee (*TMS, ACI, and ASCE*). 2013a. TMS 402-13/ACI 530-13/ASCE 5-13: Building code requirements and specification for masonry structures. MSJC, Boulder CO.

Masonry Standards Joint Committee (MSJC) (*TMS, ACI, and ASCE*). 2013b. TMS 602-13/ACI 530.1-13/ASCE 6-13: Specification for masonry structures. MSJC, Boulder CO.

Masonry Standards Joint Committee (MSJC) (*TMS, ACI, and ASCE*). 2011. TMS 402-11/ACI 530-11/ASCE 5-11: Building code requirements and specification for masonry structures. MSJC, Boulder CO.

Masonry Standards Joint Committee (MSJC) (*TMS, ACI, and ASCE*). 2008. Building code requirements and specification for masonry structures. The Masonry Society, Boulder CO, ACI, Farmington Hills, MI, and Structural Engineering Institute of the American Society of Civil Engineers, Reston, VA.

Masonry Standards Joint Committee (MSJC) (*TMS, ACI, and ASCE*). 1995. AC1 530-95/ASCE 5-95/TMS 402-95: Building code requirements for masonry structures. ACI, Farmington Hills, MI.

Mirza, S.A., and Skrabek, B.W. 1991. Reliability of short composite beam-column strength interaction. ASCE Journal of Structural Engineering, **117**(8):2320-2339.

National Concrete Masonry Association (NCMA). 2009. Effects of confinement reinforcement on bar splice performance – summary of research and design recommendations. NCMA, Herndon, VA.

National Concrete Masonry Association (NCMA). 1999. Evaluation of minimum reinforcing bar splice criteria for hollow clay brick and hollow concrete block masonry. NCMA, Herndon, VA.

Orangun, C.O., Jirsa, J.O., & Breen, J.E. 1977. A reevaluation of test data on development length and splices. Journal of the American Concrete Institute, **74**(11): 114-122.

Pillai, S.U., Kirk, D.U., & Erki, M.A. 2008. Reinforced concrete design (4th ed.). McGraw-Hill Ryerson Limited, Toronto, ON.

Priestly, M.J.N., and Elder, D.M. 1983. Stress-strain curves for unconfined and confined concrete masonry. ACI Journal, **80**(19):192-201.

Ross, S.M. 2009. Introduction to probability and statistics for engineers and scientists. Elsevier Academic Press, Amsterdam, Netherlands.

Sanchez, D.S. 2014. The effect of splice length and distance between lapped reinforcing bars in concrete block specimens. M.Sc. Thesis, Department of Civil and Geological Engineering, University of Saskatchewan, Saskatoon, SK.

Sanchez, D.S., and Feldman, L.R. 2013. The effect of splice length and distance between lapped reinforcing bars in concrete block specimens. *In* Proceedings of the 12th Canadian Masonry Symposium, Vancouver, British Columbia (electronic compendium), Vancouver, BC, 2-5 June 2013, 11 pp.

Scollard, C.R., & Barlett, F.M. 2004. Impact of new ACI 318 flexural resistance factor on bond failures. ASCE Journal of Structural Engineering, **130**(1): 138-146.

Suter, G.T., and Fenton, G.A. 1985. Splice length tests of reinforced masonry walls. *In* Proceedings of the 3rd American Masonry Conference, Arlington, TX, 3-5 June 1985, pp. 68.1-68.14.

Uniat, D.B. 1983. Lap splices of deformed bars in reinforced concrete block masonry walls. M.Eng. thesis, Dept. of Civil and Environmental Eng., Carleton University, Ottawa, ON.

Watanabe. 1985. Bond and anchorage of reinforcement in masonry. Proceedings of the First Joint Technical Coordinating Committee on Masonry Research, U.S.-Japan Coordinated Program for Masonry Building Research, Tokyo, Japan, 10 pp.

APPENDIX 4A: BLOCK COMPANION SPECIMENS

This appendix presents individual test results for all masonry block companion specimens tested in this study, as discussed in Section 4.1.1. The blocks for the first construction phase were received in two batches, referred to as batches A and B in all subsequent tables. Table 4A-1 presents the compressive strength testing results for each individual block tested. Six specimens of each block type, flat and frogged, were tested for the two batches from Phase 1 and the single batch from Phase 2, in accordance with ASTM C140 (ASTM 2012b). These specimens are labelled by the letters A through F in Table 4A-1. Table 4A-2 presents the results of absorption testing. Three specimens of each block type, flat and frogged, were tested for the two batches from Phase 1 and the single batch from Phase 2, in accordance with ASTM C140 (ASTM 2012b). Table 4A-3 presents the actual as-measured dimensions for blocks. Figure 4A-1 shows the dimensions of the blocks that were measured. Three specimens of each block type, flat and frogged, were tested for the two batches from Phase 1 and the single batch from Phase 2, in accordance with ASTM C140 (ASTM 2012b). Dimensions were measured to the nearest 0.01 mm using calipers. The minimum face shell and web thicknesses of 32 mm and 26 mm, respectively, as specified by the Canadian Concrete Masonry Producers' Association (CCMPA 2012) were met for all blocks.

Table 4A-1. Block Compressive Strength Testing Results

Phase	Block Type	Compressive Strength (MPa)						Avg. Comp. Strength (MPa)	COV (%)
		Spec. A	Spec. B	Spec. C	Spec. D	Spec. E	Spec. F		
1 Batch A	Flat	19.9	18.8	22.4	18.2	21.7	18.4	19.7	10.6%
	Frog.	22.5	21.1	20.5	17.4	19.9	15.7		
1 Batch B	Flat	23.9	20.6	27.7	24.3	18.1	24.6	23.6	11.0%
	Frog.	21.7	24.3	24.9	24.6	21.9	26.2		
2	Flat	28.6	27.3	26.8	26.3	25.9	26.8	27.4	5.12%
	Frog.	30.0	29.2	25.1	28.3	26.9	27.3		

Table 4A-2. Block Absorption Testing Results

Phase	Specimen		Oven-Dry Density [kg/m^3]	Moisture Content [%]	Net Volume [mm^3]
1 Batch A	Frogged	Spec. A	1850	11.9%	7300000
		Spec. B	1890	12.9%	7420000
		Spec. C	1870	10.3%	7390000
	Avg.		1870	11.7%	7370000
	Flat	Spec. A	1890	10.3%	7400000
		Spec. B	1960	21.2%	7440000
		Spec. C	1880	9.43%	7410000
	Avg.		1910	13.6%	7420000
1 Batch B	Frogged	Spec. A	1870	25.8%	7400000
		Spec. B	1870	35.1%	7340000
		Spec. C	1880	5.00%	7360000
	Avg.		1870	22.0%	7370000
	Flat	Spec. A	1870	17.9%	7440000
		Spec. B	1890	3.96%	7370000
		Spec. C	1860	33.2%	7370000
	Avg.		1870	18.3%	7400000
2	Frogged	Spec. A	1870	21.8%	7390000
		Spec. B	1920	27.5%	7340000
		Spec. C	1910	25.9%	7330000
	Avg.		1900	25.1%	7350000
	Flat	Spec. A	1860	20.1%	7450000
		Spec. B	1900	21.1%	7490000
		Spec. C	1900	22.5%	7510000
	Avg.		1890	21.2%	7480000

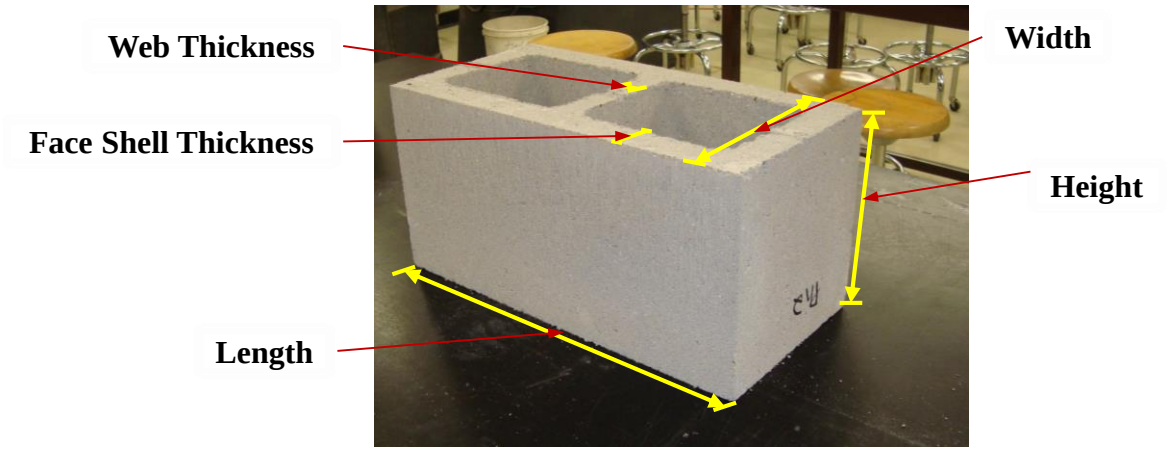

Figure 4A-1. Dimensions of masonry blocks

Table 4A-3. Block Dimension Testing Results

Phase	Specimen	Width (mm)			Height (mm)			Length (mm)			Face Shell Thickness (mm)			Web Thickness (mm)
		Top	Bottom	Avg.	Front	Back	Avg.	Front	Back	Avg.	Front	Back	Avg.	
1 Batch A	Frogged	190.30	190.42	190.36	194.15	194.01	194.08	390.0	391.0	390.5	32.38	34.13	33.26	27.96
		190.71	190.22	190.47	191.66	191.77	191.72	390.0	390.0	390.0	32.6	33.57	33.09	28.3
		190.40	190.10	190.25	191.49	189.70	190.60	390.0	391.5	390.8	31.9	34.92	33.41	28.24
	Avg.			190.36			192.13			390.4			33.25	28.17
	Flat	191.00	190.65	190.83	192.02	192.44	192.23	390.0	389.5	389.8	33.28	34.08	33.68	27.13
		190.49	190.95	190.72	190.79	191.00	190.90	390.0	390.0	390.0	33.08	34	33.54	26.96
		191.97	190.97	191.47	191.57	191.75	191.66	390.0	390.5	390.3	33.52	34.27	33.90	27.49
	Avg.			191.01			191.60			390.0			33.71	27.19
1 Batch B	Frogged	189.96	190.24	190.10	190.37	189.91	190.14	390.0	391.0	390.5	33.19	33.2	33.20	28.4
		189.69	190.51	190.10	189.58	189.14	189.36	390.5	391.5	391.0	33.71	33.38	33.55	28.61
		190.28	190.26	190.27	189.66	188.73	189.20	390.0	390.5	390.3	33.19	33.35	33.27	28.4
	Avg.			190.16			189.57			390.6			33.34	28.47
	Flat	190.87	190.78	190.83	190.82	189.75	190.29	390.5	390.0	390.3	33.15	33.9	33.53	27.48
		191.12	190.68	190.90	190.13	190.47	190.30	390.0	391.0	390.5	33.81	33.34	33.58	27.43
		190.77	190.59	190.68	190.09	189.25	189.67	390.0	390.5	390.3	33.12	34.06	33.59	27.33
	Avg.			190.80			190.09			390.3			33.56	27.41
2	Frogged	190.17	190.27	190.22	191.50	190.16	190.83	391.0	390.0	390.5	30.99	35.04	33.02	28.16
		190.09	190.46	190.28	190.95	191.00	190.98	390.0	390.0	390.0	31.15	35.08	33.12	28.34
		189.61	190.19	189.90	191.05	190.17	190.61	390.0	390.5	390.3	35.54	30.94	33.24	28.41
	Avg.			190.13			190.81			390.3			33.12	28.30
	Flat	191.12	191.11	191.12	191.01	190.24	190.63	390.0	390.0	390.0	33.65	34.08	33.87	27.14
		191.58	191.16	191.37	190.51	190.93	190.72	390.0	390.0	390.0	34.56	33.05	33.81	27.7
		191.96	191.14	191.55	190.16	190.36	190.26	390.0	390.0	390.0	34.81	33.07	33.94	27.61
	Avg.			191.35			190.54			390.0			33.87	27.48

APPENDIX 4B: MORTAR CUBE COMPANION SPECIMENS

Presented herein are the individual test results for all mortar cube companion specimens tested in this study, as discussed in Section 4.1.3. Six mortar cubes were cast for each batch of mortar produced, and these specimens are designated by the letters A through F in the subsequent tables. Table 4B-1 details the compressive strength results for the 18 batches of mortar produced in the first construction phase, including the compressive strength of each of the six mortar cubes tested and the average compressive strength of each batch. Table 4B-2 similarly details the compressive strength results for the 16 batches of mortar produced in the second construction phase.

Table 4B-1. Phase 1 Mortar Cube Compressive Strength Testing Results

Batch Number	Compressive Strength (MPa)						Average Compressive Strength (MPa)
	Spec. A	Spec. B	Spec. C	Spec. D	Spec. E	Spec. F	
1	10.6	10.8	10.5	10.7	11.5	10.3	10.7
2	15.6	16.4	16.2	16.5	15.2	15.5	15.9
3	28.6	25.2	25.2	25.3	24.7	26.8	26.0
4	19.8	19.2	18.1	20.4	20.3	25.7	20.6
5	21.1	21.4	22.9	21.1	20.8	20.3	21.3
6	16.8	18.3	15.1	17.2	18.7	16.4	17.1
7	21.6	21.4	20.4	19.6	19.9	18.8	20.3
8	16.3	20.1	20.8	22.7	23.4	22.6	21.0
9	16.5	18.4	18.9	21.0	18.4	19.9	18.9
10	22.4	23.5	23.2	20.6	20.5	21.9	22.0
11	27.6	25.2	24.8	25.7	24.7	25.3	25.6
12	21.1	22.7	22.0	22.2	23.0	23.6	22.4
13	17.6	18.4	17.0	17.9	17.8	18.1	17.8
14	13.6	13.0	12.4	13.1	15.3	14.3	13.6
15	24.6	23.9	22.2	25.2	23.4	23.5	23.8
16	25.4	23.5	26.4	25.6	24.3	n/a[1]	25.0
17	21.6	22.8	22.8	23.5	24.1	23.9	23.1
18	23.6	23.9	29.1	30.9	27.7	31.8	27.8
Average (MPa)							20.7
COV (%)							21.6%

[1]Data was not saved for this specimen and is thus excluded from the calculated average.

Table 4B-2. Phase 2 Mortar Cube Compressive Strength Testing Results

Batch Number	Compressive Strength (MPa)						Average Compressive Strength (MPa)
	Spec. A	Spec. B	Spec. C	Spec. D	Spec. E	Spec. F	
1	26.9	24.8	26.2	25.5	23.3	25.9	25.4
2	21.9	20.9	21.1	24.2	23.6	22.6	22.4
3	19.5	20.2	20.3	20.8	21.9	20.2	20.5
4	19.7	20.5	20.8	19.0	17.9	21.0	19.8
5	23.2	23.8	22.5	24.5	27.3	24.3	24.3
6	20.4	21.1	22.9	22.2	24.6	20.6	22.0
7	17.4	20.7	21.9	18.8	20.6	17.8	19.5
8	20.4	19.6	21.8	24.2	23.6	21.4	21.8
9	19.4	20.9	20.4	17.4	18.6	18.3	19.2
10	21.6	22.8	23.7	22.7	30.3	29.7	25.1
11	18.4	20.0	20.0	21.0	21.4	19.9	20.1
12	20.4	22.1	21.4	22.0	25.8	26.8	23.1
13	22.3	20.4	21.4	19.3	20.9	20.4	20.8
14	21.7	22.7	22.2	19.3	21.8	22.2	21.7
15	33.0	28.6	33.3	32.6	32.1	30.3	31.6
16	27.1	27.6	29.4	27.4	27.0	27.1	27.6
Average (MPa)							22.8
COV (%)							14.7%

APPENDIX 4C: GROUT CYLINDER COMPANION SPECIMENS

Presented herein are individual test results for the grout cylinder companion specimens tested in both phases of construction, as discussed in Section 4.1.4. Three grout cylinders were cast for each batch of grout produced, and these specimens are designated by the letters A through C in the subsequent tables. Table 4C-1 details the compressive strength results for the 34 batches of grout produced in the first construction phase, including the compressive strength of each of the three grout cylinders tested and the average compressive strength of each batch. Table 4C-2 similarly presents the Phase 2 grout cylinder compressive strength testing results.

Table 4C-1. Phase 1 Grout Cylinder Compressive Strength Testing Results

Batch Number	Compressive Strength (MPa)			Avg. Comp. Strength (MPa)
	Specimen A	Specimen B	Specimen C	
1	12.6	12.2	12.6	12.5
2	10.9	11.8	12.1	11.6
3	11.5	14.2	15.7	13.8
4	15.4	13.8	17.2	15.5
5	13.4	9.91	11.1	11.5
6	13.7	9.01	14.5	12.4
7	15.7	5.50[1]	8.69	12.2
8	14.3	16.7	15.9	15.6
9	3.40[1]	3.40[1]	3.51[1]	3.44
10	9.2	4.39[1]	12.3	10.7
11	11.3	10.3	12.0	11.2
12	10.8	9.46	12.7	11.0
13	13.0	11.5	11.5	12.0
14	11.0	10.8	9.32	10.4
15	12.0	10.9	8.84	10.6
16	2.45[2]	2.63[2]	2.28[2]	2.45
17	10.7	8.40	8.93	9.36
18	n/a[3]	11.8	11.1	11.4
19	11.3	11.2	9.69	10.7
20	9.75	7.72	9.73	9.07
21	9.44	10.5	10.6	10.2
22	10.1	11.8	11.0	11.0
23	13.0	8.73	8.74	10.2
24	11.3	12.7	11.7	11.9
25	12.3	13.7	13.3	13.1
26	11.8	11.7	11.2	11.5
27	8.02	11.1	13.8	11.0
28	11.6	12.4	13.0	12.4
29	13.0	8.5	11.1	10.9
30	11.1	13.0	11.7	12.0
31	12.4	11.5	13.0	12.3
32	12.1	13.5	11.8	12.4
33	11.8	11.4	11.6	11.6
34	12.7	9.54	12.2	11.5
Average (MPa)				11.7
COV (%)				12.3%

[1]Specimen identified as physical outlier due to sulphur cap that was not adequately bonded to the grout cylinder or was slanted, and excluded from the calculated averages.
[2]Specimens identified as statistical outlier using ASTM E178 (ASTM 2012a) procedures, thus excluded from the calculated averages.
[3]Data was not saved for this specimen, and it was thus excluded from the calculated averages.

Table 4C-2. Phase 2 Grout Cylinder Compressive Strength Testing Results

Batch Number	Compressive Strength (MPa)			Avg. Comp. Strength (MPa)
	Specimen A	Specimen B	Specimen C	
1	10.0	15.3	13.2	12.8
2	14.3	14.1	13.4	13.9
3	15.5	14.3	11.0	13.6
4	11.5	13.4	12.2	12.4
5	12.3	15.4	12.3	13.3
6	17.4	13.5	12.7	14.5
7	12.2	13.9	15.0	13.7
8	15.8	n/a[1]	16.2	10.7
9	14.3	13.5	13.0	13.6
10	17.0	15.8	10.8	14.6
11	13.9	16.3	16.3	15.5
12	13.6	13.9	14.9	14.1
13	13.6	10.4	12.7	12.3
14	24.6	27.3	25.2	25.7
15	17.0	17.9	18.4	17.7
16	16.4	18.8	17.0	17.4
17	15.8	15.6	19.2	16.8
18	16.7	16.1	20.3	17.7
19	16.8	12.6	18.5	16.0
20	16.0	18.4	15.6	16.7
21	14.2	17.5	n/a[1]	15.8
22	19.2	n/a[1]	15.4	17.3
23	16.3	17.0	15.2	16.2
24	18.2	18.9	18.8	18.6
25	17.0	15.4	16.8	16.4
26	16.6	16.2	16.5	16.4
27	20.2	20.1	20.8	20.4
28	17.1	16.8	20.4	18.1
29[2]	31.7[2]	31.5[2]	26.1[2]	29.8
30	16.5	18.5	16.8	17.2
31	22.5	20.8	21.0	21.4
32	23.0	23.2	20.9	22.3
33	18.1	17.8	15.6	17.2
Average (MPa)				16.9
COV (%)				22.0%

[1]Specimen was not tested on account of damage to specimen prior to testing, and was thus excluded from the calculated averages.

[2]Batch identified as physical outlier due to higher cement content included in this mixture.

APPENDIX 4D: GROUT PRISM COMPANION SPECIMENS

Presented herein are individual test results for all grout prism companion specimens tested in this study, as discussed in Section 4.1.5. Table 4D-1 presents the compressive strength results for the grout prisms cast and tested in Phase 1. Table 4D-2 presents the results for the grout prisms cast and tested in Phase 2.

Table 4D-1. Phase 1 Grout Prism Compressive Strength Testing Results

Batch Number	Compressive Strength (MPa)
1	12.0
2	9.84
3	12.1
4	15.6
5	11.6
6	11.0
7	12.2
8	13.5
9	7.11
10	11.9
11	12.8
12	12.2
13	11.7
14	12.0
15	12.9
16[1]	5.16[1]
17	11.8
18	14.5
19	12.0
20	10.7
21	14.5
22	12.1
23	11.6
24	12.3
25	11.4
26	11.7
27	14.4
28	12.2
29	12.0
30	10.6
31	13.1
32	14.4
33	15.9
34	12.7
Average (MPa)	12.3
COV (%)	13.5%

[1]Specimen was identified as a statistical outlier using ASTM E178 (ASTM 2012a) procedures and was thus excluded from the calculated average.

Table 4D-2. Phase 2 Grout Prism Compressive Strength Testing Results

Batch Number	Compressive Strength (MPa)
1	17.4
2	17.1
3	16.8
4	17.1
5	16.7
6	18.0
7	19.6
8	16.1
9	13.2
10	19.4
11	18.2
12	16.8
13	15.5
14	27.0
15	17.9
16	19.4
17	16.5
18	20.4
19	15.8
20	21.9
21	20.1
22	15.6
23	14.1
24	18.2
25	19.1
26	17.9
27	21.4
28	21.8
29	29.0[1]
30	21.3
31	23.0
32	23.0
33	22.0
Average (MPa)	19.0
COV (%)	17.6%

[1]Specimen was identified as physical outlier due to higher cement content included in this mixture.

APPENDIX 4E: REINFORCEMENT COMPANION SPECIMENS

Presented herein are the test results for all reinforcing bar companion specimens, as discussed in Section 4.1.7. Table 4E-1 presents the results of individual bar tests from Phase 1. Nine specimens of each bar size from Phase 1 were tested, although reliable LVDT data through the strain-hardening region was only obtained for two specimens of each bar size. Table 4E-2 presents the results of individual bar tests from Phase 2. Six specimens of each bar size from Phase 2 were tested, and reliable LVDT data was obtained for four and five of the No. 20 and 25 bar sizes, respectively. No physical or statistical outliers were identified for either phase.

Table 4E-1. Phase 1 Reinforcement Testing Results

Bar Size	Spec. No.	Yield Strength, f_y (MPa)	Modulus of Elasticity, E_s (GPa)	Strain at Initiation of Strain Hardening, ε_{sh}	Modulus at Init. of Strain Hardening, E_{sh} (MPa)	Ultimate Tensile Strength, f_{ult} (MPa)
No. 20	1	437	200	n/a[1]	n/a[1]	601
	2	439	n/a[1]	n/a[1]	n/a[1]	595
	3	439	203	n/a[1]	n/a[1]	606
	4	445	201	n/a[1]	n/a[1]	598
	5	443	n/a[1]	n/a[1]	n/a[1]	605
	6	451	n/a[1]	n/a[1]	n/a[1]	611
	7	443	203	n/a[1]	n/a[1]	601
	8	441	205	0.0125	10000	600
	9	440	202	0.0145	4170	598
	Avg.	442	202	0.0135	7080	602
	COV	0.961%	0.759%	10.5%	58.2%	0.811%
No. 25	1	476	207	0.0185	5360	633
	2	482	207	n/a[1]	n/a[1]	640
	3	480	n/a[1]	n/a[1]	n/a[1]	643
	4	476	n/a[1]	n/a[1]	n/a[1]	637
	5	474	n/a[1]	n/a[1]	n/a[1]	636
	6	483	n/a[1]	n/a[1]	n/a[1]	647
	7	481	n/a[1]	n/a[1]	n/a[1]	639
	8	476	207	0.0150	5880	641
	9	477	n/a[1]	n/a[1]	n/a[1]	641
	Avg.	478	207	0.0168	5620	640
	COV	0.631%	0.0789%	14.8%	6.61%	0.625%

[1]LVDT data not available

Table 4E-2. Phase 2 Reinforcement Testing Results

Bar Size	Spec. No.	Yield Strength, f_y (MPa)	Modulus of Elasticity, E_s (GPa)	Strain at Initiation of Strain Hardening, ε_{sh}	Modulus at Init. of Strain Hardening, E_{sh} (MPa)	Ultimate Tensile Strength, f_{ult} (MPa)
No. 20	1	428	n/a[1]	n/a[1]	n/a[1]	586
	2	428	206	0.0110	3750	582
	3	428	211	n/a[1]	n/a[1]	586
	4	430	200	0.0117	6100	582
	5	432	200	0.0133	4810	583
	6	428	n/a[1]	n/a[1]	n/a[1]	580
	Avg.	429	204	0.0120	4890	583
	COV	0.406%	2.50%	9.82%	24.1%	0.412%
No. 25	1	466	208	0.0115	n/a[1]	622
	2	468	211	0.0128	4690	625
	3	469	200	0.0120	4060	625
	4	467	208	0.0130	4560	620
	5	467	182	n/a[1]	n/a[1]	625
	6	470	197	0.0135	4350	626
	Avg.	468	201	0.0126	4420	624
	COV	0.320%	5.36%	6.38%	6.20%	0.357%

[1]LVDT data not available

APPENDIX 4F: LOAD-DEFLECTION CURVES FOR WALL SPLICE SPECIMENS

Presented herein are the load versus midspan deflection curves for all wall splice specimens constructed and tested in this study. Figure 4F-1(a) shows the load versus midspan deflection curves for replicates 1, 2, and 3 of the W200(No.20)-2.5 specimen configuration. Figure 4F-1(b) shows the load versus midspan deflection curves for replicates 4, 5, and 6 of the W200(No.20)-2.5 specimen configuration. Figure 4F-2(a) shows the load versus midspan deflection curves for replicates 1, 2, and 3 of the W200(No.20)-3.5 specimen configuration. Figure 4F-2(b) shows the load versus midspan deflection curves for replicates 4, 5, and 6 of the W200(No.20)-3.5 specimen configuration. Figures 4F-3 through 4F-7 show the load versus midspan deflection curves for the three replicates (1, 2, and 3) of the remaining wall splice specimen configurations.

The loops seen in the load-deflection curves of specimens W200(No.20)-2.5-1,2,3, W200(No.20)-3.5-1,2,3, and W250(No.20)-2.5-1,2,3 are the result of an error in the load application for one actuator. This loading error was similarly observed by Kisin (2014) in the testing of three wall splice specimens. One actuator would overshoot its load target. The control program would cause the actuator to retract momentarily in response to the overshooting, causing the loops seen in the data. However, the load-deflection curves still follow a linear relationship when the loops are excluded, which matches the behaviour seen for all other wall splice specimens. Thus, this control error did not significantly impact the results of the testing of these specimens. This control error affected the first nine wall splice specimens tested in Phase 1, after which the problem was detected. The control program was then adjusted to remediate this error for the testing of the remaining six specimens tested in Phase 1 and all 12 specimens tested in Phase 2.

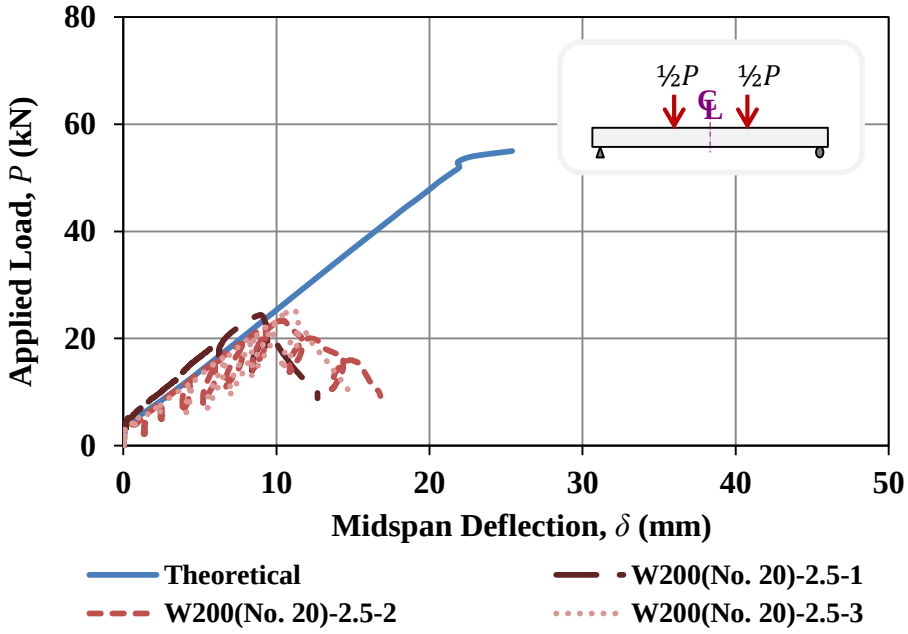

a)

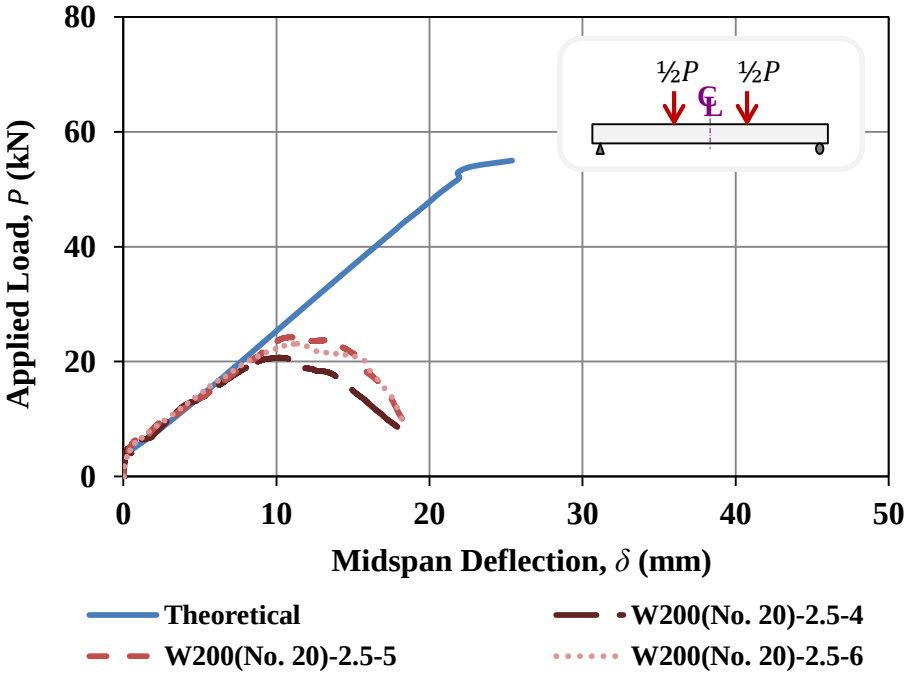

b)

Figure 4F-1. Load versus midspan deflection curve for W200(No.20)-2.5 specimens: a) replicates 1, 2, and 3, and b) replicates 4, 5, and 6

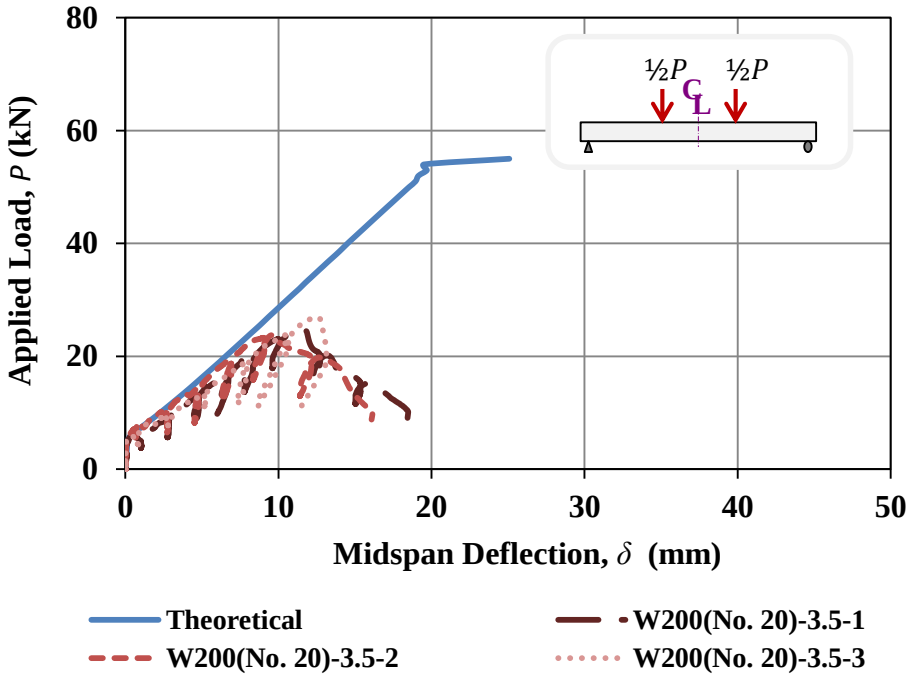

a)

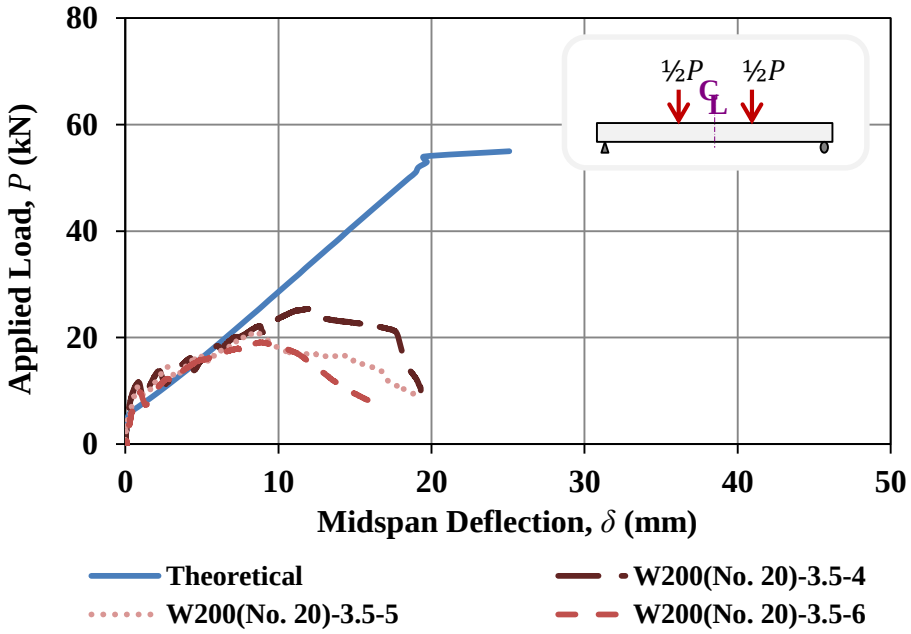

b)

Figure 4F-2. Load versus midspan deflection curve for W200(No.20)-3.5 specimens: a) replicates 1, 2, and 3, and b) replicates 4, 5, and 6

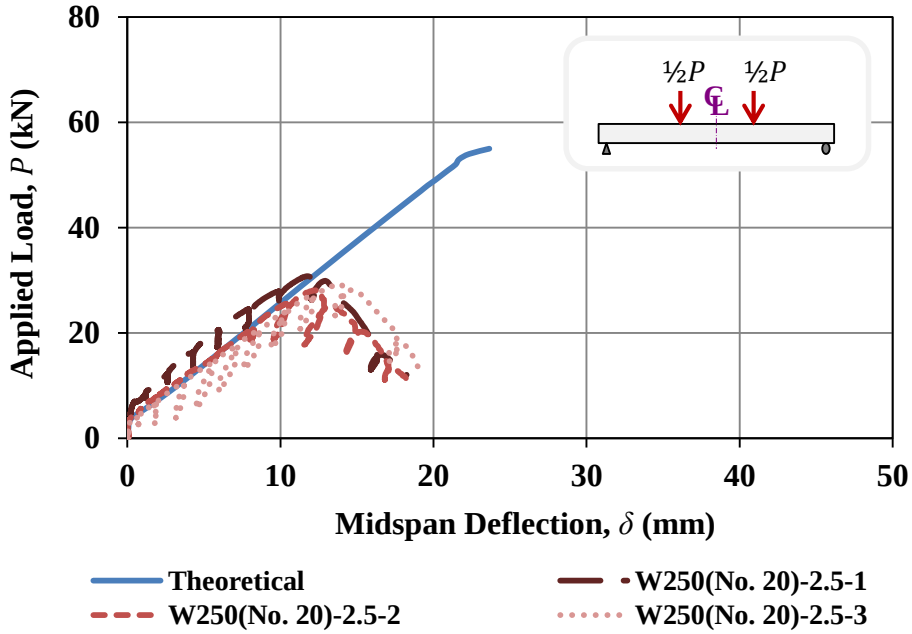

Figure 4F-3. Load versus midspan deflection curve for the W250(No.20)-2.5 specimen configuration

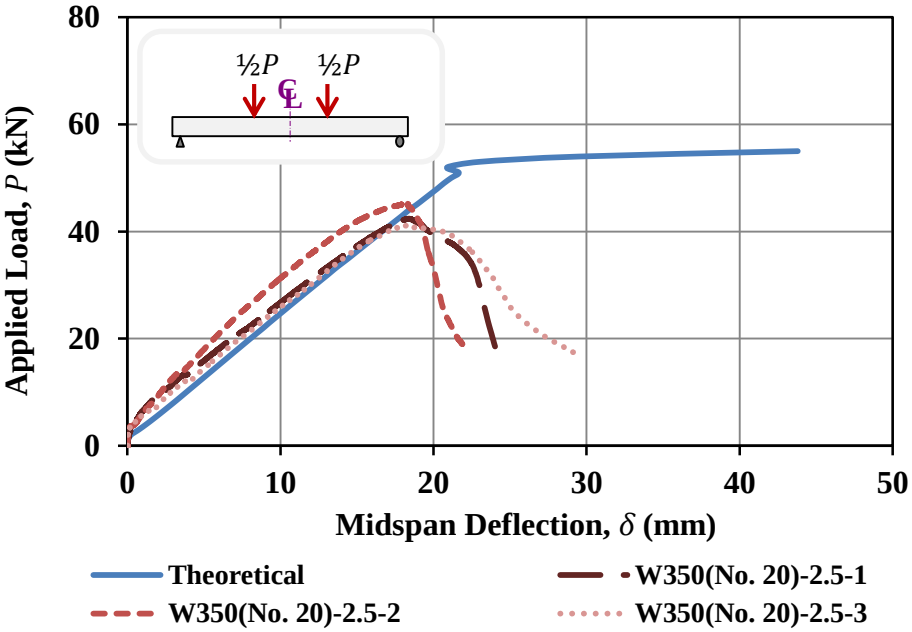

Figure 4F-4. Load versus midspan deflection curve for the W350(No.20)-2.5 specimen configuration

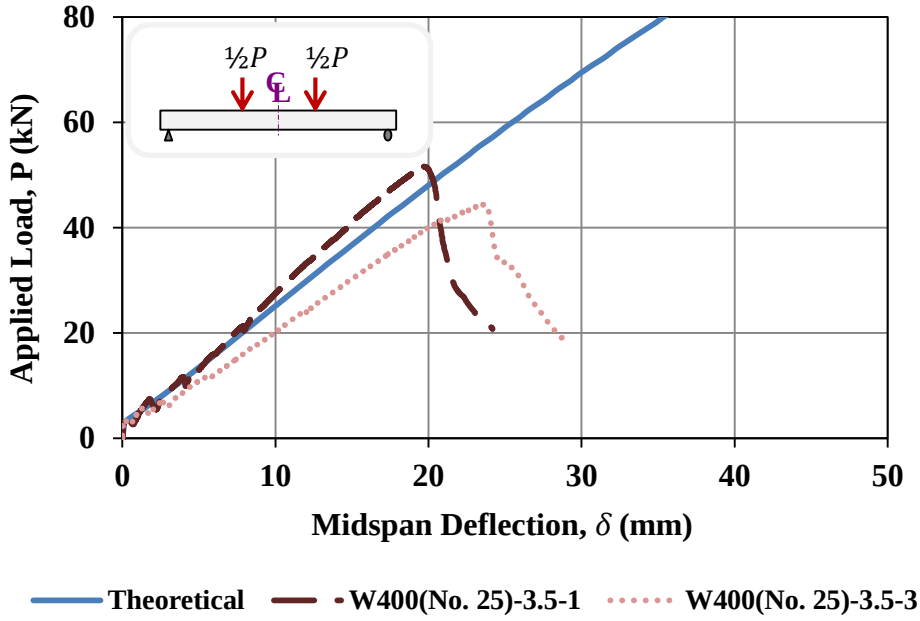

Figure 4F-5. Load versus midspan deflection curve for the W400(No.25)-3.5 specimen configuration

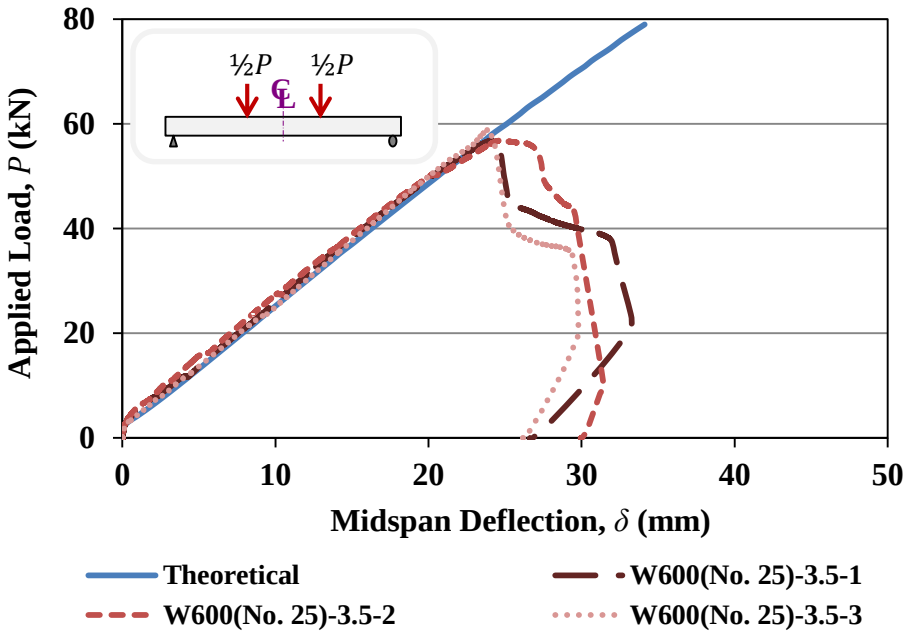

Figure 4F-6. Load versus midspan deflection curve for the W600(No.25)-3.5 specimen configuration

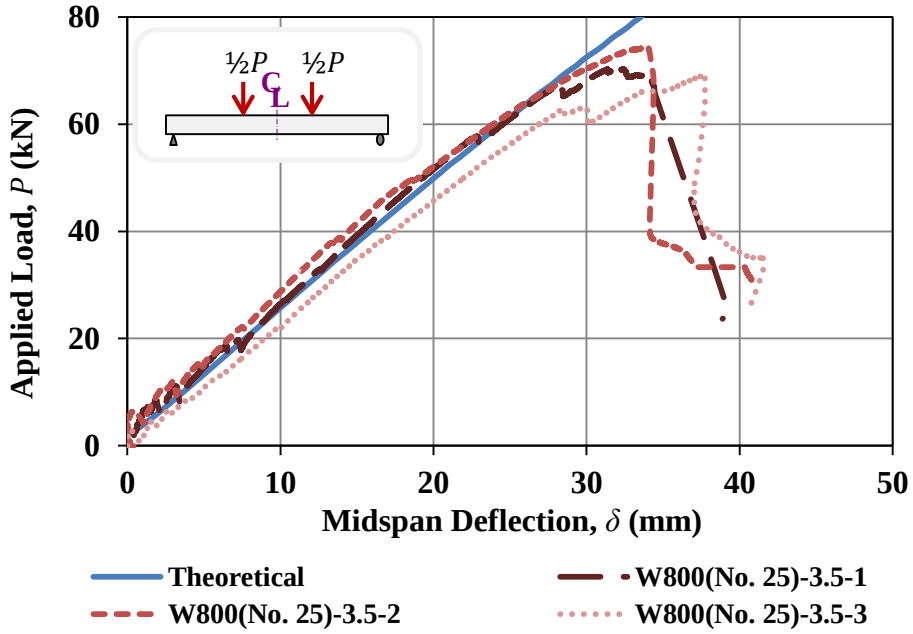

Figure 4F-7. Load versus midspan deflection curve for the W800(No.25)-3.5 specimen configuration

APPENDIX 4G: AS-MEASURED LAP SPLICE LENGTHS AND TRANSVERSE BAR SPACINGS FOR WALL SPLICE SPECIMENS

Table 4G-1 shows the as-measured lap splice lengths and transverse bar spacings for the two lap splices in each wall splice specimen. These dimensions were measured for each lap splice in each specimen using a ruler or tape measure after removal of the face shell and grout to the depth of the reinforcement, as discussed in Section 4.3.3.

The percent difference between the tensile resistance of the reinforcement for each individual specimen and the average tensile resistance of the reinforcement for the replicates of that specimen's configuration was calculated. Figure 4G-1 shows the percent difference in tensile resistance versus the difference between the nominal and actual lap splice lengths for splices 1 and 2 in all wall splice specimens. A consistent trend was not evident. The CSA A371-04 (CSA 2004e) reinforcement placement tolerance of 13 mm was met for the actual splice lengths of all but three specimens. Specimen W350(No.20)-2.5-3 had one lap splice that was 15 mm shorter than designed, and specimen W600(No.25)-3.5-1 had lap splices that were 15mm and 20 mm shorter than designed. However, the W350(No.20)-2.5-3 and W600(No.25)-3.5-1 specimens had percent differences in tensile resistance of the reinforcement of 1.70 percent and 0.434 percent, respectively. Thus, the nominal lap splice length values were used for all specimens.

Figure 4G-2 shows the percent difference in tensile resistance versus the difference between the nominal and actual transverse spacing for splices 1 and 2 in all wall splice specimens. A consistent pattern trend was not found.

Table 4G-1. Actual Lap Splice Lengths and Transverse Bar Spacings for Wall Splice Specimens

Test Specimen	Actual Splice Length, l_s (mm)		Actual Transverse Spacing, S_t (mm)	
	Splice 1	Splice 2	Splice 1	Splice 2
W200(No. 20)-2.5-1	193	198	5	15
W200(No. 20)-2.5-2	199	198	7	8
W200(No. 20)-2.5-3	202	204	11	6
W200(No. 20)-2.5-4	190	195	15	10
W200(No. 20)-2.5-5	n/a[1]	195	11	13
W200(No. 20)-2.5-6	203	197	12	8
W200(No. 20)-3.5-1	200	194	8	7
W200(No. 20)-3.5-2	204	200	11	10
W200(No. 20)-3.5-3	197	198	9	10
W200(No. 20)-3.5-4	195	198	2	11
W200(No. 20)-3.5-5	195	190	10	7
W200(No. 20)-3.5-6	195	197	7	1
W250(No. 20)-2.5-1	253	254	1	8
W250(No. 20)-2.5-2	245	249	10	12
W250(No. 20)-2.5-3	245	243	12	7
W350(No. 20)-2.5-1	n/a[1]	350	3	5
W350(No. 20)-2.5-2	338	n/a[1]	7	15
W350(No. 20)-2.5-3	345	335	10	8
W400(No. 25)-3.5-1	400	403	8	15
W400(No.25)-3.5-2	n/a[1]	n/a[1]	n/a[1]	n/a[1]
W400(No. 25)-3.5-3	401	398	11	5
W600(No. 25)-3.5-1	580	585	7	8
W600(No. 25)-3.5-2	595	590	1	3
W600(No. 25)-3.5-3	590	595	5	8
W800(No. 25)-3.5-1	805	805	8	9
W800(No. 25)-3.5-2	795	795	8	8
W800(No. 25)-3.5-3	810	n/a[1]	14	n/a[1]

[1]Measurement could not be determined because of damage to specimen that occurred during transportation of specimen or jackhammering of specimen.

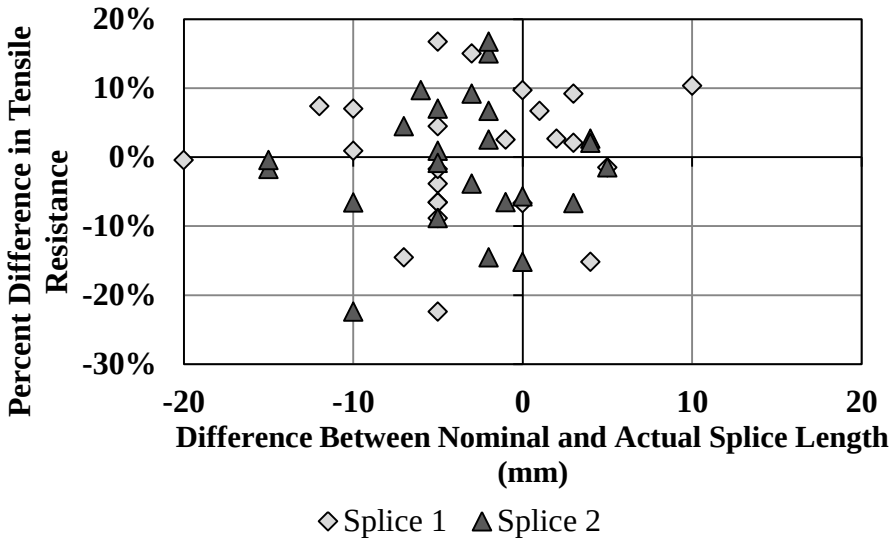

Figure 4G-1. Percent difference in tensile resistance versus difference between nominal and actual splice length

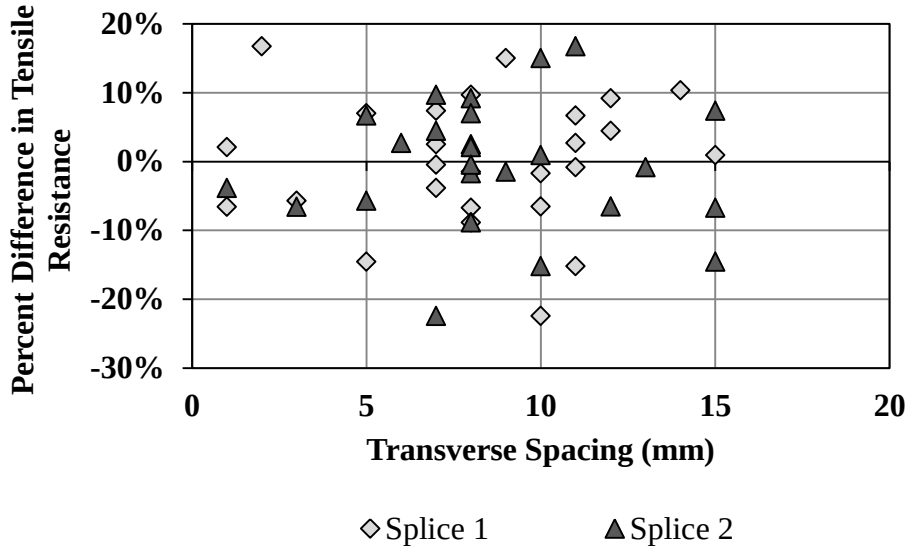

Figure 4G-2. Percent difference in tensile resistance versus actual transverse spacing

APPENDIX 4H: MOMENT-CURVATURE ANALYSIS AND THEORETICAL LOAD-DEFLECTION CURVES FOR WALL SPLICE SPECIMENS

Presented herein is a description of the numerical moment-curvature model used to determine the tensile resistance of the spliced reinforcement and the theoretical load-deflection curves for the wall splice specimens. This appendix elaborates on the remarks given in Section 4.3.4; as noted, the model is similar to that used by Ahmed (2011), Sanchez (2014), and Kisin (2014). The MathCAD code used to conduct this numerical analysis is included for a representative sample, W200(No.20)-2.5-1, and is presented on page 151 and onward.

Stress-Strain Relationship for Masonry

The stress-strain relationship for the masonry was modelled using a modified Kent-Park curve (Priestly & Elder 1983), as discussed in Section 4.3.4. This curve includes a parabolic rising curve, presented in Equation 4H.1a, and a linear falling curve, presented in Equation 4H.1b. The stress in the masonry, f_m, at a given strain ε_m, is calculated as:

$$f_m(\varepsilon_m) = K_o f'_{mt}\left[\left(\frac{2\varepsilon_m}{\varepsilon_o K_o}\right) - \left(\frac{\varepsilon_m}{\varepsilon_o K_o}\right)^2\right],\ \varepsilon_m < \varepsilon_o \qquad \{4H.1a\}$$

$$f_m(\varepsilon_m) = K_o f'_{mt}[1 - Z(\varepsilon_m - \varepsilon_o K)],\ \ \varepsilon_o < \varepsilon_m \le 0.01, \qquad \{4H.1b\}$$

$$Z = \frac{0.5}{\left[\frac{3 + 0.29 f'_m}{145 f'_{mt} - 1000}\right] - \varepsilon_o K_o}$$

where K_o is a strength enhancement coefficient, equal to 1.0 for unconfined masonry with no transverse reinforcement provided, f'_{mt} is the compressive strength of the masonry assembly determined from masonry prism testing (MPa), and ε_o is the strain corresponding to the maximum stress, equal to 0.0020 as originally proposed by Kent & Park (Priestly & Elder 1983).

Stress-Strain Relationship for Reinforcing Steel

The stress-strain relationship for the reinforcement was modelled by assuming a linear rising segment to represent its elastic region, presented in Equation 4H.2a, a straight line

corresponding to the yield plateau, presented in Equation 4H.2b, and a parabolic segment corresponding to the strain-hardening region for the reinforcement, presented in Equation 4H.2c. The stress in the reinforcement, f_s, at a given strain ε_s, is calculated as follows:

$$f_s(\varepsilon_s) = E_s\varepsilon_s \text{ , for } \varepsilon_s < \varepsilon_y \quad \{4H.2a\}$$

$$f_s(\varepsilon_s) = f_y \text{ , for } \varepsilon_y \leq \varepsilon_s < \varepsilon_{sh} \quad \{4H.2b\}$$

$$f_s(\varepsilon_s) = A'_1 + A'_2\varepsilon_s + A'_3{\varepsilon_s}^2 + A'_4{\varepsilon_s}^3 \text{ , for } \varepsilon_{sh} \leq \varepsilon_s \leq \varepsilon_{ult} \quad \{4H.2c\}$$

where ε_y is the yield strain of the reinforcement, E_s is the elastic modulus of the reinforcement, f_y is the yield strength of the reinforcement (MPa), ε_{sh} is the strain in the reinforcement at the initiation of strain-hardening, and ε_{ult} is the strain in the reinforcement at its ultimate strength. The constants A'_1, A'_2, A'_3, and A'_4 in equation **4H.2**c were determined based on the following boundary conditions:

$$f_s(\varepsilon_{sh}) = f_y \quad \{4H.3a\}$$

$$f_s(\varepsilon_{ult}) = f_{ult} \quad \{4H.3b\}$$

$$f_s'(\varepsilon_{sh}) = E_{sh} \quad \{4H.3c\}$$

$$f_s'(\varepsilon_{ult}) = 0 \quad \{4H.3d\}$$

where f_{ult} is the ultimate strength of the reinforcement (MPa), and E_{sh} is the instantaneous slope at the initiation of strain-hardening (MPa). The properties of the reinforcement used in this numerical model were determined based on testing of reinforcing bar companion specimens, as presented in Table 4.4.

Moment-Curvature Relationship for Uncracked Section

The curvature for the uncracked section, φ_{uc}, is given by:

$$\varphi_{uc} = \frac{M_a}{E_m I_g} \quad \{4H.4\}$$

where M_a is the applied moment, E_m is the elastic modulus of the masonry calculated in accordance with CSA S304.1-04 (CSA 2004a), and I_g is the moment of inertia of the

gross section calculated from the dimensions of the wall splice specimen. Equation 4H.4 is valid for applied moments less than the cracking moment, M_{cr}. As such, the curvature at the initiation of cracking, φ_{cr}, is given by:

$$\varphi_{cr} = \frac{M_{cr}}{E_m I_g} \qquad \{4H.5\}$$

Moment-Curvature Relationship for Cracked Section

A sectional analysis was used to determine the moment-curvature relationship and the tensile resistance of the spliced reinforcement for each wall splice specimen. The neutral axis depth, kd, was assumed, from which the strain in the extreme compressive fibre of the masonry, ε_{cm}, could be determined based on the assumed linear strain distribution and the given curvature, φ, as follows:

$$\varepsilon_{cm} = \varphi \cdot kd \qquad \{4H.6\}$$

The compressive zone was then divided into 100 segments, each having a thickness of $kd/100$. The centroid of the i^{th} segment was located at a distance of d_i from the neutral axis, where:

$$d_i = \frac{kd}{100}(i - 0.5), \qquad i \in 1,2 \ldots 100 \qquad \{4H.7\}$$

The strain at centroid of the i^{th} segment, ε_i, was then determined from the linear strain distribution as:

$$\varepsilon_i = \varepsilon_{cm} \cdot \frac{d_i}{kd} \qquad \{4H.8\}$$

The compressive stress in the i^{th} segment, σ_i was then found using the modified Kent-Park curve described above, where:

$$\sigma_i = f_m(\varepsilon_i) \qquad \{4H.9\}$$

The resultant compressive force for each segment was then calculated by multiplying the stress in the segment by the area of the segment, and the total compressive force in the masonry was then calculated by summating the compressive forces for each segment:

$$C = \sum_{i=1}^{i=100} \sigma_i \cdot \left(\frac{kd}{100}\right) \quad \{4H.10\}$$

The strain at the effective depth of the reinforcement, d_{eff}, equal to 95 mm, was calculated based on the linear strain distribution also:

$$\varepsilon_s = \frac{\varepsilon_{cm}}{kd} \cdot \left(d_{eff} - kd\right) \quad \{4H.11\}$$

from which the tensile force in the reinforcement was determined based on the nominal bar area of the reinforcement, A_s, and the theoretical stress-strain relationship (Equation 4H.3).

$$T = A_s \cdot f_s(\varepsilon_s) \quad \{4H.12\}$$

These calculations were conducted iteratively until the difference between the tensile force in the reinforcement and the resultant compressive force in the masonry was less than or equal to 0.5 percent. The tensile resistance of the spliced reinforcement at a given curvature, $T_r(\varphi)$, was then calculated by dividing the tensile force in the reinforcement calculated as per Equation 4H.12 by two, such that the tensile resistances are reported for an individual splice. The resulting moment at a given curvature was calculated by the following equation:

$$M = T \cdot \left[d_{eff} - kd + \frac{b \cdot kd \cdot \sum_{i=1}^{i=100}(i \cdot d_i)}{b \cdot kd \cdot \sum_{i=1}^{i=100} i}\right] \quad \{4H.13\}$$

Equation 4H.13 was used to create a database of corresponding moment and curvature values by calculating the moment corresponding to curvatures in 0.0001m^{-1} increments for 300 points. The function $\varphi_m(M)$ was then created to calculate the curvature corresponding to a given moment, M, for the cracked section, using the database of

corresponding moments and curvatures. This function was used to linearly interpolate between the curvature and corresponding moment values in the database to find the curvature corresponding to the moment entered as the argument to the function.

The error in the calculated moments corresponding to a given curvature based on the selection of 100 segments was evaluated. Figure 4H-1 shows the moment corresponding to a fixed curvature of 0.025 m^{-1} for a representative specimen W200(No.20)-2.5-1 as calculated for 50, 100, 200, 300, 400, 500, 600, 700, 800, 900, and 1000 segments. The moment at this given curvature approaches an approximate asymptotic value of 14.035 kN·m, found graphically from Figure 4H-1. The moment calculated based on 100 segments was equal to 14.025 kN·m. The error associated with the selection of 100 segments was therefore 0.07 percent. The error associated with the selection of 100 segments was also calculated for the 15 course walls. The error associated with selecting 100 segments at a fixed curvature of 0.025 m^{-1} for a representative specimen was 0.08 percent.

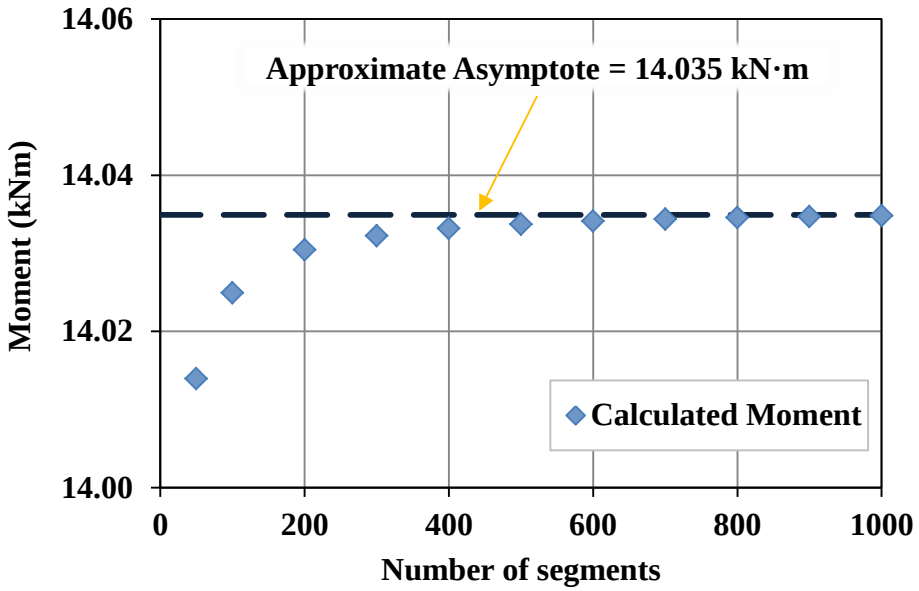

Figure 4H-1. Moment corresponding to a curvature of 0.025 m^{-1} based on number of segments, for representative sample W200(No.20)-2.5-1

Theoretical Load-Deflection Curve

The theoretical load versus midspan deflection relationship for all wall splice specimens were then determined based on the conjugate beam method, using the process described herein.

The moment of inertia of the cross-section of the wall splice specimen was needed in order to compute deflections using the conjugate beam method. The moment of inertia for the uncracked section was set equal to the gross moment of inertia for the cross section, calculated using the wall splice specimen dimensions. Bischoff's (2005) equation was used to determine the effective moment of inertia for moments greater than the cracking moment, as described in Section 4.3.4:

$$I_{eff} = \frac{I_{cr}}{1 - \left(1 - \frac{I_{cr}}{I_g}\right)\left(\frac{M_{cr}}{M_a}\right)^2} \qquad \{4H.14\}$$

where I_{cr} is the fully cracked section moment of inertia, I_g is the moment of inertia of the gross cross section, M_{cr} is the cracking moment, and M_a is the applied moment. Equation 4H.14 can be rearranged as shown by Ahmed (2011) to obtain an equation for the effective curvature, φ_e, at a given applied moment:

$$\varphi_e = \varphi_m(M_a) \cdot \left[1 - \left(\frac{M_{cr}}{M_a}\right)^2\right] + \frac{M_a}{E_m \cdot I_g}\left(\frac{M_{cr}}{M_a}\right)^2 \qquad \{4H.15\}$$

where $\varphi_m(M_a)$ is the curvature at a given moment, M_a, calculated using the function $\varphi_m(M)$ for the moment-curvature relationship for the cracked section, as described above.

The wall was divided into segments that were 10 mm wide for the purpose of calculating the theoretical midspan deflection, δ_{mid}, for a given applied load, P. Therefore, the 13 course and 15 course walls were divided into 240 segments and 280 segments, respectively. The moment at the middle of the i^{th} segment, M_{ai}, was calculated from basic principles of statics. The curvature at the middle of the i^{th} segment, φ_i, was

calculated using Equation 4H.4 if M_{ai} was less than M_{cr} or Equation 4H.15 if M_{ai} was greater than M_{cr}. The midspan deflection was then calculated as:

$$\delta_{mid} = 10\ mm \cdot \sum_{i=1}^{n/2} \varphi_i l_i \qquad \{4H.16\}$$

where n is the number of segments, equal to 240 and 280 for the 13 course and 15 course walls, respectively, and l_i is the distance from the centerline of the left support of the wall to the middle of the i^{th} segment.

The error in the applied loads as calculated using this numerical method based on the selection of the number of segments was evaluated for both heights of wall splice specimens. Figure 4H-2 shows the midspan deflection corresponding to an applied load of 30 kN for representative specimen W200(No.20)-2.5-1 as calculated for 24, 48, 120, 240, 480, and 960 segments. The midspan deflection at this applied load level approaches an asymptotic value of approximately 12.6022 mm, found graphically from Figure 4H-2. The midspan deflection calculated using 240 segments was equal to 12.6020 mm. The error associated with the selection of 240 segments was therefore 0.002 percent. Similarly, the error associated with the selection of 280 segments for the 15 course walls was 0.000 percent. Thus, the calculated midspan deflection values were relatively insensitive to the selection of the number of segments.

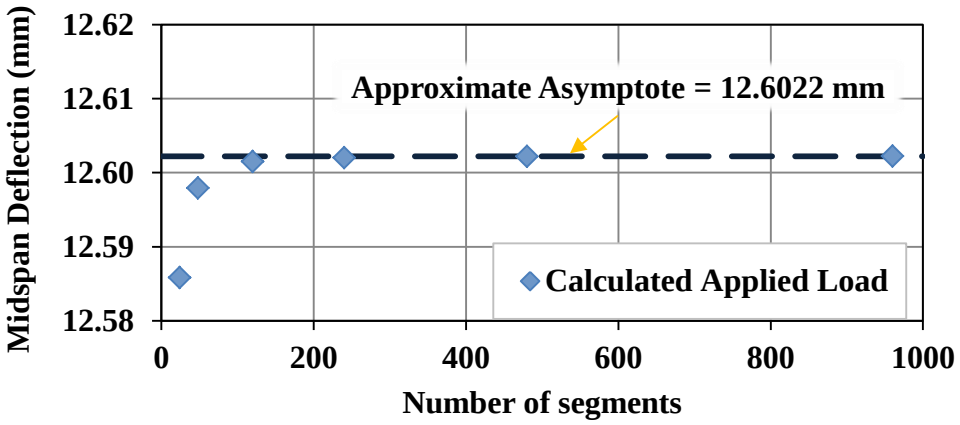

Figure 4H-2. Midspan deflection corresponding to an applied load of 30 kN based on number of segments, for representative sample W200(No.20)-2.5-1

MATHCAD CODE

Properties/Inputs:

Specimen Dimensions $b := 990mm \quad t := 190mm \quad l_m := 2400mm$

Moment of inertia for gross section: $I_g := \frac{1}{12} \cdot b \cdot t^3 = 5.659 \times 10^8 \cdot mm^4$

Loading point location: $a := \frac{1}{3} l_m = 800 \cdot mm$

Effective depth of reinforcement: $d_{eff} := 95mm$

Masonry compressive strength: $f'_{mt} := 11.05MPa$

Masonry modulus of elasticity: $E_m := 850 \cdot f'_{mt} = 9.393 \cdot GPa$

Cracking load and moment: $P_{cr} := 4.00kN \qquad M_{cr} := \frac{P_{cr} \cdot a}{2} = 1.6 \cdot kN \cdot m$

Curvature at initation of cracking: $\varphi_{cr} := \frac{M_{cr}}{E_m \cdot I_g} = 3.01 \times 10^{-4} \frac{1}{m}$

Area of steel: $A_s := 600mm^2$

Steel tensile properties: $E_s := 202GPa \quad f_y := 442MPa \quad \varepsilon_y := \frac{f_y}{E_s} = 2.188 \times 10^{-3}$

$\varepsilon_{sh} := 0.0135 \quad E_{sh} := 7084MPa \quad \varepsilon_{ult} := 0.1 \quad f_{ult} := 602MPa$

Curvature at maximum load: $\varphi_{max} := 2 \cdot 0.0069668 \cdot \frac{1}{m} = 0.0139 \frac{1}{m}$

Number of segments for compression zone in moment-curvature calculations: $n_{seg} := 100$

Length of segments of beam in conjugate beam calculations: $l_{seg} := 10mm$

Stress-Strain Relationship for Masonry

$$\varepsilon_o := 0.0020 \quad K_o := 1.0 \quad Z := \frac{0.5}{\left(\frac{3 + 0.29 \cdot \frac{f'_{mt}}{MPa}}{145 \frac{f'_{mt}}{MPa} - 1000}\right) - 0.002 K_o} = 60.225$$

Stress-Strain Curve:

$$f_m(\varepsilon_m) := \begin{cases} fm \leftarrow K_o \cdot f'_{mt} \cdot \left[2 \cdot \frac{\varepsilon_m}{\varepsilon_o \cdot K_o} - \left(\frac{\varepsilon_m}{\varepsilon_o \cdot K_o}\right)^2\right] & \text{if} \quad \varepsilon_m \le \varepsilon_o \\ fm \leftarrow K_o \cdot f'_{mt} \cdot \left[1 - Z \cdot \left(\varepsilon_m - \varepsilon_o \cdot K_o\right)\right] & \text{if} \quad \varepsilon_o < \varepsilon_m \le 0.01 \\ fm \leftarrow 0MPa \quad \text{if} \quad \varepsilon_m > 0.01 \\ fm \end{cases}$$

$$\varepsilon_m := 0 , 0.0001 .. 0.015$$

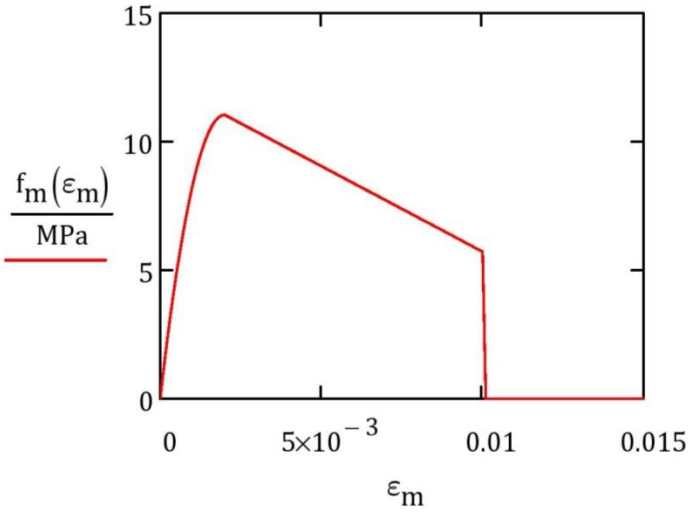

Stress-Strain Relationship for Steel

Boundary Conditions:

$$f_s(\varepsilon_{sh}) = f_y \qquad f'_s(\varepsilon_{sh}) = E_{sh} \qquad f'_s(\varepsilon_{ult}) = 0MPa \qquad f_s(\varepsilon_{ult}) = f_{ult}$$

Constants for strain-hardening curve:

$$A' := \begin{pmatrix} 1 & \varepsilon_{sh} & \varepsilon_{sh}^2 & \varepsilon_{sh}^3 \\ 1 & \varepsilon_{ult} & \varepsilon_{ult}^2 & \varepsilon_{ult}^3 \\ 0 & 1 & 2\varepsilon_{sh} & 3\varepsilon_{sh}^2 \\ 0 & 1 & 2\varepsilon_{ult} & 3\varepsilon_{ult}^2 \end{pmatrix}^{-1} \cdot \begin{pmatrix} f_y \\ f_{ult} \\ E_{sh} \\ 0 \end{pmatrix} = \begin{pmatrix} 327.094 \\ 1.002 \times 10^4 \\ -1.18 \times 10^5 \\ 4.523 \times 10^5 \end{pmatrix} \cdot MPa$$

Stress-Strain Curve:

$$f_s(\varepsilon_s) := \left| \begin{array}{l} fs \leftarrow E_s \cdot \varepsilon_s \quad \text{if} \quad \varepsilon_s < \varepsilon_y \\ fs \leftarrow f_y \quad \text{if} \quad \varepsilon_y < \varepsilon_s \le \varepsilon_{sh} \\ fs \leftarrow A'_1 + A'_2 \cdot \varepsilon_s + A'_3 \cdot \varepsilon_s^2 + A'_4 \cdot \varepsilon_s^3 \quad \text{if} \quad \varepsilon_{sh} < \varepsilon_s \le \varepsilon_{ult} \\ fs \leftarrow 0MPa \quad \text{if} \quad \varepsilon_s > \varepsilon_{ult} \\ fs \end{array} \right.$$

$$\varepsilon_s := 0 , 0.0001 .. 0.11$$

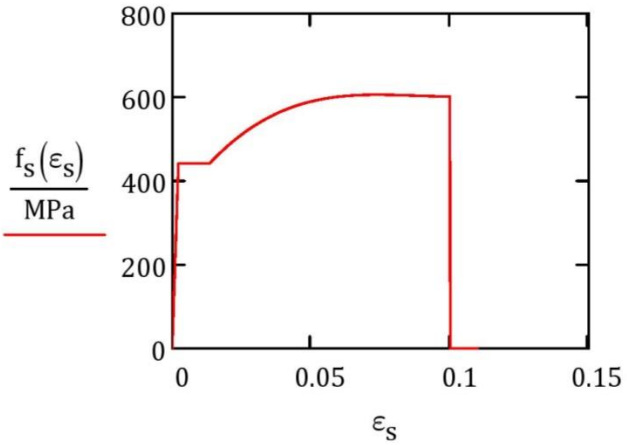

Tension in reinforcement as a function of curvature:

$$T_r(\varphi) := \left| \begin{array}{l} \text{for} \quad kd \in 90mm , 89.9mm .. 0mm \\ \quad \left| \begin{array}{l} \varepsilon_{cm} \leftarrow \varphi \cdot kd \\ C \leftarrow 0kN \\ \text{for} \quad i \in 1 , 2 .. n_{seg} \\ \quad \left| \begin{array}{l} d_i \leftarrow \dfrac{kd}{n_{seg}} \cdot (i - 0.5) \\ \varepsilon_i \leftarrow \varepsilon_{cm} \cdot \dfrac{d_i}{kd} \\ \sigma_i \leftarrow f_m(\varepsilon_i) \\ C \leftarrow C + \sigma_i \cdot b \cdot \dfrac{kd}{n_{seg}} \end{array} \right. \\ fs \leftarrow f_s\left[\dfrac{\varepsilon_{cm}}{kd} \cdot (d_{eff} - kd)\right] \\ T \leftarrow A_s \cdot fs \\ kd_f \leftarrow kd \quad \text{if} \quad \dfrac{|C - T|}{T} \leq 0.005 \end{array} \right. \\ \varepsilon_{cm\_f} \leftarrow kd_f \cdot \varphi \\ \varepsilon_{s\_f} \leftarrow \dfrac{\varepsilon_{cm\_f}}{kd_f} \cdot (d_{eff} - kd_f) \\ T \leftarrow A_s \cdot f_s(\varepsilon_{s\_f}) \\ \dfrac{T}{2} \end{array} \right.$$

$$T_r(\varphi_{max}) = 48.6 \cdot kN$$

Moment as a function of curvature for cracked section:

$$
\begin{aligned}
M(\varphi) := \ & \text{if} \quad \varphi > 0\text{m}^{-1} \\
& \quad \text{for} \quad kd \in 90\text{mm}, 89.9\text{mm} .. 0\text{mm} \\
& \quad\quad \varepsilon_{cm} \leftarrow \varphi \cdot kd \\
& \quad\quad C \leftarrow 0\text{kN} \\
& \quad\quad \text{for} \quad i \in 1, 2 .. n_{seg} \\
& \quad\quad\quad d_i \leftarrow \frac{kd}{n_{seg}} \cdot (i - 0.5) \\
& \quad\quad\quad \varepsilon_i \leftarrow \frac{\varepsilon_{cm}}{kd} \cdot d_i \\
& \quad\quad\quad \sigma_i \leftarrow f_m\left(\varepsilon_i\right) \\
& \quad\quad\quad C \leftarrow C + \sigma_i \cdot b \cdot \frac{kd}{n_{seg}} \\
& \quad\quad fs \leftarrow f_s\left[\frac{\varepsilon_{cm}}{kd} \cdot \left(d_{eff} - kd\right)\right] \\
& \quad\quad T \leftarrow A_s \cdot fs \\
& \quad\quad kd_f \leftarrow kd \quad \text{if} \quad \frac{|C - T|}{T} \leq 0.005 \\
& \quad \varepsilon_{cm\_f} \leftarrow kd_f \cdot \varphi \\
& \quad C_m \leftarrow 0\text{kN} \\
& \quad \text{for} \quad i \in 1, 2 .. n_{seg} \\
& \quad\quad d_{f_i} \leftarrow \frac{kd_f}{n_{seg}} \cdot (i - 0.5) \\
& \quad\quad \varepsilon_{f_i} \leftarrow \frac{\varepsilon_{cm\_f}}{kd_f} \cdot d_{f_i} \\
& \quad\quad \sigma_{f_i} \leftarrow f_m\left(\varepsilon_{f_i}\right)
\end{aligned}
$$

(continued on next page)

$$C_m \leftarrow C_m + \sigma_{f_i} \cdot b \cdot \frac{kd_f}{n_{seg}}$$

$$\varepsilon_{s\_f} \leftarrow \frac{\varepsilon_{cm\_f}}{kd_f} \cdot \left(d_{eff} - kd_f\right)$$

$$T \leftarrow A_s \cdot f_s\left(\varepsilon_{s\_f}\right)$$

$$Mr \leftarrow T \cdot \left[d_{eff} - kd_f + \frac{b \cdot \frac{kd_f}{n_{seg}} \cdot \sum_{n=1}^{n_{seg}} \left(n \cdot d_{f_n}\right)}{b \cdot \frac{kd_f}{n_{seg}} \cdot \sum_{n=1}^{n_{seg}} n} \right]$$

$Mr \leftarrow 0kN \cdot m \quad if \quad \varphi = 0m^{-1}$

Mr

$\varphi_{test} := 0m^{-1}, 0.005m^{-1} .. 0.45m^{-1}$

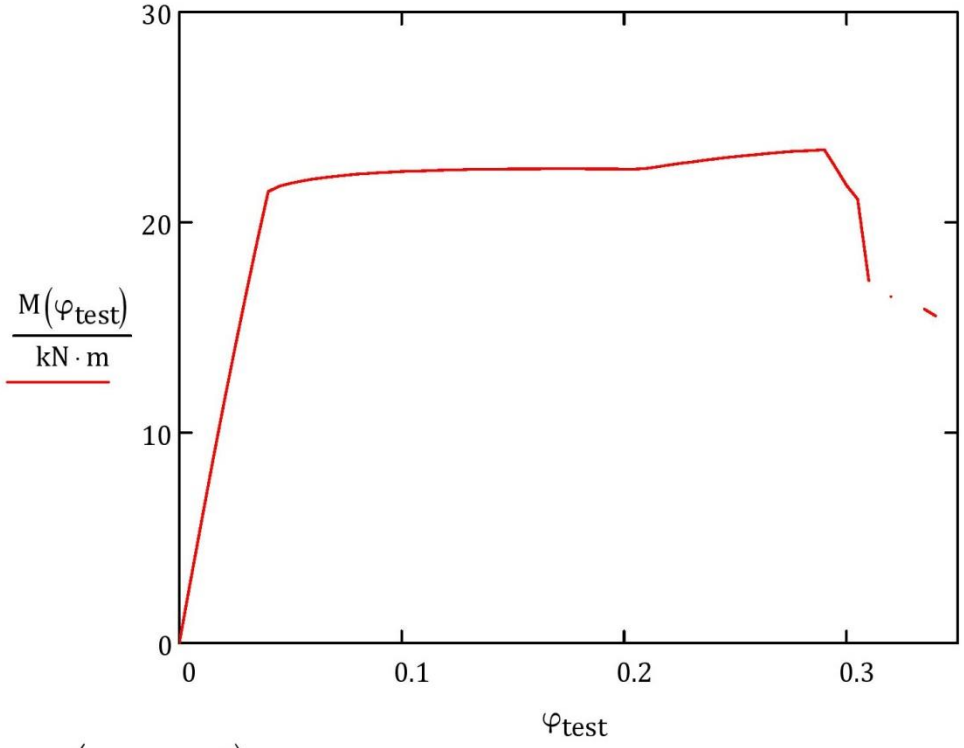

e.g $M\left(0.025m^{-1}\right) = 14.02494 \cdot kN \cdot m \qquad M_{max} := M\left(\varphi_{max}\right) = 8.02 \cdot kN \cdot m$

Database of Moment Values for Given Curvature:

$$M_{database} := \left| \begin{array}{l} \text{for} \quad i \in 1 .. 300 \\ \quad \left| \begin{array}{l} j \leftarrow (i-1) \cdot 0.001\text{m}^{-1} \\ Mom_i \leftarrow M(j) \end{array} \right. \\ Mom \end{array} \right.$$

$$\varphi_{database} := \left| \begin{array}{l} \text{for} \quad i \in 1 .. 300 \\ \quad \left| \begin{array}{l} j \leftarrow (i-1) \cdot 0.001\text{m}^{-1} \\ \varphi_i \leftarrow j \end{array} \right. \\ \varphi \end{array} \right.$$

$M_{database} =$

	1
1	0
2	0.591
3	1.179
4	1.764
5	2.352
6	2.934
7	3.514
8	4.091
9	4.665
10	5.237
11	5.807
12	6.374
13	6.939
14	7.501
15	8.06
16	...

$\cdot \text{kN} \cdot \text{m}$

$\varphi_{database} =$

	1
1	0
2	$1 \cdot 10^{-3}$
3	$2 \cdot 10^{-3}$
4	$3 \cdot 10^{-3}$
5	$4 \cdot 10^{-3}$
6	$5 \cdot 10^{-3}$
7	$6 \cdot 10^{-3}$
8	$7 \cdot 10^{-3}$
9	$8 \cdot 10^{-3}$
10	$9 \cdot 10^{-3}$
11	0.01
12	0.011
13	0.012
14	0.013
15	0.014
16	...

$\frac{1}{\text{m}}$

Curvature at a Given Moment for Cracked Section:

$$\varphi_m(M) := \left|\begin{array}{l} \varphi m \leftarrow 0m^{-1} \quad \text{if} \quad M = 0kN\cdot m \\ \text{if} \quad M \neq 0m^{-1} \\ \quad \left|\begin{array}{l} \text{for} \quad i \in 2, 3 .. 452 \\ \quad \text{if} \quad M < M_{database_i} \\ \quad\quad \left|\begin{array}{l} \varphi_1 \leftarrow \varphi_{database_i} \\ \varphi_2 \leftarrow \varphi_{database_{i+1}} \\ M_1 \leftarrow M_{database_i} \\ M_2 \leftarrow M_{database_{i+1}} \\ \varphi_{m\_int} \leftarrow \varphi_2 + (\varphi_1 - \varphi_2)\cdot\left(\frac{M - M_2}{M_1 - M_2}\right) \\ \text{break} \end{array}\right. \\ \varphi m \leftarrow \varphi_{m\_int} \end{array}\right. \\ \varphi m \end{array}\right.$$

e.g. $\varphi_m\left(\frac{1}{2}M_{max}\right) = 6.861\times10^{-3}\frac{1}{m}$ $\varphi_m\left(M_{max}\right) = 0.014\frac{1}{m}$

Moment based on applied load at location l along wall:

$$M_a(P, l) := \left|\begin{array}{l} \frac{P}{2}\cdot l \quad \text{if} \quad 0mm \le l < a \\ \frac{P}{2}\cdot a \quad \text{if} \quad a \le l < 2a \\ \frac{P}{2}\left(l_m - l\right) \quad \text{otherwise} \end{array}\right.$$

Deflection at midspan for any applied load, P:

$\delta_{mid}(P) :=$ | $defl \leftarrow 0mm$

$n \leftarrow \frac{l_m}{l_{seg}}$

for $i \in 1 .. n$

$l_i \leftarrow i \cdot l_{seg} - 0.5 \cdot l_{seg}$

$M_{ai} \leftarrow M_a(P , l_i)$

$\varphi_i \leftarrow \frac{M_{ai}}{E_m \cdot I_g}$ if $M_{ai} \le M_{cr}$

$\varphi_i \leftarrow \varphi_m(M_{ai}) \cdot \left[1 - \left(\frac{M_{cr}}{M_{ai}}\right)^2\right] + \frac{M_{ai}}{E_m \cdot I_g} \cdot \left(\frac{M_{cr}}{M_{ai}}\right)^2$ otherwise

$\delta_{mid} \leftarrow l_{seg} \cdot \sum_{i=1}^{\frac{n}{2}} (\varphi_i \cdot l_i)$

δ_{mid}

$P_{applied} := 0kN , 1kN .. 55kN$

e.g. $\delta_{mid}(30kN) = 12.602\,mm$

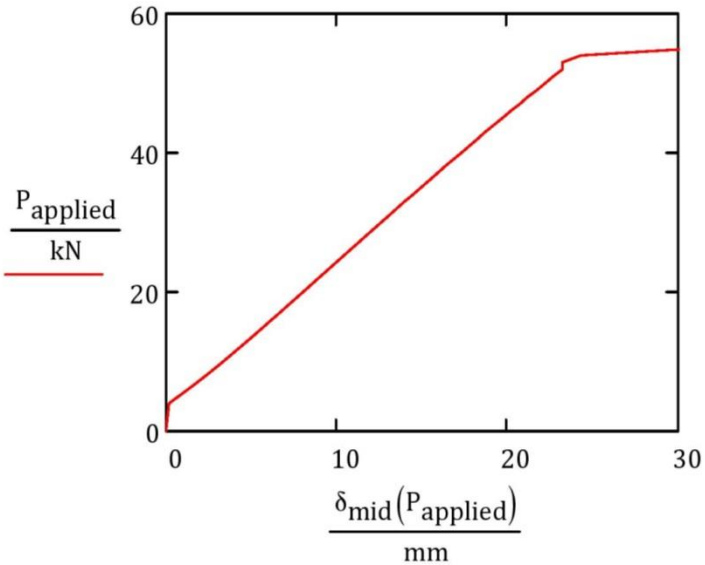

Theoretical Load-Deflection Value Databases

$\delta_{database} :=$ for $i \in 1 .. 55$
$j \leftarrow (i - 1) \cdot 1kN$
$\delta_i \leftarrow \delta_{mid}(j)$
δ

$P_{database} :=$ for $i \in 1 .. 55$
$j \leftarrow (i - 1) \cdot 1kN$
$P_i \leftarrow j$
P

$\delta_{database} =$

	1
1	0
2	0.046
3	0.092
4	0.138
5	0.185
6	0.732
7	1.283
8	1.821
9	2.342
10	2.849
11	3.347
12	3.834
13	4.313
14	4.789
15	...

$\cdot mm$

$P_{database} =$

	1
1	0
2	1
3	2
4	3
5	4
6	5
7	6
8	7
9	8
10	9
11	10
12	11
13	12
14	13
15	...

$\cdot kN$